VIBRATIONAL SPECTROSCOPY STUDIES OF BIOMOLECULAR SYSTEMS: FROM AMINO ACIDS TO MICROORGANISMS

By

Amira Cecilia Padilla Jiménez

A dissertation submitted in partial fulfillment of the requirements for the degree of

DOCTOR OF PHILOSOPHY

In

APPLIED CHEMISTRY
(Environmental Chemistry)

UNIVERSITY OF PUERTO RICO
MAYAGÜEZ CAMPUS
2014

Approved by:

_____	_____
Carlos Ríos-Velázquez, Ph.D. Member, Graduate Committee	Date
_____	_____
Martha L. López-Moreno, Ph.D. Member, Graduate Committee	Date
_____	_____
Nilka M. Rivera-Portalatín, Ph.D. Member, Graduate Committee	Date
_____	_____
Nairmen Mina-Camilde, Ph.D. Member, Graduate Committee	Date
_____	_____
Samuel P. Hernández-Rivera, Ph.D. President, Graduate Committee	Date
_____	_____
L. Antonio Estévez De Vidts, Ph.D. Representative of Graduate Studies	Date
_____	_____
René S. Vieta-Rivera, Ph.D. Chairperson of the Department	Date

© Copyright 2014
Amira C. Padilla-Jiménez
All rights reserved

This dissertation contains portions that have been published in *Nanomaterials*, in the Proceedings of SPIE *Defense, Security, and Sensing* (proceedings.spiedigitallibrary.org), and in *Optical Engineering*.

Abstract

Vibrational spectroscopy: infrared and Raman, was applied to the study of two amino acids and ten bacterial strains with the purpose of developing rapid methods of identification and discrimination. Use of spectroscopic techniques in characterization of signatures of biological agents has gained considerable attention in recent years, mainly because of the high sensitivity and selectivity that can be attained through their practice. They can also be easily adapted to portable equipment to obtain fingerprint information of biomolecules and microorganisms in the field.

In this research, various spectroscopic studies were conducted, both in the lab and in field applications. In the first study the most stable conformations and orientations of L-tryptophan (L-Trp) on silver (Ag) and gold (Au) nanoparticles (NPs) was determined using Raman spectroscopy. The objective of the work was to determine if L-Trp molecules interact with the Ag/Au NPs through the carboxylate end, through the amino group end, or through both using surface enhanced Raman spectroscopy (SERS). The work also focused on how parameters such as analyte concentration, average nanoparticle size and pH affected the binding of L-Trp to the NPs surfaces. In a second related study Ag/Au NPs were synthetized using a laser ablation technique and SERS activity of prepared NPs was evaluated with L-histidine (L-His).

In other studies quantum cascade laser spectroscopy (QCLS) was used to identify biochemical components of bacterial cell wall of various microorganism species from vibrational modes of molecular components in the biosamples. Principal component analysis (PCA) and partial least squares analysis coupled to discriminant analysis (PLS-DA) of QCL spectra were used to classify and discriminate between gram-positive and

gram-negative bacteria at a 95% confidence level. Results demonstrate that the QCLS techniques used: reflection and transmission, accompanied with powerful multivariate analyses techniques were successful in detecting and classifying the microorganisms studied by means of their characteristic spectral information.

Resumen

Espectroscopia vibracional: Infrarroja y Raman, se aplicó al estudio de dos aminoácidos y diez cepas bacterianas con el propósito de desarrollar métodos rápidos de identificación y discriminación. El uso de técnicas espectroscópicas en caracterización de firmas o señales de agentes biológicos ha ganado considerablemente la atención en los últimos años principalmente debido a la alta sensibilidad y selectividad que se puede lograr a través de su práctica. También se pueden adaptar fácilmente a equipos portátiles para obtener información de la huella dactilar de biomoléculas y microorganismos en el campo.

En esta investigación, se llevaron a cabo diversos estudios espectroscópicos, tanto en el laboratorio como en aplicaciones de campo. En el primer estudio se determinó las conformaciones más estables y orientaciones de L-triptófano (L-Trp) sobre nanopartículas (NPs) de plata (Ag) y oro (Au) usando espectroscopia Raman. El objetivo del trabajo fue determinar si las moléculas de L-Trp interactúan con las NPs Ag/Au a través del grupo carboxilato, a través del grupo amino, o a través de ambos, usando espectroscopia Raman de superficie aumentada (SERS). El trabajo también se centró sobre cómo parámetros tales como la concentración del analito, el tamaño promedio de las nanopartículas y el pH afectaron la unión de L-Trp a las superficies de las NPs. En un segundo estudio relacionado, las NPs de Ag/Au se sintetizaron utilizando la técnica de ablación por láser y se evaluó la actividad SERS de las NPs preparadas con L-histidina (L- His).

En otros estudios se utilizó la espectroscopia láser de cascada cuántica (QCLS) para identificar los componentes bioquímicos de la pared celular bacteriana de varias

especies de microorganismos a partir de los modos vibracionales de los componentes moleculares en las muestras biológicas. El análisis de componentes principales (PCA) y el análisis de mínimos cuadrados parciales junto con el análisis discriminante (PLS-DA) de los espectros de espectroscopia con láseres de cascada cuántica (QCL por sus siglas en inglés) se utilizaron para clasificar y discriminar entre bacterias gram-positivas y gram-negativas a un nivel de confianza del 95%. Los resultados demuestran que las técnicas de QCL usadas: reflectancia y transmisión, acompañadas de poderosas técnicas de análisis multivariable fueron efectivos en la detección y clasificación de los microorganismos estudiados a través de su información espectral característica.

Dios me dijo:

A*l mirarte por un solo momento*

M*ientras descansas de tus quehaceres*

I*nvitas a darte mi bendición en tus tormentos*

R*eforzando en ti todo lo que eres, para*

A*nimarte a que logres todo lo que quieres.*

This thesis is dedicated to God

To my Mother for her entirety,

To my precious sons: Gustavo Adolfo and my little one Adolfo Andrés.

Acknowledgments

This work was carried out at the Department of Chemistry, University of Puerto Rico at Mayagüez Campus, and was possible due to the support of several persons and institutions that collaborated directly and indirectly with my research. I wish to recognize their support.

First of all, I want to give thanks to God, for the strength that He gave me through all the way that I have crossed and for allowing me to achieve one of my desired goals. My deepest gratitude goes to Professor Samuel P. Hernández-Rivera, my advisor, because he gave me the opportunity to perform research under his guidance and supervision. I received his counseling and unconditional support to convert this research into a scientific contribution. I would like also, to mention Professors Martha Laura López-Moreno and Carlos Ríos-Velázquez for their valuable suggestions and collaboration throughout this investigation. To members of my other graduate committee Professors Nilka Rivera-Portalatín and Nairmen Mina-Camilde, special thanks for their comments and revision of this manuscript.

I would like to express my gratitude to Gabriel Cruz from the Chemical Lab at Hewlett Packard-PR for the FE-SEM micrographics and to Boris Rentería from NANO-Materials Processing Lab for the Zeta potential measurement of nanoparticles.

I am grateful to Mr. Wilmer Carrión-Roca who was instrumental in expediting the opportunity to do research in QC Analytical laboratories during my doctoral internship at Abbvie Biotechnology, Ltd., and special thanks go to Mrs. Antonia Pérez and Dr. David Acevedo for their continuous technical support in Abbvie.

I wish to mention the help that was given to me by the working team of Abbvie Biotechnology Ltd., whose names are: Rebecca Molina, Jezenia Carrero, Limaris Santos, Yolanda Rentas, Javier Rosado, David Hernandez, Aurelio Garcia, Oswaldo, Guiovanny, Vanessa Saavedra, Michelle Dasta, Noel Vargas, Angel Malave, Luis Cortes, Zorellys Fuentes, Sahudi Ocasio, Debbye Figueroa, Keila Torres, Aneudy Vera, Orlando Amador, Nilda Mendez, Mayra Aquino, Samuel Colon, Maraneysa Torres, Andres Calvo, Leticia Portalatin, Melvin Morales, Rose Cuevas, Loyda Hernandez, Jessica Concepcion, Rosan Rivera, Eva Rosario and Rafael Hernandez.

With pleasure I thank to all my lab mates: José Luis Ruiz-Caballero, John R. Castro-Suarez, Jorge Castellanos, Carlos Ortega-Zúñiga, Nataly Galán-Freyle, Amanda Figueroa, Dr. Gloria M. Herrera-Sandoval, Dr. William Ortiz-Rivera, Dr. Leonardo C. Pacheco-Londoño, Dr. Pedro M. Fierro-Mercado and Iris Vasquez-Ayala, thanks for all the shared moments and for the great help. Sincere thanks to Jose Antonio Ríos for his unconditional friendship and unlimited support during all the phases of my Ph.D degree.

This work was conducted in collaboration with the Center for Chemical Sensors Development at the Chemistry Department of the University of Puerto Rico–Mayagüez sponsored by the Department of Defense, Agreement Number: W911NF-11-1-0152. Support from the U.S. Department of Homeland Security under Award Number 2008-ST-061-ED0001 is also acknowledged.

Last, but most important, I would like to thank my family, that still in the distance, they have provided me their greatest love, prayers and sacrifices for the time away, specially to my mother who gave me the most valuable advice and my sons Gustavo

Adolfo and Adolfo Andrés, they are the source of inspiration, motivation and all the success that I have accomplish in my professional and personal life. Thank you very much to all!!!!!!.

Table of Contents

List of Table

List of Figures

Chapter 1

INTRODUCTION

1.1. From amino acids to microorganisms

Biophysical research at the molecular level focuses on the study of molecules present as constituent of all living creatures. The development of new techniques that help to elucidate how complex biological processes are carried out by all living organisms, such as: digestion, respiration, reproduction and other important physiological functions have advanced the state of the art of these important areas of biophysical research. Organic molecules such as carbohydrates, lipids, proteins, and nucleic acids are chemical compounds found in all living cells at different concentration levels. Proteins are the most abundant and more varied of these biomolecules with larger diversity of functions in the body. They play key roles both in intra and extra cellular processes. Knowledge of the functions of the body requires a detailed study of the structure and properties of proteins. All known types of proteins are formed by only 20 amino acids in which one is attached to an adjacent via a covalent bond formed by dehydration, called a peptide bond. These units can form a variety of combinations, which are of the order of thousands different structures designed to develop a multitude of biological activities.

Amino acids are classified into three groups such as essential, nonessential and conditional, depending if they can or cannot be made by the body and must be supplied by food and supplements. Tryptophan (Trp) and histidine (His) are two essential amino

acids that are important, both physiologically and in biophysics and biomedicine. Amino acids consist of a central carbon atom attached to a carboxyl group (–COOH), an amino group ($–NH_2$), a hydrogen atom, and a side group (–R) that may be a hydrogen or an organic group and determines the properties of particular amino acids, because the side group differs from one amino acid to another. L-tryptophan (L-Trp) is a large neutral amino acid with a 3-methylindole side chain [1]. This group makes L-Trp highly hydrophobic. However, in spite of the hydrophobic nature of the indole ring it may be found both on the surface and within protein molecules [2]. Similarly, L-histidine (L-His) is an α-amino acid with an imidazole ring as side group, which has an aromatic behavior with six π electrons that can give rise to assembling interactions represented by two equally important resonance structures [3]. L-His is used to develop and maintain healthy tissues in all parts of the body, for the reason that, is the only amino acid that ionizes within the physiological pH range. Decarboxylation of L-His produces a biogenic amine called histamine, via the enzyme histidine decarboxylase that is produced by enteric bacteria. Histamine is considered a toxic compound above 50 mg/kg according to Food and Drug Administration (FDA) guidelines [4].

Most studies published on these compounds are based on spectroscopic and chromatographic methodologies [5-12]. However, vibrational spectroscopy has demonstrated to be crucial for the detection of biomolecules because each compound has characteristic vibrations in a determined frequency range that can be used for identification and quantification. In particular, Raman spectroscopy in its various modalities has played unique roles in characterization of biological materials [13], and some of its modalities allow analyzing these compounds at low limits of detection, which

can be useful in a number of applications in fields such as clinical analysis, monitoring environmental pollution, defense and security applications among many other disciplines.

Raman spectroscopy is a powerful analytical tool that can be used to analyze a single molecular species or mixtures of various molecular species. Surface enhanced Raman scattering (SERS) spectroscopy, which is routinely used for detecting analytes at very low concentrations and has been very successful in the detection of biocompounds. SERS is a useful technique resulting in an enhanced increase of intensities of Raman signals from molecules attached to nanometer sized metallic structures. Specific chemical information for each compound (in this case amino acids) can be obtained using SERS. This work was aimed at using SERS to determine how bio-analytes such as L-Trp and L-His interact with metallic nanoparticle surfaces: Ag and Au.

Amino acids are part of proteins present in prokaryotes organisms such as bacteria. Study of these microorganisms is very important in pharmaceutical and food industries. The usual components of the culture media are amino acids. The concentration of amino acids in the culture media limits the growth and survival of bacterial cells. Culture media should contain appropriate composition of nutrients, pH and osmolality for the type of microorganisms under study. Once these parameters are determined, media quantities and the frequency with which it should be replaced with fresh medium can be calculated. The medium formulation depends mainly on the microorganisms to be cultured.

The main purpose of vibrational spectroscopy techniques has been the identification, discrimination and classification of microorganisms. Recent approaches to the

identification of medically relevant microorganisms, cyanobacteria, lactic acid bacteria and yeasts and the use of multivariate techniques to achieve this have been published [14-20].

The bacterial strains used and studied in this research were: *Bacillus thuringiensis (Bt), Bacillus pumilus (Bp), Bacillus subtilis (Bs), Bacillus licheniformis (Bl), Escherichia coli (Ec), Staphylococcus epidermidis (Se), Micrococcus luteus (Ml), Staphylococcus aureus (Sa), Pseudomonas aeruginosa (Pa), Acinetobacter genomospecies 3 (Ag3)*. *Bacillus thuringiensis*, *Bacillus subtilis*, *Bacillus pumilus* and *Bacillus licheniformis*, which are gram-positive bacteria, have the ability to form endospores, a latent state that is highly resistant to chemical and thermal extremes. As bacillus specie, they have a bacterial life cycle in which they grow as vegetative cells forming endospores as defense mechanisms [21]. Endospores are highly resistant to environmental stresses such as high temperature, radiation, strong acids, disinfectants, etc. They are able to tolerate extreme environments thus making them suitable for transporting as part of a biological attack [22]. *Bs*, considered as an organism “Generally Recognized as Safe” (GRAS), is a non-harmful microorganism to humans with a low degree of virulence [23]. It does not produce significant quantities of extracellular enzymes or possess other virulence factors that would predispose it to cause infection [24]. *Bp,* generally shows high resistance to UV light exposure, desiccation, and the presence of oxidizers such as hydrogen peroxide [25]. Isolated strains of *Bp* produce a complex of lipopeptides called pumilacidins, known to have toxic effects on epithelial cells. Other symptoms that result from the infection include dizziness, headache, chills, back pain, stomach cramps and diarrhea [26]. Furthermore, a report was published concluding that a strain of *Bp* was

responsible for the development of cutaneous lesions morphologically similar to those caused by *Bacillus anthracis* (Anthrax) [27]. Likewise, *Ml* is also a gram-positive, spherical, aerobe, saprotrophic bacterium that belongs to the Micrococcaceae family [28]. It is often found in contaminated soils, oil spills, sludge, dust, water and air, and as part of the normal flora of the mammalian skin. The bacterium also colonizes the human mouth, mucosae, oropharynx and upper respiratory tract. It has a potential role in bioremediation and in biotechnology. In the form of sphere it combines two properties essential to dealing with toxic wastes: the ability to degrade toxic organic pollutants and tolerance to metals [29]. *Se,* another sphere forming gram-positive bacterium is also part of our normal flora, usually the skin. However, *Se* can be found as contaminant reflecting ease of contamination of processing units. Organisms being part of the normal floral of the body easily contaminates food and biotechnology industrial products during handling and processing by personnel. Favorable growth environment for microorganisms is prevented by high sugar concentration [30]. *Se* is heat resistant and thrives well in fairly high concentration of sugar which also contributes to its survival in processed products. These bacterial species have previously been associated with drug contaminations [31, 32]. Oligotrophic bacteria such as *pseudomonas* are capable of reproducing and forming biofilms under conditions that are usually considered to be nutrient restricted. Such organisms are found in low nutrient environments like drinking water, attaining population densities of 10^6 to 10^7 cells/mL in distilled water [33]. The presence of *Pa,* has been invoked as a means of assessing the hygiene quality of drinking water, and in certain circumstances, provides an indication of the general

cleanliness of the water distribution system and can survive under different storage and treatment conditions [34].

1.2. Literature review for SERS

Many studies involving identification of biomolecules using Raman spectroscopy have been conducted recently. Raman spectroscopy combined with chemometrics has recently become a widespread technique for analysis, detection and chemical profiling of a variety compounds. This was discussed by Buckley and Matousek [35] in 2011. The first measurement of a surface Raman spectrum from pyridine [36] (heterocyclic organic compound) adsorbed on an electrochemically roughened silver electrode was reported by Fleischmann and coworkers in 1974, although it was not recognized as such at that time. Koglin and Séquaris in 1986 published on surface enhanced Raman scattering (SERS) of biomolecules and discussed the advantages and applications of SERS and surface enhanced resonance Raman scattering (SERRS) from biomolecules adsorbed on a metal surface [37]. Thousands of papers have been published on SERS since its discovery three decades ago. Kneipp, et al. provided a comprehensive review on SERS and a critical analysis and prospects of single-molecule Raman Spectroscopy [36]. The SERS phenomenon has two simultaneously operative mechanisms not completely understood: the electromagnetic field mechanism (EM) proposed by Jeanmaire and Van Duyne in 1977 and the molecular or chemical (CHEM) enhancement mechanism proposed by Albrecht and Creighton in 1977. In the CHEM mechanism, enhancement of the Raman signal is related to specific interactions, i.e., electronic coupling between the molecule and the metal, involves charge transfer between the chemisorbed species and the metal surface. EM SERS enhancement

arises from the presence of surface plasmons on the substrate, where surface plasmons are electromagnetic waves that propagate along the surface parallel to the metal/dielectric interface. The molecule must be directly adsorbed to the roughened surface to experience the chemical enhancement. In 2001 Haynes and Van Duyne, clarified and documented that the EM enhancement is strongly dependent on size, shape, and material of the nanoscale roughness features [39]. These characteristics determine the resonant frequency of the conduction electrons in a metallic nanostructure. In 2005 Haynes, McFarland and Van Duyne reported that electromagnetic enhancement relies on Raman-active molecules being confined within EM fields and contributes an average enhancement factor ≥ $10^{4\text{-}12}$ [40]. However, a key problem in analytical application of SERS is to develop stable and reproducible SERS-active substrates that can provide a large enhancement factor [40]. There is a general consensus that the most critical aspect of performing a SERS experiment is the choice and/or fabrication of the noble-metal substrates. Because SERS intensities depend on the excitation of the called localized surface plasmon resonances (LSPR), it is important to control the factors influencing the LSPR to maximize signal strength and ensure reproducibility.

The SERS effect discovered in the seventies is largely attributed to the interaction of light with matter. Specifically, SERS is related to the inelastic scattering (or Raman scattering) of certain molecules in the presence of specially prepared roughened or discontinuous metallic nanostructures. Bantz et al. in 2011 summarized a variety of engineered nanostructures that have been used for SERS detection [41]. During the past few years, researchers have dedicated efforts to study characterization of proteins

on different substrates. Examples of SERS substrates platforms and preparation techniques include electrochemically-roughened electrodes, laser ablation of metals (Takeshi, 2012; Haibo et al., 2012; Herrera-Sandoval, et al., 2013) [42-44]; colloidal suspensions of Ag and Au nanoparticles (Lee and Meisel, 1982) [45]; chemically etched metal surfaces and evaporated metal films (Natan and He, 2001) [46]. Tolaymat et al., 2010 describe the properties, synthesis and applications of silver nanoparticles [47].

Papers of SERS have been written with several application-specific for electrochemistry, medicine, biochemistry, and surface science (Baker and Moore, 2005; Aroca et al., 2005; Primera-Pedrozo et al., 2012; Felix-Rivera et al, 2011; Tourwé and Hubin, 2006; Stuart et al., 2006; Alexander and Le, 2007) [48-54]. In a paper on the SERS of amino acid and L-Trp [55, 56], the SERS spectra of L-Trp was reported. Authors state that both the carboxylate (COO^-) and amino groups ($-NH_2$) bind to the silver substrate. The aliphatic moiety was close to the surface and the nitrogen atom of the indole ring interacts with the surface only when L-Trp is the C-terminal residue of a peptide [57]. In addition, Kim and coworkers in 1987 showed the strong vibrational enhancements of (COO^-) symmetric stretching and $C–COO^-$ stretching, leading to the conclusion that the adsorption of the carboxylate and amino groups of L-Trp on the Ag surface was responsible for the vibrational enhancements [58].

Nabiev et al., 1988, described SERS and its application to the study of biological molecules, including SERS of imidazole ring containing histidine [59]. Other contributions have followed, for example Davis, et al., 1992, presented results on SERS of histamine at silver electrodes as a function of pH [60]. The spectroscopic analysis of L-His adsorbed on gold and silver nanoparticle surfaces was reported by Lim et al.,

2008 [61]. Wen-Chi Lin et al., 2012 investigated the SERS spectroscopy of histamine and L-histidine using nanosphere lithography (NSL) based on silver film over nanosphere (Ag-FON) substrate at optimal conditions and establishing a comparison between the sensitivity of SERS measurements based on silver nanoparticles array and Ag-FON substrates [62]. They measured SERS spectra of L-histidine and histamine at concentrations as low as 10^{-10} M.

In addition, there are several contributions from the Center for Chemical Sensors Development (CCSD), which have published several studies in detection of highly energetic materials (HEM) using SERS [63-65]. Research group members addressed the syntheses of metallic NPs based on the properties of interest. Among the desired properties the types of metallic NPs are: silver, gold, bi-metallic (alloy), etc.; size: seeds, small to large (< 3-100 nm); shape: spherical, rods, dog-bones, prisms; and optical properties: location of maximum wavelength of surface plasmon in the Vis region. Furthermore the fixation of NPs and nanostructures on substrates using micro-patterned laser image formation obtained by physical reduction for detection of explosives and other analytes (nitrogenous bases, nucleosides, nucleotides, amino acids and the biological content of bacteria) have also been discussed. The broad applications of SERS have motivated researchers to continue the development of novel SERS substrates to prolong substrate lifetime, to provide stable and optimized enhancement factors that permit studies of biomolecules in diverse environments.

1.3. Objectives

The objective of this research was to perform detection, identification and discrimination (classification) studies of biomolecular systems. Raman spectroscopy was used to study aromatic amino acids: L-Trp and L-His and their interactions with Ag and Au NPs. Infrared spectroscopy: FT-IR and QCLS were used to develop detection and characterization techniques to discriminate live bacterial cells by their spectral signatures. The microorganisms studied were: *Bacillus thuringiensis, Bacillus pumilus, Bacillus subtilis, Bacillus licheniformis, Escherichia coli, Staphylococcus epidermidis, Micrococcus luteus, Staphylococcus aureus, Pseudomonas aeruginosa, and Acinetobacter genomospecies* 3.

1.3.1. Specific objectives

- To establish the most stable conformation and orientation of L-Trp, and L-His on gold and silver nanoparticles surfaces and to determine how these parameters are affected by nanoparticle size and colloidal pH values.
- To determine how bio-analytes such as L- Trp, and L-His interact with metallic NPs (Au and Ag), by how they adsorb or bind to the NPs surfaces.
- To identify and classify isolated bacterial colonies (*Bacillus subtilis, Bacillus pumilus, Bacillus licheniformis, Micrococcus luteus, Staphylococcus epidermidis and Acinetobacter genomospecies 3*) based on chemical composition.
- To establish growth curves for microorganisms studied transferring species from a mixed culture allowing a single colony to grow in a sterile medium

- To fully distinguish each bacterium species by the use of several spectroscopic techniques, such as FT-IR, Raman spectroscopy and QCLs and to use multivariate analysis to discriminate between bacterial samples isolated as PCA and PLS-DA.
- Perform microbial environmental control (MEC) sampling and testing from air (viable) on surfaces that are collected at specified places on a random in order to recover the amount of bacteria found in air, and on surfaces in the aseptic manufacturing area on pharmaceutical industry.

1.4. Overview of the dissertation

1.4.1. Chapter 2

This investigation focused on interactions of Ag and Au NPs with L-Trp to determine the effects of the carboxylate and amino end groups on these interactions. Ag/Au NPs were synthesized using citrate reduction for SERS measurements of L-Trp in the 100 – 3500 cm^{-1} spectral range. Experimental protocols included use of electrolytes (NaCl) for colloid activation which resulted in high intensity SERS signals. NPs surface charges were modified by changing the pH (2-11) of these precious metallic colloidal suspensions. SERS spectra suggest that relatively large size NPs are favored in achieving high sensitivity detection. The prominently enhanced intensities of the COO^- group stretch in the SERS spectra strongly suggest that the carboxylate group attaches to Ag NPs, whereas for Au NPs a new band at ~ 2136 cm^{-1} was observed suggesting that the amino group of L-Trp is attached to Au in its neutral form. SERS spectra were modeled using density functional theory (DFT) on molecular models in which L-Trp

interacted with limited surface models of Ag/Au NP substrates in neutral and ionic forms.

Keywords: L-tryptophan, silver/gold nanoparticles, surface enhanced Raman scattering.

1.4.2. Chapter 3

Gold and silver nanoparticles (NPs) were prepared in water by laser ablation methodologies. The average characteristic (longer) size of the NPs obtained ranged from 3 to 70 nm. 4-Aminobenzebethiol (4-ABT) was chosen as the surface enhanced Raman scattering (SERS) probe molecule to determine the optimum irradiation time and the pH of aqueous synthesis of the laser ablation-based synthesis of metallic NPs. The synthesized NPs were used to evaluate their capacity as substrates for developing analytical applications based on SERS measurements. L-His was used as the target compound in the SERS experiments. The results demonstrate that gold and silver NP substrates fabricated by the methods developed show promising results for SERS-based studies and could lead to the development of micro sensors.

Keywords: laser ablation; Au and Ag NP; Raman spectroscopy; SERS; L- histidine.

1.4.3. Chapter 4

Investigations focusing on devising rapid and accurate methods for developing signatures for microorganisms that could be used as biological warfare agents detection, identification, and discrimination have recently increased significantly. QCL based spectroscopic systems have revolutionized many areas of defense and security

including this area of research. In this contribution, infrared spectroscopy detection based on QCLS was used to obtain the mid-infrared (MIR) spectral signatures of *Bacillus thuringiensis, Escherichia coli,* and *Staphylococcus epidermidis.* These bacteria were used as microorganisms that simulate biothreats (biosimulants) very realistically. The experiments were conducted in reflection mode with biosimulants deposited on various substrates including cardboard, glass, travel bags, wood, and stainless steel. Chemometrics multivariate statistical routines, such as principal component analysis (PCA) regression and partial least squares (PLS) coupled to discriminant analysis (DA) were used to analyze the MIR spectra. Overall, the investigated infrared vibrational techniques were useful for detecting target microorganisms on the studied substrates and the multivariate data analysis techniques proved to be very efficient for classifying the bacteria and discriminating them in the presence of highly IR-interfering media.

Keywords: microorganisms; QCLS; multivariate analysis; principal component analysis; partial least squares-discriminant analysis.

1.4.4. Chapter 5

Development of capabilities for detection, identification and discrimination of microorganisms, such as bacteria, is important in defense and security applications. This research involves detection of bacteria using spectroscopic techniques such as Fourier transform infrared (FT-IR) spectroscopy and quantum cascade laser spectroscopy (QCLS). Zinc selenide discs were used as support media for bacterial samples. Three strains of bacteria were analyzed: *Escherichia coli, Staphylococcus epidermis* and *Bacillus thuringiensis*. Partial least squares (PLS) combined with

discriminant analysis (DA) were employed as chemometric tools for classification and to differentiate between bacterial strains using transmission mode QCLS. FT-IR spectra were used as reference. Spectral differences of the bacterial membrane were used to determine that these microorganisms were present in the samples analyzed.

Keywords: Transmission mode QCLS, FT-IR spectroscopy, bacteria, zinc selenide discs, partial least squares-discriminant analysis.

1.4.5. Chapter 6

Developing capabilities for detection and identification of microorganisms, such as bacteria, is a top priority for the pharmaceutical industries, because bacteria might be present as contaminants, even in clean rooms and ultra-clean process facilities. At a Biotechnology Lab facilities a series of experiments aimed to detect and discriminate for unwanted bacteria were proposed. Study of known bacteria such as *Bacillus subtilis, Bacillus pumilus, Bacillus licheniformis, Micrococcus luteus, Staphylococcus epidermidis and Acinetobacter genomospecies 3* in process rooms are needed to identify microorganisms in short time scales in order to minimize possible health hazards as well as production downtimes causing financial deficits. These types of bacteria were analyzed using spectroscopic techniques such as FT-IR, QCLS systems to determine whether these microorganisms are present in air and on surfaces in the aseptic manufacturing area on pharmaceutical industry. In addition, they were discriminated based on spectral differences of the bacterial membrane using multivariate tools such as principal component analysis (PCA).

Keywords: microorganisms; quantum cascade lasers; multivariate analysis; principal component analysis; Anodisc™ aluminum oxide filter.

1.5. References

[1]. Zaheer, Z., Ahmad-Malika, M., Al-Nowaiser, F.M., Khana. Z., Preparation of silver nanoparticles using tryptophan and its formation mechanism, *Colloids and Surfaces B: Biointerfaces* (2010) 81: 587–592.

[2]. Cao, X., Fischer, G., Infrared Spectral, Structural, and Conformational Studies of Zwitterionic L-Tryptophan, *J. Phys. Chem. A* (1999) 103: 9995-10003.

[3]. Wang, L., Sun, N., Terzyan, S., Zhang, X. and Benson D.R., A Histidine/Tryptophan π-Stacking Interaction Stabilizes the Heme-Independent Folding Core of Microsomal Apocytochrome b5 Relative to that of Mitochondrial Apocytochrome b5, *Biochemistry-US* (2006) 46: 13750-13759.

[4]. FDA. U.S. Food and Drugs Administration. Fish and Fishery Products Hazard and Control Guide. (1997).

[5]. Trucksess, M.W., Separation and isolation of trace impurities in L-tryptophan by HPLC, *Journal Chrom.* (1993) 630: 147-150.

[6]. Staruszkiewics, W., Waldron, E., Bond, J., Decomposition in Foods. Fluorometric Determination of Histamine in Tuna: Development of Method, *Journal of the AOAC,* (1977) 60(5): 1125-1136.

[7]. Seiler, N., Chromatography of biogenic amines generally applicable separation and detection method, *J. Chromatogr.* (1997) 143: 221-246.

[8]. Bartolomeo, M. P. and Maisano, F., Validation of a Reversed-Phase HPLC Method for Quantitative Amino Acid Analysis, *J. Biomol Tech.* (2006) 17(2): 131–137.

[9]. Zambrano, A; Rodríguez, N; Tovar, M., Histamine determination by chemical methods in tunas and sardines analyzed it the Institute National of Hygiene, *Rev. Inst. Nac. Hig.* (2000) 31: 22-25.

[10]. Bhandare, P., Madhavan, P., Rao, B.M., Rao, N.S., Determination of arginine, lysine and histidine in drug substance and drug product without derivatization by using HILIC column LC technique, *J. Chem. Pharm. Res.* (2010) 2(5), 580-586.

[11]. Ben-Gingirey, B., Craven, C. and An, H., Histamine formation in albacore muscle analyzed by OAOC and enzymatic methods, *J. Food Sci.* (1998) 63(2), 210-214.

[12]. Cinquina A. L, Longo F, Calì A, De Santis L, Baccelliere R, Cozzani R., Validation and comparison of analytical methods for the determination of histamine in tuna fish samples*, J Chromatogr. A*, (2004) 1032: 79–85.

[13]. Curl R. F., Capasso F., Gmachl C, Kosterev A.A., McManus, B., Lewicki R., Pusharsky M., Wysocki G., Tittel, F.K., Quantum cascade lasers in chemical physics, *Chem. Phys. Lett.* (2010) 487(1-3): 1-18.
[14]. Padilla-Jiménez, A.C., Ortiz-Rivera, W., Ríos-Velázquez, C., Vázquez-Ayala, I., Hernández-Rivera S.P., Detection and discrimination of microorganisms on various substrates with quantum cascade laser spectroscopy, *J. Opt. Eng.* (2014) 53(6) 061611-10.
[15]. Naumann, D., Helm, D., and Labischinski, H., Microbiological characterizations by FT-IR spectroscopy, *Nature* (1991) 351(6321): 81-82.
[16]. Helm, D., Labischinski, H., and Naumann, D., Elaboration of a procedure for identification of bacteria using Fourier-Transform IR spectral libraries: a stepwise correlation approach. *J. Microbiol. Methd.* (1991) 14(2): 127-142.
[17]. Curk, M.C., Peledan, F., and Hubert, J.C., Fourier transform infrared (FTIR) spectroscopy for identifying Lactobacillus species, *FEMS Microbiol. Lett.* (1994) 123(3): 241-248.
[18]. Goodacre, R., Timmins, E.M., Rooney, P.J., Rowland, J.J., Kell, D.B., Rapid identification of Streptococcus and Enterococcus species using diffuse reflectance-absorbance Fourier transform infrared spectroscopy and artificial neural networks. *FEMS Microbiol. Lett*. (1996) 140(2-3): 233-239.
[19]. Helm, D., Labischinski, H., Schallehn, G., and Naumann, D., Classification and identification of bacteria by FT-IR spectroscopy, *J. Gen. Microbiol.* (1991) 137(1): 69-79.
[20]. Mariey, L., Signolle, J.P., Amiel, C., and Travert, J., Discrimination, classification, identification of microorganisms using FTIR spectroscopy and chemometrics. *Vib. Spectrosc.* (2001) 26(2): 151-159.
[21]. Felix-Rivera, H., González, R., Rodríguez, G.D., Primera-Pedrozo, O.M., Ríos-Velázquez, C., Hernández-Rivera, S.P., Improving SERS Detection of Bacillus thuringiensis using Silver Nanoparticles Reduced with Hydroxylamine and with Citrate Capped Borohydride, *Int. J. Spectrosc.,* (2011) 2011: 989504.
[22]. Johnson, T.J., Valentine, N.B., Sharpe, S. W., Mid-infrared versus far-infrared (THz) relative intensities of room-temperature Bacillus spores, Chem. Phys. Lett. (2005) 403: 152–157.
[23]. Westers, L., Westers, H., Quax, W.J., Bacillus subtilis as cell factory for pharmaceutical proteins: a biotechnological approach to optimize the host organism, *BBA-Mol. Cell. Res.* (2004) 1694: 299–310.
[24]. Edberg, S.C. 1991 US EPA human health assessment: Bacillus subtilis. U.S. Environmental Protection Agency, Washington, D.C.
[25]. Kempf, M.J., Chen, F., Kern, R., Venkateswaran, K., Recurrent isolation of hydrogen peroxide-resistant spores of Bacillus pumilus from a spacecraft assembly facility, *Astrobio*l (2005) 5(3): 391–405.

[26]. From, C., Hormazabal, V., Granum, P., Food poisoning associated with pumilacidin-producing Bacillus pumilus in rice, *Int. J. Food Microbiol.* (2007) 115: 319-324.
[27]. Tena, D., Martinez-Torres, J., Perez-Pomata, M., Saez-Nieto, J., Rubio, V., Bisquert, J. Cutaneous infection due to Bacillus pumilus: Report of 3 cases, Clin. Infect. Dis. (2007) 44: 40-42.
[28]. Madigan, M., Martinko, J., Brock Biology of Microorganisms (11th ed.) Prentice Hall, (2005).
[29]. Sandrin, T.R. and R.M. Maier. Impact of metals on the biodegradation of organic pollutants, Environ. Health Persp. (2003) 111: 1093-1101.
[30]. Frazier W.C. and Westhoff, D.C., Food microbiology: 3rd edition, Mc-Graw Hill Book Co. New York, 71-75, 1994.
[31]. Ibezim, E. C, Esimone, C. O., Ofeofule, S. I., Chah, K. F., Evaluation of the microbiological quality of some commercially available syrups and suspensions in Nigeria. J phytomed, therap., 7(1&2):18-25, 2002.
[32]. Takon, A. I and Antai, S. P., Microbial contamination of expired and unexpired aqueous and suspension drugs sold in some patent medicine stores in calabar. Nig. J. Microbiology, 20 (2), 1096-1103, 2006.
[33]. McFeters, G.A., Broadaway, S.C., Pyle, B.H., Egozy, Y. Distribution of bacteria within operating laboratory water purification systems, *Appl. Environ. Microbiol.* (1993) 59: 1410-1415.
[34]. Legnani, P., Leoni, E., Turin, D., Valenti, C., Survival and growth of Pseudomonas aeruginosa in natural mineral water: a 5-year study, *Int. J. Food Microbiol.* (1999) 53: 153-158.
[35]. Buckley, K. Matousek, P., Non Invasive Analysis of Turbid Samples using Deep Raman Spectroscopy, *Analyst* (2011) 136(15): 3039-3050.
[36]. Fleischmann, M., Hendra, P.J., McQuillan, A., Raman Spectra of Pyridine Adsorbed at a Silver Electrode, J. Chem. Phys. Lett. (1974) 26: 163-166.
[37]. Kloglin, E. and Sequaris J., Surface Enhanced Raman Scattering (SERS) Spectroscopy of biomolecules, in Topics in Current Chemistry, Springer-Verlag: Berlin, (1986) 134, 1-57.
[38]. Kneipp, K., Kneipp, H., Itzkan, I., Dasari, R., Feld, M., Ultrasensitive Chemical Analysis by Raman Spectroscopy, *Chem. Rev.* (1999) 99: 2957-2975.
[39]. Haynes, C.; Van Duyne, R., Nanosphere Lithography: A Versatile Nanofabrication Tool for Studies of Size-Dependent Nanoparticle Optics, *J. Phys. Chem. B.* (2001) 105, 5599-5611.
[40]. Haynes, C.; McFarland, A.; Van Duyne, R., Surface-Enhanced Raman Spectroscopy, *Anal. Chem.* (2005) 77: 338A-346A.

[41]. Bantz, K.; Haynes C., Surface-Enhanced Raman Scattering Substrates Fabricated Using Electroless Plating on Polymer-Templated Nanostructures, *Langmuir* (2008) 24: 5862-5867.
[42]. Takeshi, T., Preparation of Nanoparticles Using Laser Ablation in Liquids, In Laser Ablation in Liquids, Pan Stanford Publishing, USA (2012), pp. 207–268.
[43]. Haibo, Z., Shikuan, Y., Weiping, C., Formation of Nanoparticles under Laser Ablation of Solids in Liquids, Laser Ablation in Liquids, Pan Stanford Publishing, USA (2012), pp. 327–396.A
[44]. Herrera-Sandoval, G.M., Padilla-Jimenez A.C. and Hernández-Rivera S.P., Surface Enhanced Raman Scattering (SERS) Studies of Gold and Silver Nanoparticles Prepared by Laser Ablation, Nanomaterials (2013) 3, 158-172.
[45]. Lee P.C., Meisel, D., Adsorption and surface-enhanced Raman of dyes on silver and gold sols, *J. Phys. Chem.* (1982) 88: 3391.
[46]. Natan, M.; He, L., Novel Surface Enhanced Raman Scattering (SERS) - Active Substrates and Method for Interfacing Raman Spectroscopy with Capillary Electrophoresis (CE), (2001). Patent WO0125757.
[47]. Tolaymat, T., El Badawy, A., Genaidy, A., Scheckel, K., Luxton, T., Suidan, M., An evidence-based environmental perspective of manufactured silver nanoparticle in syntheses and applications: A systematic review and critical appraisal of peer-reviewed scientific papers. *Scien. Tot. Environ.* (2010) 408: 999 – 1006.
[48]. Baker, G; Moore, D., Progress in Plasmonic Engineering of Surface Enhanced Raman-Scattering Substrates: Toward Ultra-trace Analysis, *Anal. Bioanal. Chem*. (2005) 382: 1751-1770.
[49]. Aroca, R.F.; Alvarez-Puebla, R.; Pieczonka, N.; Sanchez-Cortez, S.; Garcia-Ramos, J., Surface-enhanced Raman Scattering on Colloidal Nanostructures. *Adv. Colloid Interface Sci.* (2005) 116: 45-61.
[50]. Primera-Pedrozo, O.M., Rodríguez, G.D.M., Castellanos, J., Felix-Rivera, H., Resto, O., Hernández-Rivera, S.P., Increasing surface enhanced Raman spectroscopy effect of RNA and DNA components by changing the pH of silver colloidal suspensions, *Spectrochim. Acta A* (2012) 87: 77-85.
[51]. Félix-Rivera, H., González, R., Rodríguez, G.D.M., Primera-Pedrozo, O.M., Ríos-Velázquez, C., Hernández-Rivera. S.P., Improving SERS Detection of Bacillus thuringiensis Using Silver Nanoparticles Reduced with Hydroxylamine and with Citrate Capped Borohydride, Int. J. Spectrosc., (2011) 2011: 989504.
[52]. Tourwé, L., Hubin, A., Preparations of SERS-active Electrodes Via *ex situ* electrocrystallization of Silver in a Halide free Electrolyte. *Vib. Spectrosc.* (2006) 41: 59- 67.
[53]. Stuart, D., Yuen, J., Shah, N., Lyandres, O., Yonzon, C., Glucksberg, M., Walsh, J., Van Duyne, R., In Vivo Glucose Measurement by Surface Enhanced Raman Spectroscopy, *Anal. Chem.* (2006) 78: 7211-7215.

[54]. Alexander, T.A., Le, D.M., Characterization of a Commercialized SERS-Active Substrate and its Application to the Identification of Intact Bacillus Endospores. *Appl. Opt*. (2007) 46: 3878-3890.
[55]. Lee, H., Suh, S, Kim, M., Raman spectroscopy of L-tryptophan-containing peptides adsorbed on a silver surface, *J. Raman Spectrosc.* (1988) 19: 491-495.
[56]. Aliaga, A.E., Osorio-Román, I., Leyton, P., Garrido, C., Cárcamo, J., Caniulef, C., Célis, G., Díaz F., Clavijo, E., Gómez-Jeria, J.S., Campos-Vallette, M.M., Surface-enhanced Raman scattering study of L-tryptophan, *J. Raman Spectrosc.* (2009) 40: 164-169.
[57]. Chuang, C.H., Chena, Y.-T., Raman scattering of L-tryptophan enhanced by surface plasmon of silver nanoparticles: vibrational assignment and structural determination, *J. Raman Spectrosc.* (2009) 40: 150–156.
[58]. Kim, S., Kim, M., Suh, S., Surface-enhanced Raman scattering (SERS) of aromatic amino acids and their glycyl dipeptides in silver sol, *J. Raman Spectrosc.* (1987) 18: 171-175.
[59]. Nabiev, I., Efremov, R., Chumanov G., Surface-enhanced Raman scattering and its application to the study of biological molecules, *Sov. Phys. Uspekhi,* (1988) 31(3): 241–262.
[60]. Davis, K., McGlashenf M., and Morris M., Surface-Enhanced Raman Scattering of Histamine at Silver Electrodes, *Langmuir*, (1992) 8: 1654-1658.
[61]. Lim J., Kim Y., Yeong s., Lee, S., Joo S., Spectroscopic analysis of l-histidine adsorbed on gold and silver nanoparticle surfaces investigated by surface-enhanced Raman scattering, Spectrochimica Acta Part A (2008) 69,286–289
[62]. Wen-Chi L., Tsong-Ru T., Hsiang-Lin H., Chyuan S.& Hai-Pang C., SERS Study of Histamine by Using Silver Film over Nanosphere Structure, Plasmonics, (2012) 7, 709-716.
[63]. Fierro-Mercado, P., Hernández-Rivera, S.P., Highly sensitive filter paper substrate for SERS trace explosives detection, *Int. J. Spec.,* (2012), Article ID 716527.
[64]. Pacheco-Londono, L.C., Aparicio-Bolaño, J., Primera-Pedrozo, O.M., Hernandez-Rivera, S.P., Growth of Ag, Au, Cu, and Pt nanostructures on surfaces by micropatterned laser-image formations. Appl. Optics, (2011) 50(21): 4161-69.
[65]. Ortiz-Rivera W., Pacheco-Londoño, L. C., Castro-Suarez, J. R., Felix-Rivera, H., Hernandez-Rivera, S. P., Vibrational spectroscopy standoff detection of threat chemicals. 2011, *Proc. SPIE Int. Soc. Opt. Eng.,* 8031: 803129.Proc. SPIE (2011) 8031.

Chapter 2

SERS STUDY OF L-TRYPTOPHAN ADSORBED ON Ag/Au NANOPARTICLES

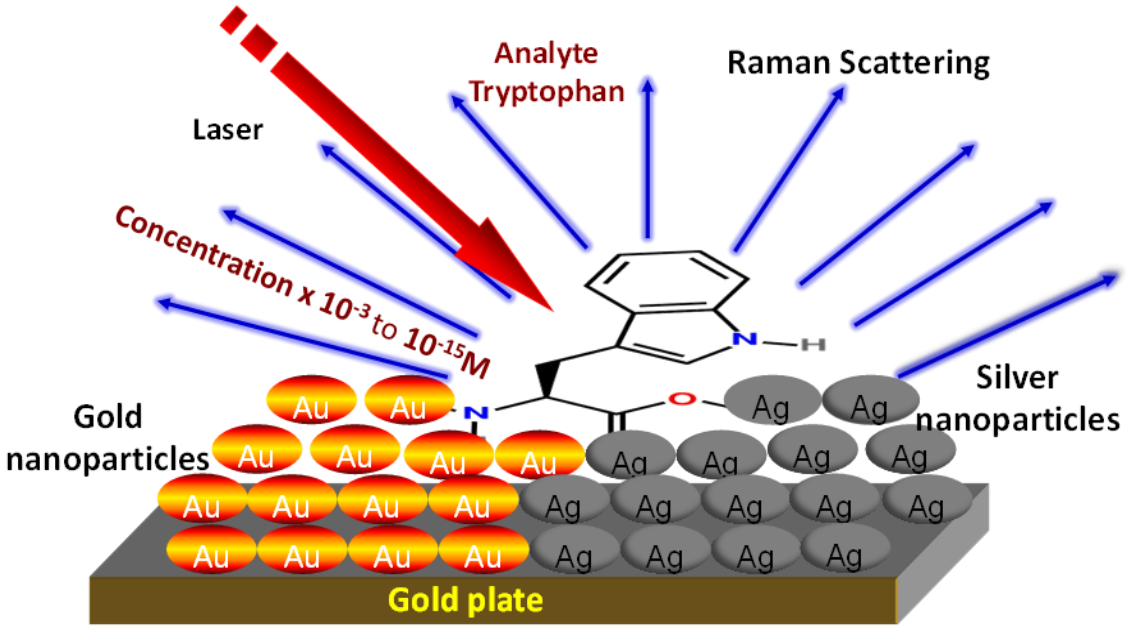

SERS of L-Trp on Au/Ag NPs.

2.1. Introduction

L-Tryptophan (L-Trp) is a rather large neutral essential amino acid, when compared to others, which has a 3-methyl indole side chain. This side chain is highly hydrophobic, but in spite of this, it may be found both on the surface and in the interior of protein molecules [1]. Aromatic π electrons allow it to interact strongly with other molecules containing electrons in π orbitals. While L-Trp has no ionizable groups, the relatively unreactive indole N-H bond, (pKa 9.5), may act as a hydrogen bond donor. In addition

to biological functions, L-Trp absorbs strongly between 275 and 280 nm, which allows for protein concentration to be determined in solution by UV-VIS spectrophotometry [2]. L-Trp is the only substance that can be converted into serotonin, which in turn is converted into melatonin. L-Trp clearly plays an important role in balancing mood and sleep patterns, is a precursor to a number of neurotransmitters in the brain, is involved in the production of B vitamin, niacin [3], and to list just a few potential applications, studies have also demonstrated its beneficial role in treating Down's syndrome and aggressive behavior. However, L-Trp levels are altered in cancer patients, so they often have very low levels of serotonin, which can contribute to a depressed mood and decreased chances of survival [4]. Although L-Trp levels in the diet are essential for physiological functions, in excess it can be converted into cancer-promoting metabolites that can interact with nitrite to produce mutagenic nitrosamines [5].

Recent advances in nanoscale science concerning the development of novel nanomaterials, exhibiting outstanding physical, chemical and biological properties have allowed the improvement of robust and highly sensitive and selective detection methods that are expected to address some deficiencies of conventional technologies [6]. Within this context gold (Au) and silver (Ag) nanoparticles (NPs) have been developed as powerful tools in sensing and imaging applications due to their unique optical properties. Although Ag exhibits many advantages over Au, such as higher extinction coefficients, sharper extinction bands, higher ratio of scattering to extinction, and extremely high field enhancements, it has been employed far less in the development of sensors, with the exception of sensors based on surface enhanced Raman scattering (SERS). The reason for this is the lower chemical stability of Ag NPs

when compared to Au NPs [7]. Despite the great excitement about the potential uses of Au NPs for medical diagnostics, as tracers, and for other biological applications, researchers are increasingly aware that potential NPs toxicity must be investigated before any in vivo applications of Au NPs can move forward [8]. Au and Ag NPs absorb visible light in the 400 to 700 nm range, which makes them perfect SERS substrates for this light scattering phenomenon [9]. SERS has been used for determining the orientation of molecules adsorbed on NPs surfaces [10]. This fact has great potential for application in biophysical studies, in addition to the increase in Raman intensity by as much as 106 to 1012 fold and the possibility of obtaining vibrational spectra at very low sample concentrations [11-12].

A previous SERS study of L-Trp with Ag NPs concluded that the analyte was bound to the Ag surface through both the carboxylate (COO^-) and amino groups (NH_2). The aliphatic moiety was close to the surface of the NPs and the nitrogen atom of the indole ring was bound to the surface only when L-Trp was the C-terminal residue of a peptide [12]. In addition, Kim and coworkers [13] showed the strong vibrational enhancements of (COO^-) symmetric stretching and C–COO^- stretching, leading to the conclusion that the adsorption of the carboxylate and amino groups of L-Trp on the Ag surface were responsible for the vibrational enhancements [14]. However, for a more detailed SERS investigation of L-Trp with NPs size, colloidal pH is required. It is expected that surface charges of the NPs in turn influence the SERS phenomenon observed and the interaction between the analyte and the metal surface [15]. Also calculations optimized using density functional theory (DFT) on a molecular model in which L-Trp interacts as

neutral, cationic and anionic forms with Ag and Au surfaces should contribute to gain insight on L-Trp – NPs substrate interactions.

2.2. Experimental section

2.2.1. Reagents

Hydrogen tetrachloroaurate (III) hydrate ($HAuCl_4.3H_2O$, 99.9985% Au; 49% Au, Puratrem) and silver nitrate ($AgNO_3$, 99.9995%-Ag, Puratrem) were purchased from Strem Chemicals (Newburyport, MA, USA). Sodium citrate dihydrate ($C_6H_5Na_3O_7.2H_2O$, ≥ 99%, FG), sodium hydroxide (NaOH, reagent grade, ≥ 98%, pellets, anhydrous) and L-Trp ($C_{11}H_{12}N_2O_2$, 99%) were acquired from Sigma-Aldrich Chemical Co. (Milwaukee, WI, USA) and were used as received without further purification. All sample solutions were prepared with ultra-high purity (UHP, 18.2 MΩ) Milli-Q water. Glass vessels for the preparation of Ag/Au NPs were thoroughly cleaned using aqua regia and rinsed with UHP water before using. Aluminum and gold coated glass slides (1 cm × 1 cm) were used for solid samples and for colloidal samples.

2.2.2. Preparation of Au and Au colloids

Colloidal Ag NPs were prepared with a modification of the method reported by Lee and Meisel [16]. After preparation, colloids were stored at 8^{o}C for future use. The obtained Ag NPs suspensions were characterized by using UV-Vis spectrophotometry to ensure that the reaction was complete with absorption λ_{max} ≈ 410 nm. Synthesized Ag NPs had an average size of 68 nm, a Zeta potential of -43.6 mV and pH 7.35. Au NPs were synthesized using the citrate reduction method. Solutions of 200 mL of chloroauric acid 1.0 mM solution per 50 mL of $HAuCl_4$ (0.01%) were reduced with 1% sodium citrate.

The metal ion and reducing agent solutions were degasified with N_2 and placed in incubator for 15 min to produce the growth solution of Au NPs. A typical synthesis consisted of dissolving 50.0 mL $HAuCl_4$ (0.01%) and 300 µL to 500 µL of 1% sodium citrate. The solutions were left undisturbed in an incubator for 12 h, until color changed from colorless to violet and had a pH 4.10. Colloids obtained were also stored at 8 ^oC for future use.

2.2.3. Instrumentation

Electronic absorption spectra of Ag/Au NP colloids were obtained using an Agilent model 8453 UV-Vis spectrophotometer. Spectra were recorded in the range of 200 to 800 nm. Quartz cells, 1.0 cm path length were used for the experiments and data were collected in absorbance mode. Average hydrodynamic radius and zeta potentials measurements at 25 ^oC of colloidal suspensions at different pH values were performed in a Nano Series Zetasizer (Malvern Instruments Ltd., Worcestershire, UK). SEM images for Ag/Au NPs morphology were obtained on a JEOL-JSM 6500 and a Philips/FEI SEM model XL30s. Samples for SEM analysis were prepared by depositing 5 µL of the metallic NPs suspensions on ultrathin carbon film/holey carbon 400 mesh copper grids (01824, Ted Pella, Inc., Redding, CA, USA). A Raman microspectrometer, model RM-2000 (Renishaw, Inc., Hoffman Estates, IL, USA) was used.

2.2.4. Raman experiments

Normal Raman (NR) and SERS experiments were performed with a 785 nm laser. For Au SERS samples 10 s integration and 3 accumulations were acquired. Spectra were recorded in the Raman shift range of 100-3500 cm^{-1} for normal and SERS spectra. Small amounts of the solid compounds were transferred to stainless steel microscope slides and NR spectra were collected in the Raman shift of interest. Laser power at the sample was kept bellow 10 mW. Stock solutions of L-Trp at concentrations range of 5 x 10^{-3} to 5 x 10^{-13} M were prepared using UHP water. 10 µL aliquots of a L-Trp 5 x 10^{-3} M solution were transferred onto aluminum slides and Raman signal for this sample with optimum pH was recorded.

For SERS measurements solutions of L-Trp and NaCl (for colloid activation) were transferred to a micro centrifuge vial and mixed by vigorous manual agitation, with a final pH of 7.35 (Ag) and 4.52 (Au). SERS spectra were acquired immediately and at 10 min intervals and checked at 24 h after mixing to ensure that the analyte was adsorbed on the NP surface [17]. A small volume of samples were transferred onto aluminum microscope slides (Ag) and gold coated slide (Au) and spectra were acquired at laser powers of 10 to 20 mW. In order to confirm results, Raman and SERS measurements were repeated several times for each sample. Since changes in dispersant media such as the ones induced by pH, ionic strength and even analytes are capable of promoting nanoparticle aggregation, NaOH and HCl solutions were used to adjust the pH of colloidal NPS suspensions from 2.0 to 11.0. SERS spectra for each sample were acquired every 20 min after mixing with the NPs at a specified pH [18].

2.2.5. Computational methods

In this study the neutral or zwitterion ($^{+}H_3NCH(R)COO^{-}$) and the cationic ($^{+}H_3NCH(R)COOH$) and anionic ($NH_2CH(R)COO^{-}$) forms of the molecular structure L-Trp were optimized using the density functional theory (DFT) at the B3LYP (Becke, three-parameters, Lee-Yang-Parr) level of theory with 6-311G basis set, using Gaussian 03 program [19].

Vibrational Raman frequencies were computed at the same level of theory and compared with experimental spectra. In order to have an insight in the interaction of L-Trp with the metal NPs surface, a calculations with surfaces of ten Ag/Au atoms were performed. Initially, the energies and vibrational Raman frequencies calculation were done of for the surface using DFT at B3LYP level with LANL2DZ (Los Alamos effective core potential with double zeta function). To evaluate the interaction of the different forms of L-Trp with the Ag/Au surfaces, two methods for optimization and frequency calculations were computed. First calculations were performed with the possible molecular forms of L-Trp (neutral, cationic and anionic) and the Ag/Au surfaces. These calculations were done using pseudo potentials for Ag/Au with LANL2DZ basis set and for L-Trp structures with 6-31G basis set. This combination was used in order to save computational costs. The second method of calculation was accomplished using the LANL2DZ basis set for both Ag/Au atoms and L-Trp structures. These methods were done freezing the Ag/Au atoms.

2.3. Results and discussion

2.3.1. Nanoparticles characterization

Ag and Au NPs were synthesized as described in the experimental section. Ag NPs were also reduced chemically using sodium borohydride [20]. These chemical reductions produced very small spherical NPs. However, NPs obtained did not perform as well as citrate reduced NPs in terms of yielding high surface enhancement factors (SFE) of L-Trp. This behavior has been attributed to the optical properties of metallic nanostructures that depend more markedly on shape than on size [21]. UV–Vis absorption spectroscopy is one of the most widely used, simple and sensitive techniques for characterization of metallic NPs synthesized via spectral location of wavelength max and the width of the absorption band of the electronic surface plasmon. The presence of only one plasmon component (transverse) indicated that the colloids consist primarily of nanospheres for both Ag and Au NPs [22]. The λ_{max} was on the averages located at 410 nm for Ag and 530 nm for Au. SEM was used to further confirm the nearly spherical Au NPs and nearly spherical form of Ag NPs, as is shown in figure 2.1.

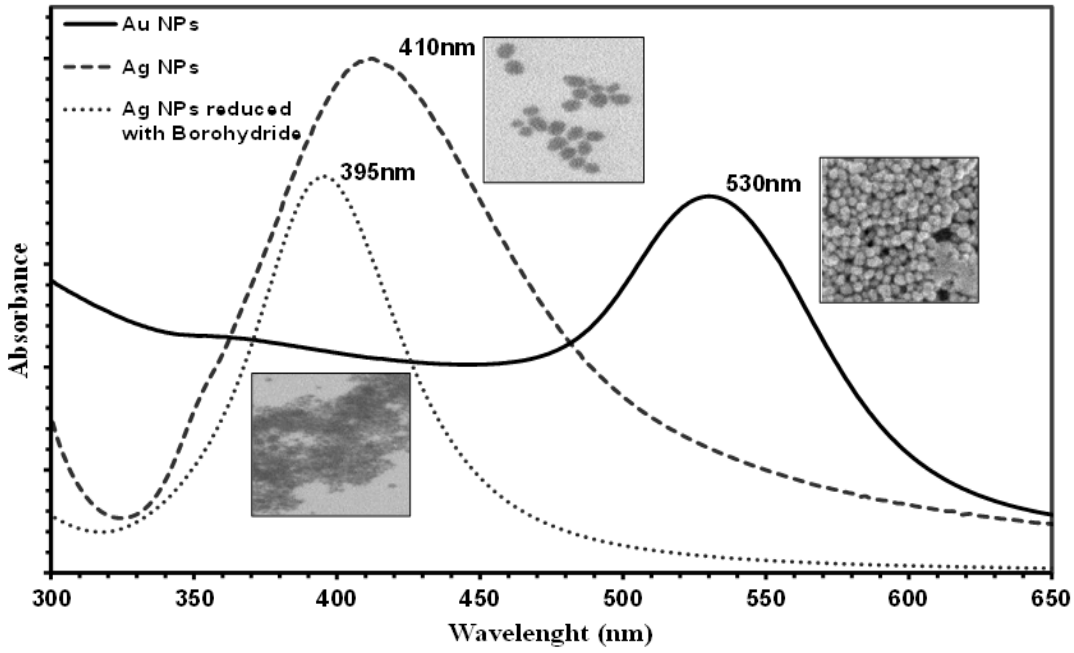

Figure 2.1. UV-Vis spectra of prepared Ag NPs and Au NPs.

2.3.2. Optimization of geometries of L-Trp on NP substrates models

Figs. 2.2 (a)-(c) show the graphical representations of optimized input and output geometries used in the calculations of the various molecular species of L-Trp: zwitterion, cationic and anionic forms. These were based on optimized structures of the neutral, cationic and anionic forms of L-Trp. Also included are the 10-atom surfaces representation of Ag (1,0,0) and Au (1,0,0) NPs. All optimized structures were confirmed to be minimum energy conformations. The optimized structures of L-Trp species and the model NPs surfaces are shown in Fig. 2.2 (b) for Ag/L-Trp and in Fig. 2.2 (c) for Au/L-Trp.

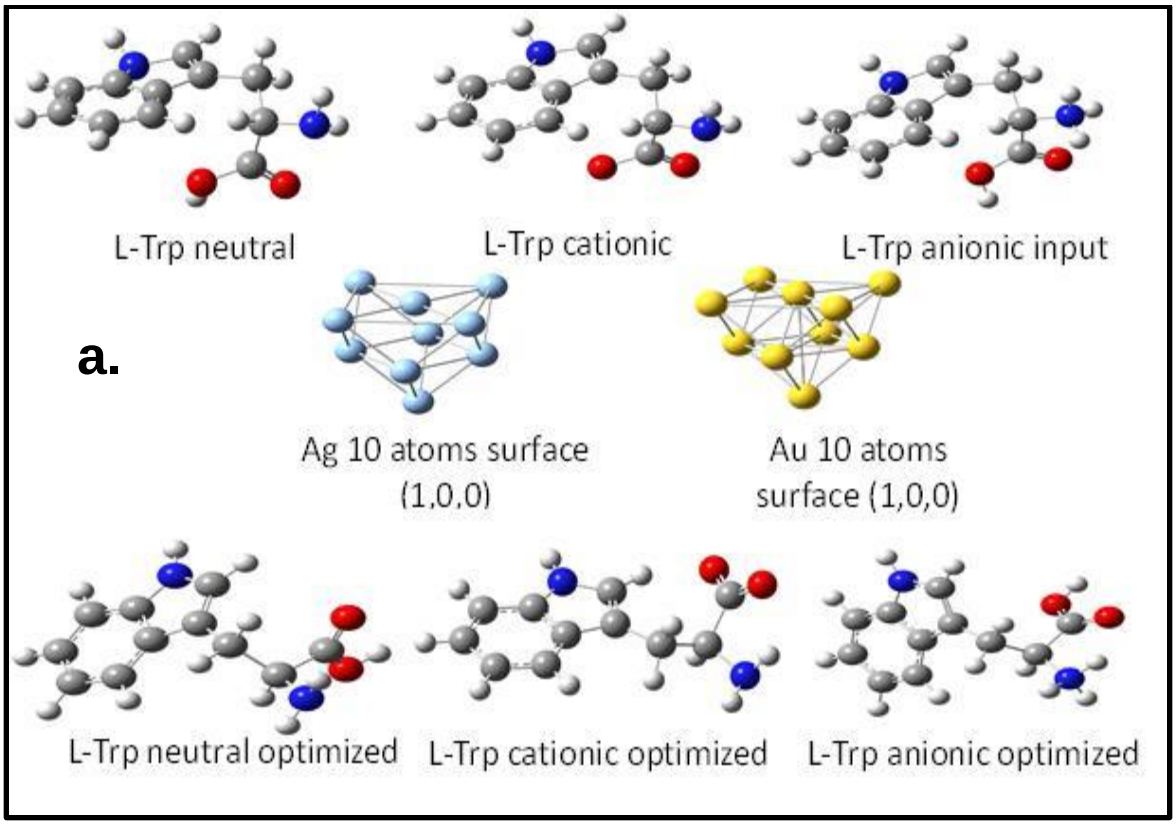
L-Trp neutral
L-Trp cationic
L-Trp anionic input
a.
Ag 10 atoms surface (1,0,0)
Au 10 atoms surface (1,0,0)
L-Trp neutral optimized
L-Trp cationic optimized
L-Trp anionic optimized

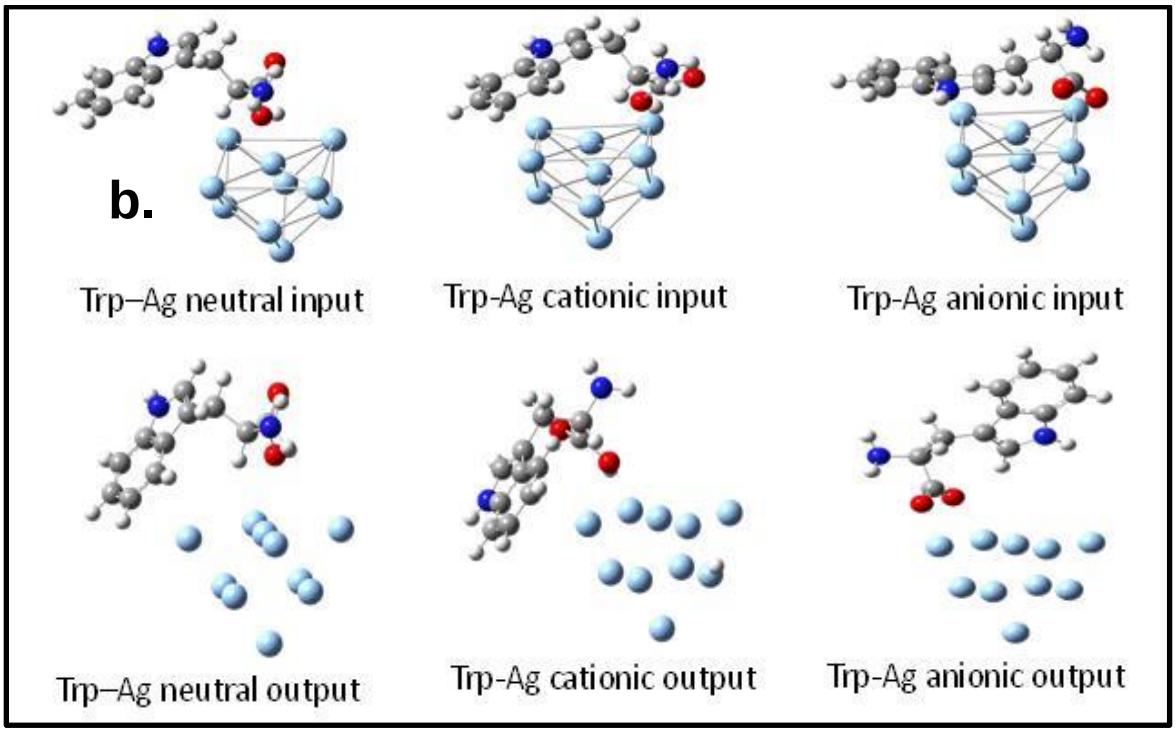
b.
Trp–Ag neutral input
Trp-Ag cationic input
Trp-Ag anionic input
Trp–Ag neutral output
Trp-Ag cationic output
Trp-Ag anionic output

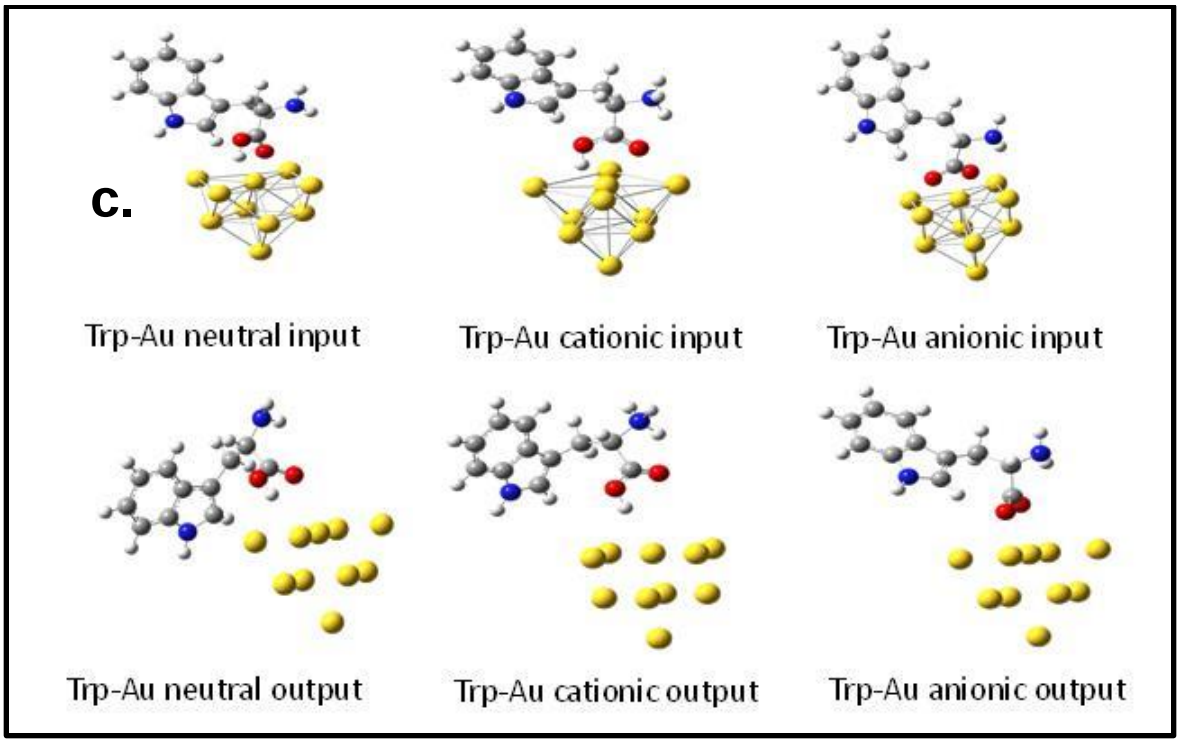

Figure 2.2. Optimized geometries of inputs and outputs for calculations of L-Trp with Ag/Au NPs: (a) L-Trp zwitterion, cationic and anionic forms of L-Trp and 10-atom surfaces representations for Ag(1,0,0) and Au(1,0,0); (b) Ag NPs surface interacting with L-Trp molecular forms; (c) Au NPs surface representation interacting with L-Trp molecular forms.

2.3.3. Raman spectra

Raman spectra of dilute solutions of L-Trp were measured to determine the SERS activity of the NPs for the desired application. NR of solid L-Trp, and SERS spectra at a low concentration (10^{-13} M for Ag and 10^{-8} M for Au) compared with L-Trp in aqueous solution (10^{-3} M) are shown in Figure 2.3. Peak positions are listed in Table 1 together with corresponding tentative assignments. Based on the position of the peaks and their relative intensities an estimate can be made on how the molecules are attached to the NPs surface. These assignments were compared to previously published data on L-Trp [23-25]. Calculated Raman shift spectra using DFT at B3LYP level with LANL2DZ

basis set, measured SERS and Raman band positions and assignments are also listed in Table 2.1.

SERS spectra are slightly different than those from NR spectra. Although similar peaks are present in these spectra, there are also significant differences; including peaks that have different relative heights, different shape, and new peaks are present. L-Trp has three different ionic forms depending on the pH of the solution: cationic ($^{+}H_3NRCOOH$, pKa_1 = 2.4), the zwitterion ($^{+}H_3NRCOO^{-}$, pH < 9.0) forms in which the amino group is protonated as NH_3^{+} in the solid and in aqueous solutions and the anionic form (NH_2RCOO^{-}, pKa_2 = 9.4) [26]. These structures are shown in Figure 2.3.

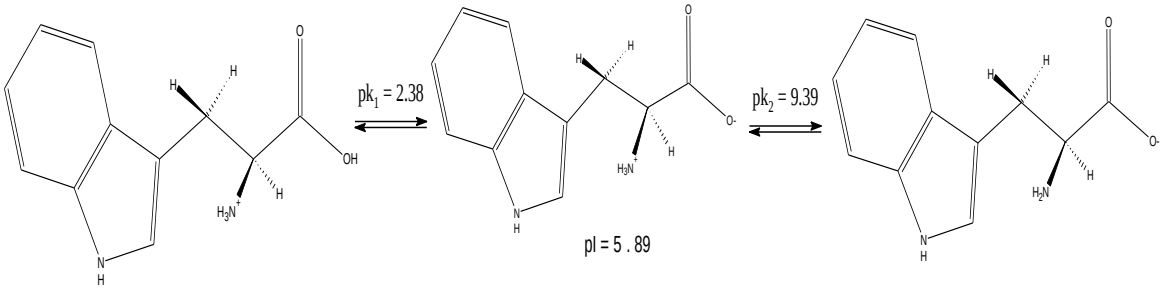

Figure 2.3. Three different ionic molecular forms of L-Trp.

The results clearly indicate enhancement of intensities of Raman signals and thus demonstrate the effectiveness of the SERS colloidal suspensions for carboxylate group and amino group in their structure of amino acid. SERS spectra of L-Trp on Ag and Au were found to be quite similar (Figure 2.3).

It is notable that new bands were saw in the ~2130 – 2254 cm^{-1} range for Au NPs SERS spectra, showed in each case a weaker absorption at 2254 cm^{-1}, assigned as overlapping asymmetric stretches, and a medium absorption at 2132 cm^{-1}, assigned as the approximately symmetric stretch $COAu_2$ [27], but disappearing at pH close to the pK_a of L-Trp, whereas it was absent for the Ag SERS spectrum as shown in Figure 2.3.

Table 2.1. Comparison and assignment of Raman shift spectra for L-Trp: DFT calculated (neutral species), NR of solid; NR in aqueous solution; adsorbed on Ag and Au NP.

NR L-Trp Solid	NR L-Trp Aqueous solution	SERS DFT Calculations Ag	SERS DFT Calculations Au	SERS Experimental Ag	SERS Experimental Au	Tentative Assignment [24-25]
				232		C-C-C oop; υAg-O
243	245	260				C-O-OH i.p
		323		329		C-NH_2 oop
352			359		359	C-C-C oop
	380	385		385	386	def. R.
	395			396	398	def. oop R, r
408	412					C-C-C oop
430						C-NH_2 i.p
472		467-476				βCC R, r, γCH_2
526	514			523	520	βN-H (r) ν R, r
537	533			529	536	δ(r), β i.p.
	551	579		574	574	β(R) oop; γCH_2
598		590 -599	595			δ(r), β i.p.
	607			604	607	γCH_2; N-H oop
630		620	640			αNH_2; βC-O
689	679					ν R, r
710	722	724		718	711-721	Def. R, r, υ CN
749		748	744-748	740		θ(R), θ (r); ωH(R); γCH_2
757	759		758			θ(R), θ (r)
768		771-778	775-778			Def. R, r, α COO^-
		787-793	788- 790			β(R)CC; β(r)
808					824	γCH_2, υ C-COO^-
846		845	843- 845			βCH(r) oop,
858	859	869		858	864	δH(R), βCH(NH) (r)
877		878	878	868		βH(R), αH(r)
		891-893	889			C-C-C i.p
933	929	902	902		942	C-H oop, υ CC (r); υ CNC (r)
974		969-975	969			δCH(r); γCH_2; βCH; γNH_2
993			980- 984			δCH_2;
1010	1011	1010	1015	1011	1009	θ(R), θ (r); βH(R)
		1028-1031	1024-1037			α (R)s, βH(C), β H (R)
1066	1060	1065				νCN , γNH_3^+ i.p.
1079			1081- 1085	1090	1083	αH (r), ω NH_3^+
1112		1103	1100-1109			βH(C)
		1125	1124	1137	1132	ω NH_3^+, βH(C)
1143	1140	1148-1154	1153- 1154			αH (R), ω NH_3^+, βCH
1167	1170	1169-1174	1174	1170	1168	γCH_2, αH(R);

1213			1204- 1206			υ(r), υ C-COO^-
1235	1243	1237	1236- 1241	1242	1243	αH(R), γH(r)
1264	1264	1267	1250- 1259		1251	γH(R), γH(r), βCH
	1276		1277	1284	1289	βH (CH_2)
1300		1291-1296	1296			υCN
1318	1319	1318	1316-1318			υ(R), υ(r); ωCH_2
1337		1324-1326	1326	1331	1334	νCN, βCH
1342	1345			1343		βCH, βH (CH_2)
1361		1360-1361	1360- 1365			ωCH_2, βCH
	1374	1375	1376- 1374			υ(r), υ(R)
		1380	1380		1387	γCH(R);υ(r); βCH(NH); δCH_2
	1399	1391-1398	1398	1396		$υ_s$ COO^-
		1404	1405			υ C-C
1427		1416	1416			υ COO^-;υ C-C
1457		1450-1453	1441- 1450		1457	α CH_2, δ NH_2
1461	1461	1459	1459	1463	1464	υ(r), υ(R), υs NH_3^+
1490		1489-1492	1479- 1492			βCH(R)
	1504		1506			δ CH_2; υ(R)CC, βCH;
		1513-1517	1517			υ C-C
			1541		1541	βCH (r) (NH)
1560	1557			1560		υ(r), υ(R)
1581		1587	1587		1578	υ(R)CC, βCHalk; βCH(r) (NH) i.p
	1603	1598		1595	1594	α NH_3^+
		1618	1618			υ(R)CC, βCH_{alk}; βCH (r) (NH), δ CH_2
1628	1638		1653			βCC, $υ_{as}$ COO^-; α CCO
	1659-1666	1659-1661	1667			α NH_3^+
					2136	υas CN; υC-H
					2254	υs CN; υN-H
2950			2952		2942	υas H(R)
3059			3065		3083	υs NH_3^+ ; υC-H

Symbols for vibrational modes: υ = stretching; β = bending; α = scissoring; γ = rocking; ω = wagging; δ = twisting; θ = ring; R = phenyl ring; r = indole/pyrrole ring; i.p = in plane; oop = out of plane; s = symmetric; as = antisymmetric.

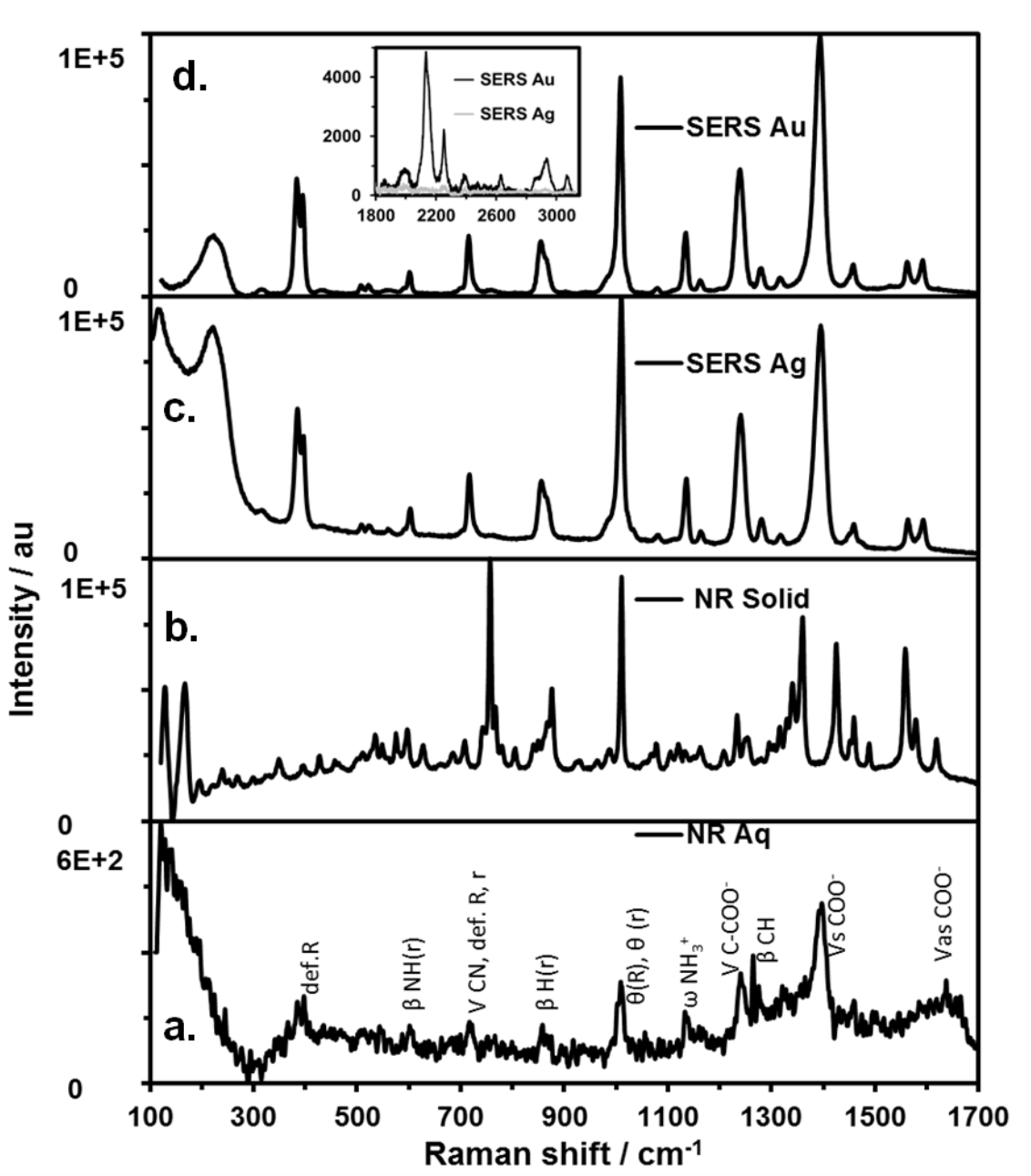

Figure 2.4. Comparison of Raman spectra of L-Trp: (a) NR spectrum aqueous; (b) NR spectrum of solid; (c) SERS spectrum on Ag NPs and (d) SERS spectrum on Au NPs.

L-Trp has a carboxylate ($–COO^-$) group, an amino ($–NH_2/–NH_3^+$) group and a side group consisting of 3-methyl indole. These are the possible active sites for binding to NPs surfaces. Group stretching modes for ($–COO^-$) were observed at 1427 and 1628 cm^{-1}. The band located at 1560 cm^{-1} corresponds to a deformation of the $–NH_3^+$ group. Group stretching modes for ($–NH_2/–NH_3^+$) were observed at 3065 and 3246 cm^{-1}, respectively, in the NR spectra for the solid and for aqueous solutions of L-Trp [13]. However, SERS spectra do not present enhancements of these signals ($–NH_2/–NH_3^+$) with Ag NPs but, were observed with Au NPs colloids. Hence, the orientation of the molecule on the silver and gold surface can be inferred from aromatic C–H stretching vibrations, ring stretching vibrations, the ring breathing mode, in-plane and out-of-plane vibrations and the SERS surface selection rules [28-29]. Also, the C–H stretching vibrations were observed in SERS on Au surface at 2942 cm^{-1}.

The C-C ring breathing mode and C-C-C trigonal bending were tentatively assigned to the bands at 748 - 757 cm^{-1} and 1001-1010 cm^{-1} of L-Trp. The modes were observed as a strong band at 1011 cm^{-1} for Ag and 1009 cm^{-1} for Au in SERS spectra, respectively. Corresponding Raman band has been observed in the same region [25, 30]. Neither a considerable red shift, nor significant band broadening related to this vibration mode was identified in the SERS spectra of L-Trp indicating that a low probability of a direct ring π-orbital to metal interaction. The spectral intensities in the NR solid L-Trp, NR aqueous L-Trp solution observed at 1318, 1326, 1337, 1342, 1360-1361, 1380, 1416-1427, 1441-1457, 1479-1492, 1557-1560, 1578-1587, 1616-1618 cm^{-1} were assigned to carbon vibrations in indole ring stretching. The degenerate frequency for in plane carbon bending vibrations was observed at 529 and 536 in

SERS Ag/Au and 574 cm^{-1}. A split into two non-symmetric components is observed at 380 and 395 cm^{-1} assigned by degenerate carbon out-to-plane bending vibrations. The C-H stretching vibrations are associated with the presence of bands at 2950-2952 and 3059-3065 cm^{-1}. The presence of the ring C-H stretching band in a SERS spectrum is indicative of a tilted orientation of the aromatic ring moiety on a metal substrate and it has also been well documented in the literature [31, 32]. In this work the aromatic ring C-H stretching band were not observed in SERS spectra on Ag, indicating that the indole ring was adsorbed flat on the Ag surface. The orientation of L-Trp on the Au NPs surface suggests that there is a certain angle between the ring plane and the Au surface for the appearances of both in-plane modes and out-of-plane modes and that not shown in the SERS spectra. The frequencies in the NR solid L-Trp, NR aqueous L-Trp solution at 1079, 1167, 1235-1243 and 1276 cm-1, are assigned to C-H in plane bending vibration. These frequencies were observed at 1090/1083, 1170/1168, 1242/1243 and 1284/1289 cm-1 in the SERS spectra of L-Trp on Ag/Au colloidal suspension respectively. The C-H out-of-plane bending vibrations in the NR solid L-Trp, NR aqueous L-Trp solution have assigned at 845, 933-929 and 974 cm^{-1}. The weak bands at 1463 and 1457 cm^{-1} in SERS spectra for Ag and Au respectively, correspond to the CH_2 scissoring mode. In L-Trp the wagging vibrations of CH_2 are found at 1318 cm^{-1} which is justified by the DFT calculation, but not does appear in the SERS spectra.

The carbonyl asymmetric stretching appears as a very weak band at 1618 cm^{-1} in the SERS spectrum for Ag and Au colloids calculated. The weakening of this carbonyl stretching vibration indicates that the C=O is not in direct interaction with the Ag/Au

NPs surfaces. It is also revealing to observe the υ_s ($-COO^-$) bands at 1396 cm^{-1} for Ag. This indicates that the Ag–COO^- and Au–COO^- bonds formed by the adsorption of L-Trp on Ag and Au are not ionic. The bonds would then have a covalent character. This (COO^-) group binds to the metal surface via either the oxygen lone pair electrons or the carboxylate π system [33]. The geometry of the (COO^-) on the surface, which is stated by steric hindrance between the carboxylate ion and other adjacent substituents, determines the nature of binding of these molecules on the surface.

N-H out-of-plane bending deformation is assigned to 604/607 cm^{-1} in the SERS by Ag/Au. Another important vibrational mode of L-Trp is located at 1137 cm^{-1} for Ag and 1132 cm^{-1} for Au corresponding to wagging of NH_3^+ and indicating that the amino acids have the NH_2 form twisted when lying on the Ag/Au surface as determined by a pH-dependent measurement. The NH_2 form, rather than NH_3^+, is regarded as a preferential structure when amino acids attach on the Ag surface in the SERS measurements, according to SERS studies carried out previously [34,35]. This blue shift in its frequency of approximately ± 15 cm^{-1} has been previously reported for other amino acids [13]. The band at 1066 and 1060 cm^{-1} observed in the NR solid L-Trp and NR aqueous L-Trp solution that correspond to the υ (CN) vibration was not observed in SERS spectra on Ag/Au NPs. It is probably overlapped with band at 1011 cm^{-1} for Ag and 1009 cm^{-1} for Au, having suffered a larger red shift on the Au NPs surface, because the SERS frequencies of these modes are usually very close to those observed in Raman of solid amino acids. The NH_2 scissoring modes showed up between 1590 and 1670 cm^{-1} in primary aromatic amines. The bands at 1598-1603

cm^{-1} and 1666-1661 cm^{-1} were assigned to NH_2 scissoring mode in NR solid L-Trp and NR aqueous L-Trp solution.

2.3.4. Theoretical discussion

Raman shift calculations of optimized neutral or zwitterion ($^{+}H_3NRCOO^{-}$), cationic ($^{+}H_3NRCOOH$) and anionic (NH_2RCOO^{-}) forms of L-Trp structure were compared with the experimental NR spectra of solid L-Trp and with NR spectra of aqueous solutions of L-Trp. The geometries of these optimizations are shown in Fig. 2.2. For these structures the comparison with experimental vs. calculated Raman spectra is shown in Figure 2.5.

It is possible to observe similarities between NR solid L-Trp spectrum and the calculated for neutral form of this molecule, but there are differences because the calculations were done without anharmonic corrections in order to save computational costs. The optimization of L-Trp with the Ag/Au NPs surfaces was completed with convergence criterion accepted for the neutral form, but the calculation with pseudopotential produced a deformation of L-Trp structure. For the optimization with the LANL2DZ basis set for all the atoms, it was possible to see an orientation of carboxylate group of L-Trp structure. This was oriented in the same form for the calculation with pseudopotential (Fig. 2.2).

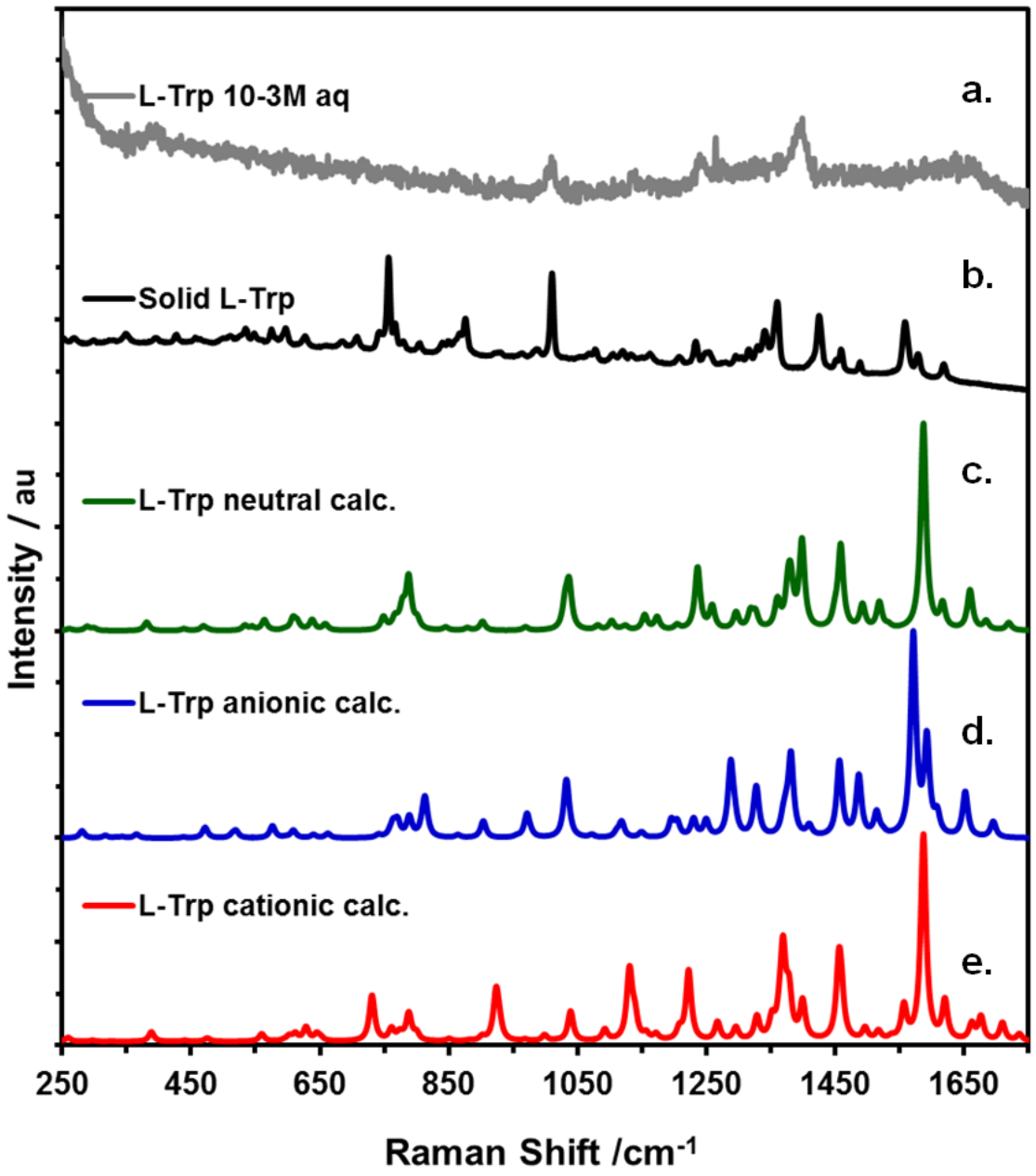

Figure 2.5. Comparison of Raman spectra of L-Trp experimental: (a) NR spectrum of Trp aqueous solution; (b) NR spectrum of solid; (c) calculated Raman spectrum zwitterion; (d) calculated Raman spectrum of anionic form; (e) calculated Raman spectrum of cationic form.

Generally, chemisorption can take place on Ag/Au NPs surface through the formation of a bond between the Ag/Au surface and the adsorbed molecule, e.g. Ag–N, Ag–O, Ag–S, or Ag–X (X = halogen) [36–38]. In order to analyze the influence of chemical enhancement on the SERS spectra, one needs to consider two possible interactions between the adsorbate and the metal surface. Physical adsorption, which is the result of relatively weak interactions between the solid surface and the adsorbate, occurs with an enthalpy of adsorption higher than −25 kJ mol^{-1}. Chemical adsorption, where the adsorbed molecules are strongly bound to the surface is accompanied with an enthalpy of adsorption lower than −40 kJ mol^{-1} [28, 39]. In the process of chemisorption, the adsorbed molecule changes its chemical structure and symmetry because of bond formation with the surface. This mechanism usually introduces wavenumber shifts [40] between vibrations of adsorbed molecules in comparison to the NR spectra of these molecules as shown in SERS Au/L-Trp spectra in Figure 2.4.

The energy gaps between the highest occupied molecular orbital (HOMO) and the lowest unoccupied molecular orbital (LUMO) for L-Trp on Ag/Au NPs surfaces were calculated at the B3LYP/6- 311G level of theory. These are represented in Fig. 2.6. The energy gap reflects the chemical activity of the molecule. The LUMO, as an electron acceptor, represents the ability to accept an electron. The HOMO represents the ability to donate an electron. The lower the HOMO-LUMO energy gap explains the eventual charge transfer (CT) interactions taking place within the molecule. In Figure 2.6 it can be observed that the Fermi level of the Ag and Au NPs surfaces are located at -446.7 kJ mol^{-1} and -509.9 kJ mol^{-1}. [Figures 2.6 (a) and (b), respectively].

a.

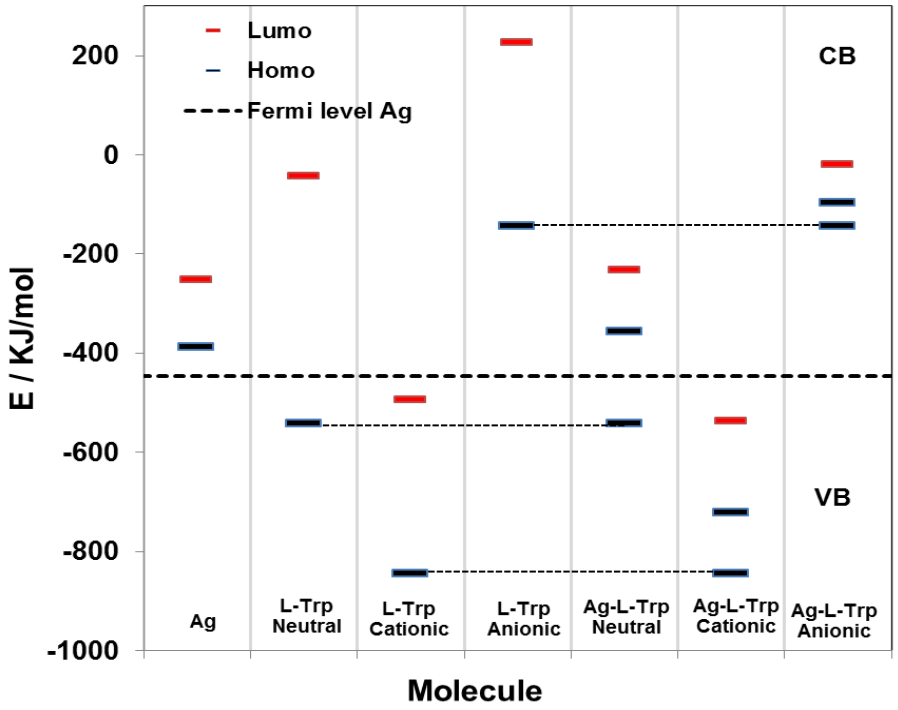

b.

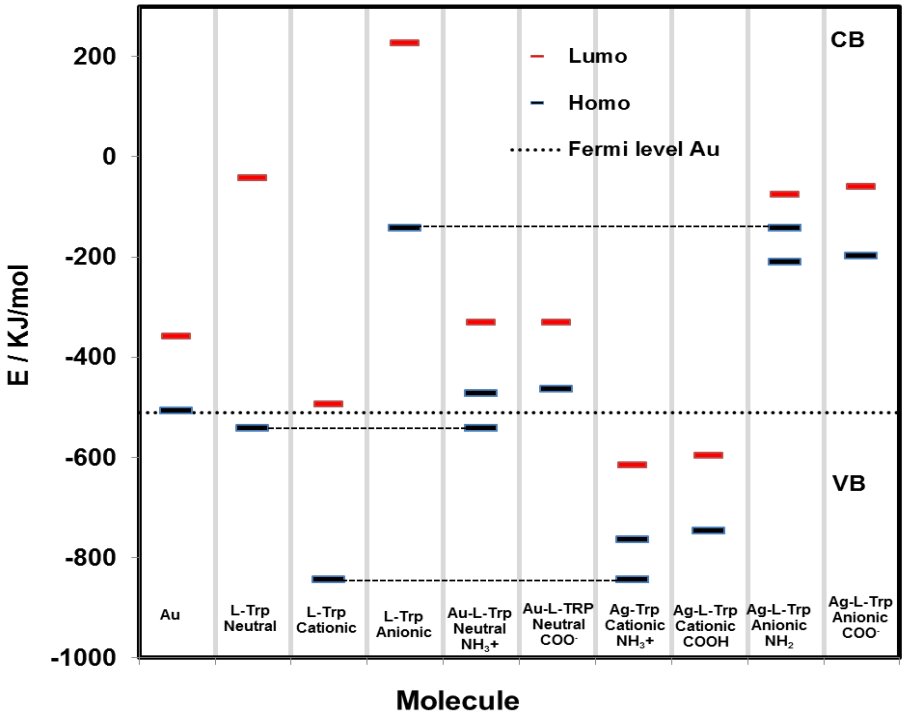

Figure 2.6. Diagram of the HOMO-LUMO energy gap of L-Trp in its three forms calculated at the B3LYP/6- 311G level on: (a) 10 atom Ag(1,0,0) surface; (b) 10 atom Au(1,0,0) surface.

The two main binding sites of the carboxylate group and the amino group were considered for the present calculation. In L-Trp, the highest occupied molecular orbital (HOMO) is located at −141.8 kJ mol^{-1}, thus precluding a CT from L-Trp to the conduction band of the Ag/Au surface. It is important to note that the energies of the first empty MOs (LUMO) of L-Trp acid (cationic form) are within the energy range of the valence band of the Ag surface, but close to level Fermi of the Au surface. This fact explains the CT from the Ag/Au surface to L-Trp and the LUMO (225.8 kJ mol^{-1}) is localized on the COO^- moiety, explaining the fact that part of this moiety is directly facing the Ag surface [13]. The adsorption energies of L-Trp on Ag and Au via the cationic form of the amino group were estimated as 107.7 kJ mol^{-1} and -12.4 kJ mol^{-1} respectively, and the adsorption energies of L-Trp on Ag and Au through the carboxylate group anionic form were estimated as -611.7 and -731.8 kJ mol^{-1}, respectively, on Ag and Au. These results are in good agreement with the interpretation that L-Trp adsorbs via the carboxylate group and the amino group (NH_2) form on Ag and for Au surface adsorbs via amino group in its protonated NH_3^+ form and the ionized carboxyl group (–COO^-). It is also informative that the difference in adsorption energy between the carboxylate and the amino group is quite a less for Au than for Ag. This may explain why the carboxylate group was weakly observed on Au but more strongly observed on Ag.

2.3.5. Effect of pH on vibrational bands of L-Trp on Ag/Au colloids

The pH can affect the way a molecule orients itself on the NPs surface of a colloidal metallic suspension. In particular, it affects the state of protonation and hence the

number and nature of binding sites of molecules on colloidal NPs [41]. Numerous reports are available in the literature focusing on interactions of L-Trp with Ag colloids [14,42], and a methodical study on the effect of gradual changes in net atomic charge distributions at different terminals of L-Trp on Ag metal interaction was also reported recently [40]. However, in this work the most probable conformation of L-Trp on Ag/Au colloidal solution was assessed varying the pH of Ag and Au NPs in the range from 2.0 to 11.0. It was important to determine if differences on the spectral profiles of the biomolecule studied evidenced the suggested orientations of L-Trp on the NPs surfaces. The Ag/Au NPs colloidal suspension then was prepared and pelleted. Zeta potentials were measured for each sample to identify the main forces that mediate interparticle interactions and to understand dispersion and aggregation processes with regards to stability of metal colloids. The measurements of “as-prepared” colloids to generate average values of −37.4 mV at pH 7.35 for Ag NPs and −34.9 mV at pH 4.10 for Au NPs confirm the moderate stability of Ag/Au nanoparticles. The larger the zeta potential, the more likely the suspension is to be stable because charged particles repel each other and thus overcome the natural tendency to aggregate. As expected, when acid solution was added to the NPs suspensions the surface charge turned to more positive values resulting in a decrease in the magnitude of the zeta potential (less negative). High zeta potential values were obtained at pH 2 and 11, therefore correlating with the decrease of SERS signal enhancement as result of aggregation and flocculation of the Ag/Au colloids.

Contrary to information contained in most SERS reports on Ag NPs a 532 nm laser excitation line did not produce highly enhanced SERS spectra or the typical highly

resolved traces when exciting the SERS spectra of L-Trp. This situation is illustrated in Figure 2.7(a). These results also demonstrate that for different diameters of spherical Ag and Au NPs, higher SERS intensities were obtained for average NPs sizes of 40-60 nm. This is shown for Au NPs in Figure 2.7(b).

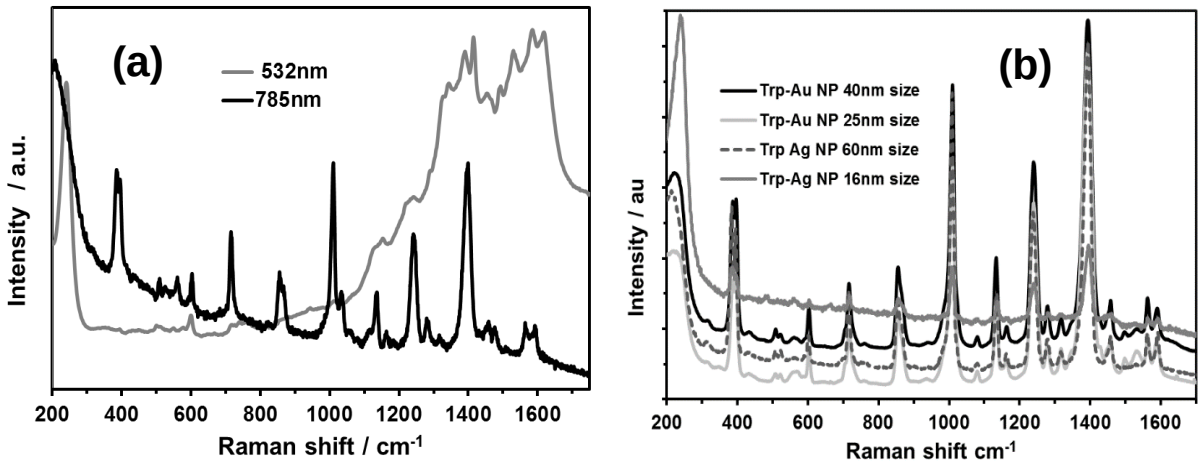

Figure 2.7. Comparison SERS spectra of L-Trp: (a) on Ag NPs at 532 nm and 785 nm; (b) on Ag/Au NPs colloidal suspensions at different average particle sizes.

Ag/Au NPs were mixed with L-Trp at different concentrations. pH of the samples were measured prior to acquiring their Raman spectra. To ensure adsorption equilibrium and pH stabilization, spectral measurements were done 20 min after preparing the mixtures. A detailed analysis on the relative variation in intensities of different vibrational bands is shown in Figures 2.8 and 2.9 for Ag and Au, respectively. Peak areas of spectra obtained at different pH, were calculated using OPUS™ software (V. 3.0; Bruker Optics, Billerica, MA). The integration was performed in the regions that showed most intense bands in the SERS spectra assigned to the bond vibration of the biomolecule. DFT calculations reveal interesting increasing of the metal–molecule interaction with the change in pH of Ag/L-Trp and Au/L-Trp.

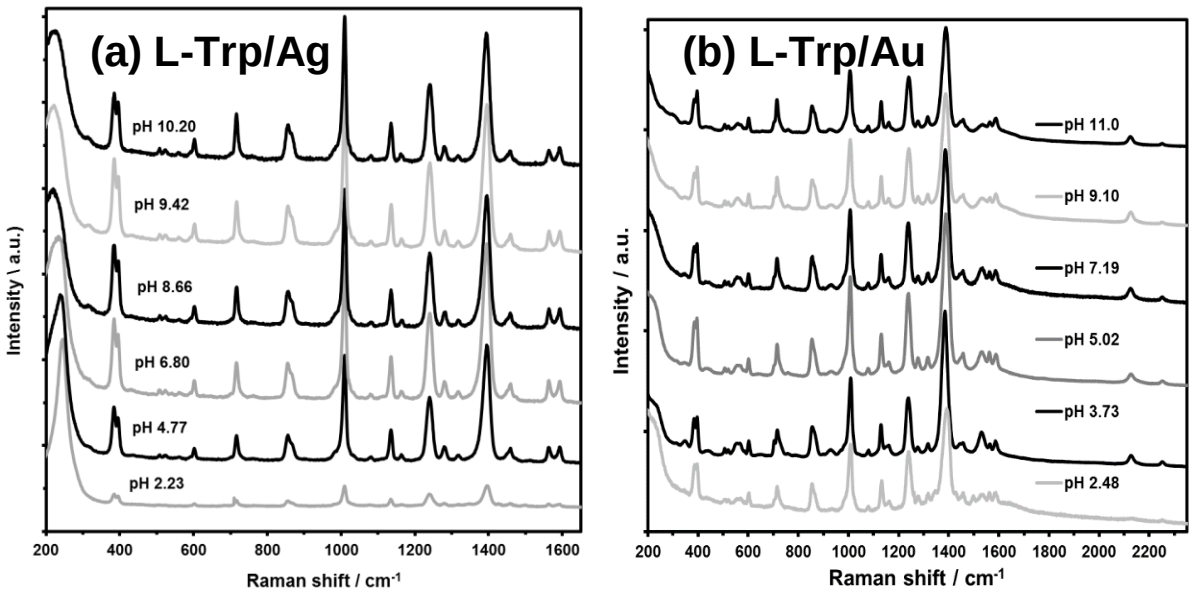

Figure 2.8. (a) SERS spectra of L-Trp at different pH at 785 nm with: (a) Ag NPs; (b) Au NPs.

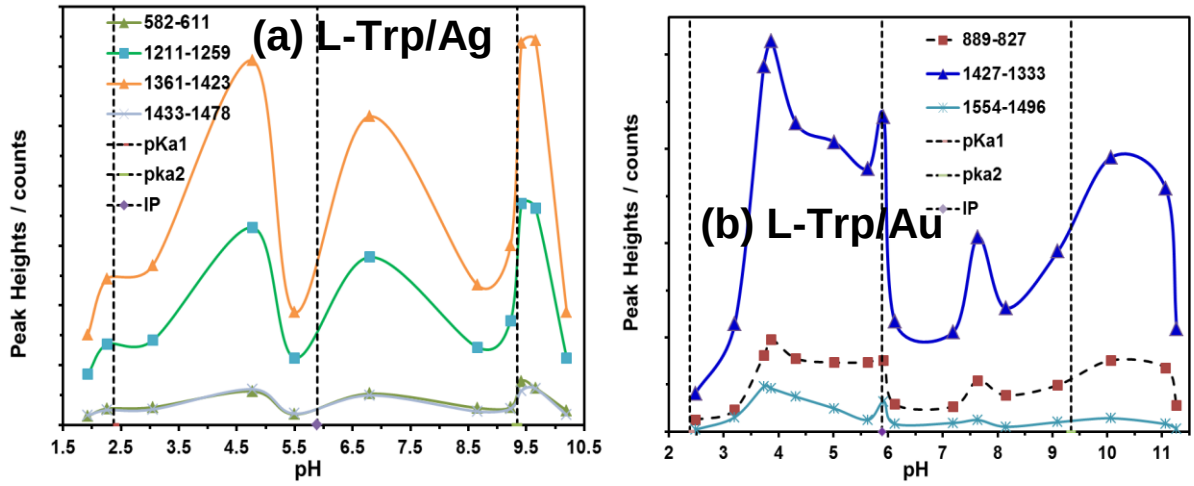

Figure 2.9. (a) Dependence of SERS signal of L-Trp with: Ag NPs; (b) Au NPs.

According to the figures shown, there is a close dependence between SERS peak areas and the pH for L-Trp species under study. At pH values below pK_a and above pK_b the spectral profile decayed markedly compared to neutral or basic pH values for Ag surface and neutral or acid pH values for Au surfaces, where is evidently observed a high intensity enhancement of the vibrational modes, until reaching a maximum

intensity at pH ~ 9.42 and pH ~ 3.73. Therefore, parameters such as analyte concentration, nanoparticle size and colloidal pH values have a significant effect in establishing the most stable conformation and orientation of L-Trp on Ag/Au NPs surfaces. According to results, L-Trp molecules interact with the Ag surface through the carboxylate group nearest at its pK_b = 9.40, at ~10^{-12} M concentration, with approximate 60 nm particle size, and with Au surface L-Trp molecules interacts through the amino group on neutral form close to its pK_a at pH 3.73, at a concentration of ~10^{-8} M and ~ 40 nm particle size. Good results were also observed at values near its isoelectric point (IP).

Enhancement factor is one of the most important information in SERS characterization as well as SERS effect comparing experimental results to theoretical calculations. The concept of SERS enhancement factor results from the increase in signal resulting from the increase of cross section of the molecules, in this case L-Trp. Enhancement factors of 10^7-10^8 can be sufficient for single molecule detection where the maximum magnitude ranges among 10^{10}-10^{14} under optimized conditions. When intensities are normalized for laser power and acquisition time the ratio of the two intensities is given by equation (*2.1*).

$$EF = \left(\frac{I_{SERS}}{I_{NR}}\right)\left(\frac{N_{NR}}{N_{SERS}}\right) \qquad \textbf{2.1}$$

To calculate the enhancement factor for SERS on Ag/Au NPs, three bands were used: 1399, 1243 and 1011 cm^{-1} in the normal Raman and for SERS spectra were 1396, 1242 and 1011cm^{-1} for Ag and 1243, 1009cm^{-1} for Au, because, these are the strongest bands on both normal Raman and SERS spectra. The corresponding peak height for 4.9 x 10^{-12} M and 4.9 x 10^{-8} M L-Trp in Ag/Au colloids solution gives the

values of the enhancement factor as $1.70x10^{10}$, $1.20x10^{10}$ and $2.40x10^{10}$ for the frequencies 1396, 1242 and 1011 cm^{-1} respectively, which is six orders of magnitude higher than previously reported for Ag.

2.4. Conclusions

We have demonstrated that Ag and Au NPs colloids of particle size average of ~ 40 to 60 nm constitute good sensing platforms for developing SERS methodologies to establish the most stable conformation and orientation of amino acids, such as L-Trp. Low limits of detection were found for this biomolecule, at ~10^{-13} M for Ag and ~10^{-8} M for Au. The intensities of the Raman signals were significantly modified by the pH of the colloidal suspensions, which induces changes in the electrostatic charge on the NPs surfaces. The binding between L-Trp molecules and the colloids should depend on the preparation and surface conditions of the NPs and the combination of electrolytes used to promote attachment of the molecules to the surface. Relative intensities of the vibrational bands in the SERS spectrum of L-Trp depend on several factors such as the excitation laser line, the nature of the metal substrate, the pH of the medium, the ionic strength, the concentration of the solution, aggregation of the colloid, and the eventual chemical interaction between the amino acid and the metal substrate. The observation of the vibrations ν_s (COO^-) and ν_s (NH_2) in SERS on Ag surface, the detection of the ν_s (NH_3^+) at ~3030 – 3130 cm^{-1} on Au surface and the non-detection of υ(C=O) modes confirm that L-Trp was adsorbed in its anionic form on Ag NPs substrates. The L-Trp molecule interacts with the Ag NPs through the $–COO^-$ and $–NH_2$ groups, while the indole ring fragment is close to the surface and interacts with Au

surface via NH_3^+ when in neutral form, depending on the pH of the colloidal suspensions. The pyrrole moiety is farther from the surface than the benzene ring. So the L-Trp molecules are probably tilted on the Ag/Au NPs surface through ionized carboxyl, and there is a certain angle between the indole rings and the Au NPs surfaces. Experiments demonstrate that the SERS spectra vary depending on the different formulas of Ag colloids [41]. The theoretical data complement the experimental results quite well.

2.5. References

[1]. J.M Berg, J.L Tymoczko, L Stryer. Biochemistry. 5th edition. New York: W H Freeman; (2002). Section 3.1, Proteins Are Built from a Repertoire of 20 Amino Acids. Available from: http://www.ncbi.nlm.nih.gov/books/NBK22379/. (accessed on 27 December 2012)

[2]. P. Joshi, V. Shewale, R Pandey, V. Shanker, S. Hussain, & S.P. Karna. J. Phys. Chem. C (2011), 115 (46), 22818–22826.

[3]. M. Dehghan-Shasaltaneh, J. Fouladi, S.Z Mousavinezhad. J. of Paramedical Sciences (JPS), (2010), 1 (2) 19-25.

[4]. N. Le Floc'h, W. Otten, E. Merlot. Amino Acids. (2011), 41(5):1195-205.

[5]. K.T. Chung, G.S. Gadupudi. Environ. Mol. Mutagen., (2011), 52 (2): 81–104.

[6]. M.M. Oliveira, D. Ugarte, D. Zanchet, A.J.G. Zarbin, J. Colloid Interf Sci., (2005) 292 429- 435

[7]. R.A. Alvarez-Puebla, E. Arceo, P.J.G. Goulet, J.J. Garrido, R.F. Aroca. J. Phys. Chem. B. (2005) 109 3787-3792.

[8]. C.J. Murphy, A.M. Gole, J.W. Stone, P.N. Sisco, A. M. Alkilany, E.C. Goldsmith and S.C. Baxter. Acc. Chem. Res., (2008), 41 (12), 1721–1730.

[9]. Y. Fleger, Y. Mastai, M. Rosenbluha, and D.H. Dressler. J. Raman Spectrosc., (2009), 40, 1572–1577.

[10]. M. Ahern, R. L. Garrell, J. Am. Chem. Soc. (1991), 113, 846.

[11]. H.I. Lee, S.W. Suh, M.S. Kim, J. Raman Spectrosc. (1988) 19, 491- 495.

[12]. A.E. Aliaga, I. Osorio-Roman, P. Leyton, C. Garrido, J. Carcamo, C. Caniulef, F. Celis, G. Díaz, E. Clavijo, J.S. Gomez-Jeria and M.M. Campos-Vallettea. J. Raman Spectrosc. (2009), 40, 164–169.

[13]. S.K. Kim, M.S. Kim, S. W. Suh, J. Raman Spectrosc. (1987), 18, 171.

[14]. C.H. Chuang and Y.T. Chen, J. Raman Spectrosc. (2009) 40, 150-156.
[15]. M. Kazanci, J.P. Schulte, C. Douglas, P. Fratzl, D. Pink, T. Smith-Palmer, Appl. Spec., (2008) 63 214-223.
[16]. P.C. Lee and D. Meisel. J. Phys. Chem. (1982). 88, 3391.
[17]. A.M. Chamoun-Emanuelli, O.A. Primera-Pedrozo, M.I. Barreto-Caban, J. Jerez-Rozo, S. P. Hernandez-Rivera. Nanoscience and Nanotechnology for Chemical and Biological Defense, American Chemical Society. (2009), 217-232.
[18]. O.M. Primera-Pedrozo, G.D.M. Rodríguez, J. Castellanos, H. Felix-Rivera, O. Resto, S.P. Hernández-Rivera. Spectrochimica Acta Part A: Molecular and Biomolecular Spectroscopy (2012) 87, 77-85.
[19]. M.J. Frisch, G.W. Trucks, H.B. Schlegel, G.E. Scuseria, M.A. Robb, J.R. Cheeseman, J.A. Montgomery, Jr., T. Vreven, K.N. Kudin, J.C. Burant, J.M. Millam, S.S. Iyengar, J. Tomasi, V. Barone, B. Mennucci, M. Cossi, G. Scalmani, N. Rega, G.A. Petersson, H. Nakatsuji, M. Hada, M. Ehara, K. Toyota, R. Fukuda, J. Hasegawa, M. Ishida, T. Nakajima, Y. Honda, O. Kitao, H. Nakai, M. Klene, X. Li, J. E. Knox, H.P. Hratchian, J.B. Cross, V. Bakken, C. Adamo, J. Jaramillo, R. Gomperts, R.E. Stratmann, O. Yazyev, A.J. Austin, R. Cammi, C. Pomelli, J.W. Ochterski, P.Y. Ayala, K. Morokuma, G.A. Voth, P. Salvador, J.J. Dannenberg, V.G. Zakrzewski, S. Dapprich, A.D. Daniels, M.C. Strain, O. Farkas, D.K. Malick, A.D. Rabuck, K. Raghavachari, J.B. Foresman, J.V. Ortiz, Q. Cui, A.G. Baboul, S. Clifford, J. Cioslowski, B.B. Stefanov, G. Liu, A. Liashenko, P. Piskorz, I. Komaromi, R. L. Martin, D. J. Fox, T. Keith, M.A. Al-Laham, C.Y. Peng, A. Nanayakkara, M. Challacombe, P.M.W. Gill, B. Johnson, W. Chen, M.W. Wong, C. Gonzalez, and J.A. Pople, Gaussian, Inc., Wallingford CT, (2004). Gaussian 03, Revision C.02.
[20]. H. Felix-Rivera, R. Gonzalez, G.D.M. Rodrıguez, O.M. Primera-Pedrozo, C. Rıos-Velazquez, and S.P. Hernandez-Rivera. Int. J. Spectrosc. (2011), 1-9.
[21]. I. Lisiecki, F. Billoudet, M.P. Pileni, J. Phys. Chem. 100 (1996) 4160–4166.
[22]. K.L. Kelly, E. Coronado, L.L. Zhao, G.C. Schatz, J. Phys. Chem. B (2003) 107, 668–677.
[23]. J.S. Suh, M. Moskovits, J. Am. Chem. Soc. (1986), 108, 4711.
[24]. X. Cao, G. Fisher, J. Phys. Chem. B (1999), 103, 9995- 10003.
[25]. G. Socrates, Infrared and Raman Characteristic Group Frequencies, Tables and Charts (3rd edn), John Wiley & Sons: Chichester, (2001).
[26]. D.L. Nelson, M.M. Cox, Principles of Biochemistry (4th edn), W.H. Freeman and Company, New York, (2005), 78.
[27]. L. Jiang, Q. Xu. J. Phys. Chem. A, (2005), 109, 6, 1026.
[28]. D.M. Ruthven, Principles of Adsorption and Adsorption Processes, John Wiley: New York, (1984).

[29]. Markovits, M. Garcia-Hernandez, J.M. Ricart and F. Illas. J. Phys. Chem. B (1999) 103, 509.
[30]. S, Mohan, N. Puviarasan and S. Bakkialakshmi. Asian J. of Chem. (1999) 4, 1137-1143.
[31]. J.S. Suh and J. Kim. J. Raman Spectrosc. (1998) 29, 143.
[32]. S.J. Bae, C. Lee, I.S. Choi, C.S. Hwang, M..S.Gong, K. Kim, S.W. Joo, J. Phys. Chem. B (2002) 106, 7076.
[33]. S.W. Joo, T.D. Chung,W. Jang, M.S. Gong, N. Geum, K. Kim, Langmuir (2002) 18, 8813.
[34]. Y.J. Kwon, D.H. Son, S.J. Ahn, M.S. Kim, K. Kim, J. Phys. Chem. (1994), 98, 8481.
[35]. E.T. Nibbering and T. Elsaesser. Chem. Rev (2004), 104, 10.
[36]. T.M. Herne, A.M. Ahern, R.L. Garrell, J. Am. Chem. Soc. (1991), 113, 846.
[37]. C.S. Allen, R.P. Van Duyne, J. Am. Chem. Soc. (1981), 103, 7497.
[38]. D. Roy, T. E. Furtak, J. Chem. Phys. (1984), 81, 4168.
[39]. R. Aroca, Surface Enhanced Vibrational Spectroscopy, JohnWiley and Sons, UK, (2006).
[40]. A.W. Adamson, Physical Chemistry of surfaces, JohnWiley and Sons: New York, 1990.
[41]. S. Bhattacharya, N. Vyas, A.K. Ojha, S. Dasguptac and A. Roya. J. Raman Spectrosc. (2012), 43, 718–723.
[42]. A. Kandakkarthara, I. Utkin, R. Fedosejevs, Appl Spectrosc. (2011), 65: 5, 507-513.

Chapter 3

SURFACE ENHANCED RAMAN SPECTROSCOPY STUDIES: GOLD AND SILVER NANOPARTICLES PREPARED BY LASER ABLATION

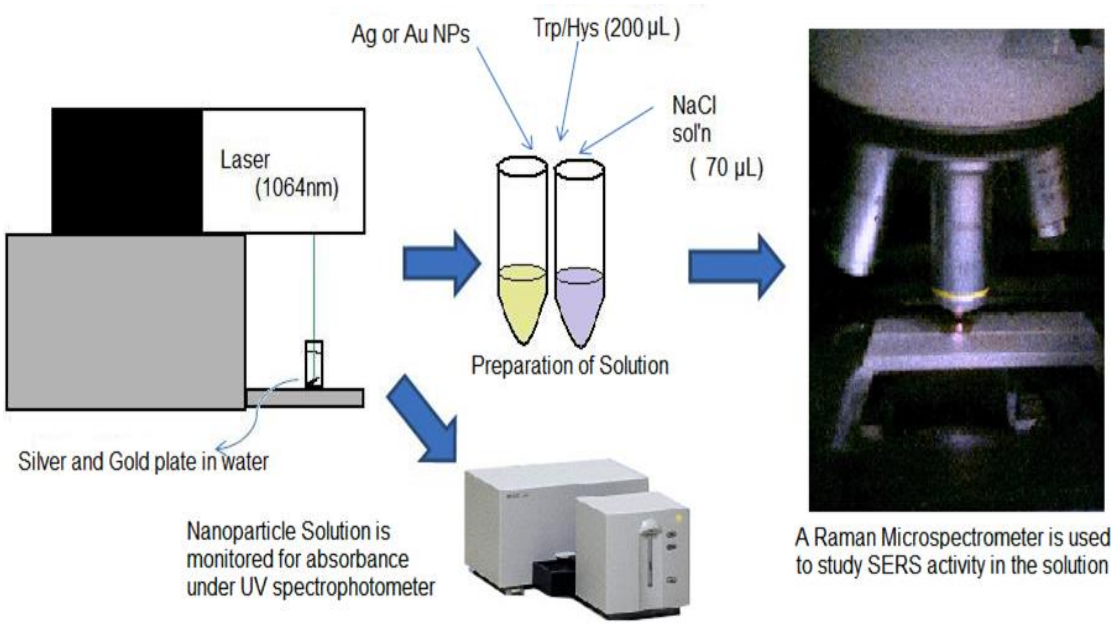

Laser ablation of metallic nanoparticles for SERS applications.

3.1. Introduction

Nanotechnology includes very important applications in several areas, such as medicine [1–5], catalysis [6–14], industrial applications [15–17] and scientific investigations. The size, shape and physicochemical properties are very important in future applications and are the main theme in studies currently conducted. There are several ways to synthesize metal (NPs). Their synthesis can be classified as either

chemical or physical methods. Some chemical methods include the chemical reduction of metal salts, the alcohol reduction process, microemulsions, thermal decomposition of metal salts and electrochemical synthesis [18, 19]. Physical methods include pulsed laser ablation, the exploding wire technique, plasma, chemical vapor deposition, microwave irradiation, supercritical fluids, sono-chemical reduction and gamma radiation [20]. Laser ablation is a very clean physical method for the preparation of metallic nanoparticles (NPs). During the last year, metal laser ablation has increased in popularity, due to the fast and simple nature of the procedure. In addition, the important advantage of this method when compared to chemical synthesis ("wet chemistry synthesis") is the preparation of high surface purity NPs in the chosen solvent. There are no counter ions and no residuals of the reducing agents remaining on the surfaces of the NPs [21–23]. To take advantage of these features, we have prepared gold (Au) and silver (Ag) NPs by laser ablation. Colloidal suspensions of prepared NPs were deposited on gold-coated slides to immobilize them and to test them for potential use as substrates for the detection of explosives using surface enhanced Raman scattering (SERS).

The use of spectroscopic techniques with intensities augmented by nanostructured metal surfaces has attracted great interest in recent years. The SERS effect discovered in the seventies is largely attributed to the interaction of light with matter. Specifically, SERS is related to the inelastic scattering (or Raman scattering) of certain molecules in the presence of specially prepared roughened or discontinuous metallic nanostructures. There are two mechanisms that explain the increase in the Raman signal. The first is explained through an electromagnetic interaction model (EM) and

the second through a chemical interaction model or charge transfer (CT) [24, 25]. Both mechanisms are thought to contribute to the signal intensity enhancement observed, although the extent of the contribution of each source of enhancement depends on the system under study. The enhancement mechanisms of the Raman signal lead to a technique with a sensitivity and selectivity that make Raman scattering a highly promising technique for further developing analytical applications [26–31]. These applications are closely related to the properties and the surface morphology of the metallic NP used. A large part of the contribution to the SERS effect is due to the increase in the inelastically scattered Raman signal intensity by the nanostructured metal systems present and the particular properties of the particles to induce greater morphological coupling with the incident radiation, resulting in intense spectroscopic signals. The molecule-surface relative orientation allows the emergence of new selection rules, resulting in the intensification of the Raman spectrum bands corresponding to the molecular vibrations of the molecular polarizability components perpendicular to the surface. The Au and Ag NPs prepared by laser ablation were deposited on various substrates and subsequently were used to evaluate their capacity as substrates with the objective of detecting amino acids such as L- histidine (L- His) for developing more analytical applications based on SERS measurements. 4-Aminobenzebethiol (4-ABT) was chosen as the surface enhanced Raman scattering (SERS) probe molecule based on affinity of the compound with Ag NPs, to determine the optimum irradiation time and the pH of aqueous synthesis of the laser ablation-based synthesis of metallic NPs.

3.2. Experimental section

3.2.1. Laser ablation NPs synthesis

Au or Ag metal foils (99.99%, Sigma-Aldrich, Milwaukee, WI, USA) were placed in a vial containing 10 mL of deionized water as ablation and heat tempering media. Laser pulses at 1064 nm, obtained using a Quanta-Ray Pro Series pulsed Nd:YAG laser from Spectra-Physics/Newport Corporation (Mountain View, CA, USA), were used to ablate the metallic foils. The laser was operated in single-shot mode (5 ns, 10 Hz). The target was irradiated using a focusing lens with a focal length of 86.4 cm. The laser power used was 0.980 mW, and the energy was 106 mJ. The ablation process was carried out for time intervals of 5, 10, 15 and 20 min of near IR laser pulse irradiation.

3.2.2. Characterization of NPs suspensions

A UV-Vis spectrophotometer (Agilent model 8453) was used to acquire the electronic absorption spectra of the NPs in water. The spectra were recorded in the range of 300 to 900 nm. Quartz cells with a 1.0 cm path length (72-Q-10, obtained from Starna Cells, Inc., Atascadero, CA, USA) were used for the experiments. The NPs morphology and size were obtained from high-resolution transmission electron microscopy (HR-TEM) images (Zeiss, model 922 operated at 200 kV). The samples for TEM analysis were prepared by depositing 5 µL of the metallic NP suspensions on ultrathin carbon film/holey carbon 400 mesh copper grids (01824 from Ted Pella, Inc., Redding, CA, USA). Zeta potential and hydrodynamic radius (HR) measurements

were obtained using a Zetasizer™ Nano Series (Malvern Instruments Ltd., Worcestershire, UK).

3.2.3. Effect of pH on the synthesis of NPs

Solutions of 1.0 mM 4-ABT were used as analytes to evaluate the pH effect on the synthesis by laser ablation of colloidal suspensions of Au and Ag NPs. The preparation method used was as described in section 3.2.1. Studies were performed only at the optimum irradiation time. Diluted solutions of NaOH and HCl were used to adjust the pH in the aqueous media used as the solvent in the synthesis of nanoparticles. After the synthesis at various pH values was studied, the UV-Vis spectra of the suspensions were obtained. The pH values of the aqueous colloidal suspensions used for synthesis were 2.6, 4.8, 8.1 and 10.3.

3.2.4. Evaluation of SERS activity

SERS spectra were excited with a 514.5 nm INNOVA 308 Argon ion laser or a 532 nm VERDI 6.0 solid-state diode laser (both from Coherent, Inc., Santa Clara, CA, USA) and a 785 nm solid-state laser (InProcess Inc., Salt Lake City, UT, USA). 4-Aminobenzebethiol (4-ABT, Sigma-Aldrich) and 1, 2-bis (4-pyridyl) ethylene (BPE, Sigma-Aldrich) were used as SERS probe analytes. Renishaw Raman Microspectrometers RM1000 and RM2000 systems were used to acquire normal Raman (NR) and SERS spectra. The laser power at the samples was typically in the range of 10–40 mW. The data acquisition time was 20 s with 2 accumulations. The spectra are presented without pre-treatments or baseline corrections.

Au and Ag NPs at different pH values were used to evaluate the effect of the pH of the colloidal suspensions on the SERS activity obtained. Thus, 1.0 mM 4-ABT solutions and L-His solutions were used to evaluate the SERS activity at different pH values. Aliquots of 5.0 µL of L- His solutions at 1.6 mM were deposited on Au NP/Au substrates. To determine the surface enhancement factor (SEF), a solution of 4-ABT at 1.0×10^{-9} M was deposited on Au NP/Au substrates (approximately 5–10 µL of Au NPs deposited on Au substrates).

3.2.5. Detection of L-His using Au NP/Au substrates

The low limit of detection (LOD) of L-His using Au NPs deposited on Au-coated glass slides and used as substrates for the NPs was calculated based on the SERS data. For the spectral measurements, aqueous solutions of histidine at concentration 1.6×10^{-2} M (bulk) and 1.6×10^{-4} M were used. Aliquots of 30 µL of Au NPs were deposited on Au-coated substrates, and Raman spectra were measured. Then, 5 µL of L-His solutions were deposited on Au NP films. The NPs used were prepared in water and place in the desiccator to permit the evaporation of the solvent and the quicker use of the substrate.

3.3. Results and discussion

This contribution focuses on developing fast and simple methods for the preparation of SERS-active substrates with high sensitivity. For this purpose, NPs were synthesized using laser ablation methods. Au and Ag NP suspensions were synthesized at different irradiation times (5, 10, 15 and 20 min). UV-Vis absorption measurements

were obtained to characterize the NPs obtained [Figures 3.1 (a.) and 3.1 (b.)]. The typical positions of the surface plasmon maximum absorption wavelength for Au NPs and Ag NPs were approximately 525 nm (Figure 3.1a) and 400 nm (Figure 3.1b), respectively. These absorption maxima correspond to spherical (or nearly spherical) NPs with a characteristic average diameter between 2 and 100 nm [32]. These results were corroborated with TEM images and the corresponding statistical and morphological analyses.

Colloidal suspensions of Au NPs of different sizes were obtained and with predominant the spherical shape. Purple colloids are typical of large Au NPs of approximately 126 ± 36 nm. Red colloid suspensions have average sizes of 11 ± 4 nm. Typical colloidal suspensions of Ag NPs have green-gray color, with spheroidal morphology, are large of approximately 132 ± 5 nm. Other Ag NPs are spherical seeds of 5 ± 1 nm and yellow color.

The effect of the irradiation time on the enhancements obtained in the SERS experiments using the metallic NPs prepared was evaluated using 4-ABT for Ag NPs. Similarly, 1,2-bis(4-pyridyl)ethylene (BPE) was used to evaluate the optimum conditions for the synthesis of Au NPs. These analytes were selected based on the affinity of the compounds with the corresponding NPs. Figures 3.2 and 3.3; display the SERS spectrum results of Au NPs at different irradiation times. The best enhancement in the Raman signals for 4-ABT was observed at 20 min of irradiation time for Ag and Au NPs. The optimized parameter (20 min of irradiation) was used during all subsequent syntheses in this work. Aliquots of 5 µL of NP suspensions at different times of analysis were deposited on Au slides of approximately 1.0 cm^2. The drops of

NP suspensions were allowed to dry in a desiccator overnight, and then, the analyte was deposited on the substrate and again placed in a desiccator.

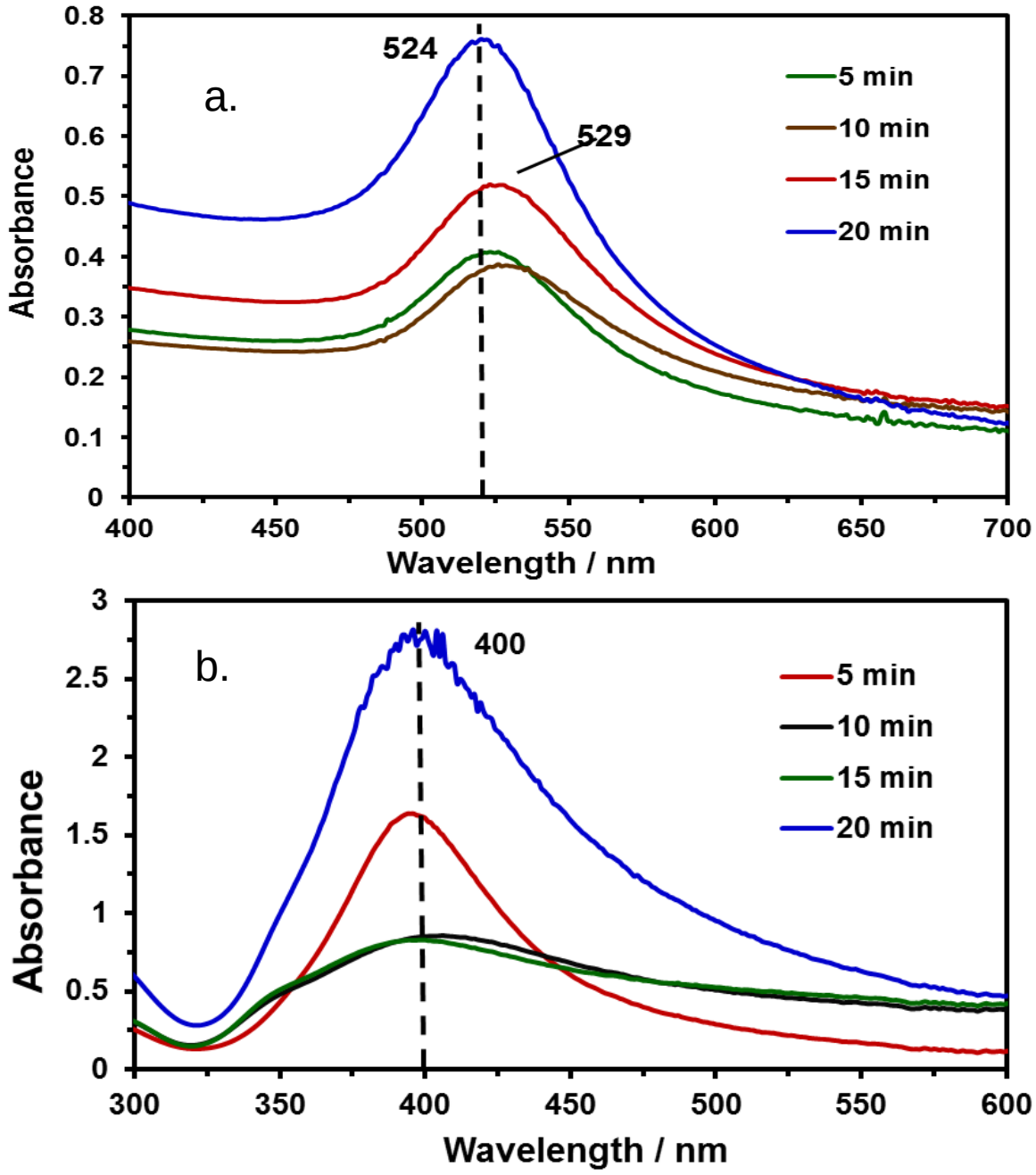

Figure 3.1. UV-Vis absorption spectra of Au and Ag nanoparticles (NPs) at various irradiation times: (a) absorption spectra of Au NPs; (b) absorption spectra of Ag NPs.

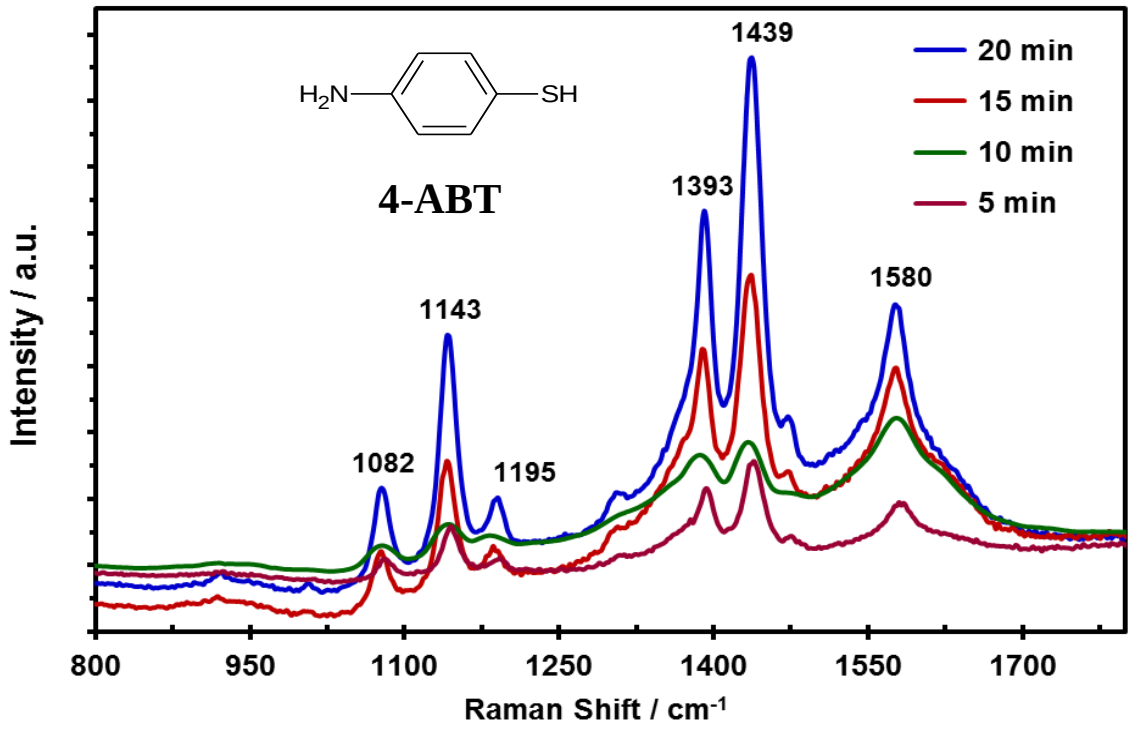

Figure 3.2. SERS spectra of 1.0 mM 4-ABT solution deposited on Au-coated glass slide with Ag NPs at various irradiation times. SERS spectra were acquired at 532 nm.

Predominant vibrational signals were observed in the Raman spectrum of 4-ABT at 1140, 1390 and 1430 cm^{-1}. These signals can be attributed to modes assigned to the 9b, 3 and 19b modes of the b2-type ring, respectively. The low intensity band at 1,080 cm^{-1} is due to the 7a mode of the a1-type ring [33–37].

Main Raman bands of BPE are observed in SERS spectrum of the probe molecules deposited on Au NPs. The peak at 994 cm^{-1} corresponds to the ring breathing mode of BPE pyridine. A blue shift of 27 cm^{-1} was observed in the SERS spectra of BPE, which includes the vibrational movement of the pyridyl nitrogen atom. Similarly, the vibrational signature observed at 1596 cm^{-1} corresponds to the C−N stretching mode of the pyridyl ring.

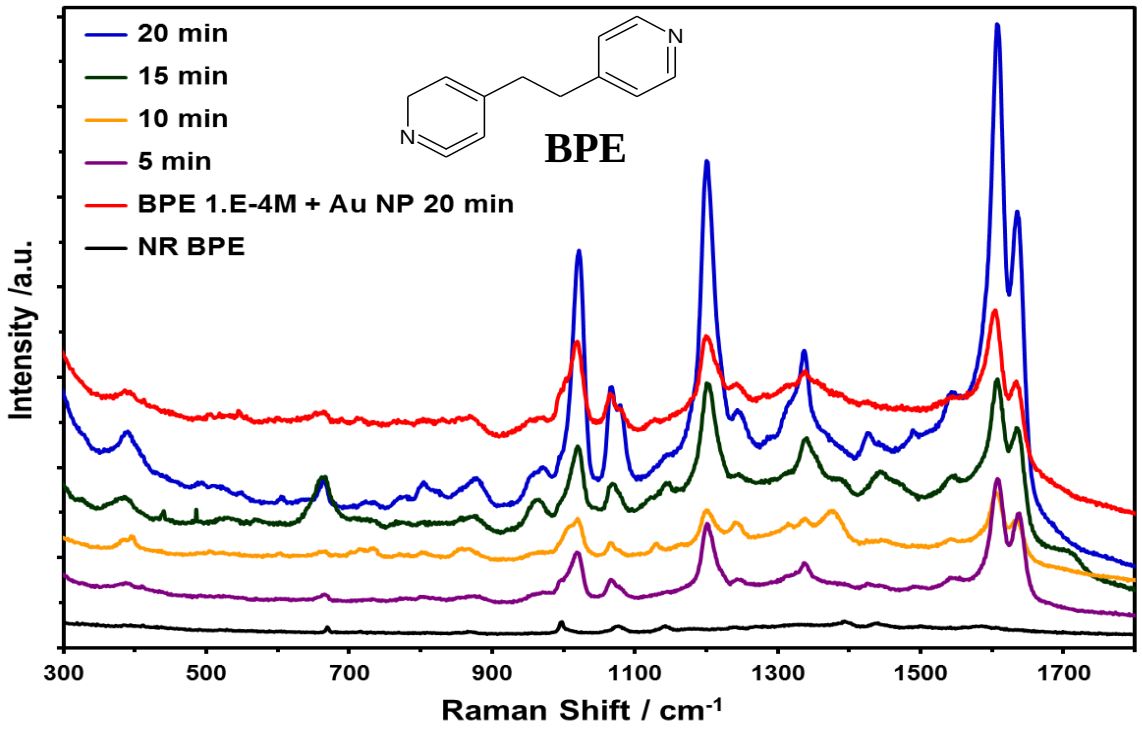

Figure 3.3. SERS spectra of 1.0 mM BPE solution in Au NPs at various irradiation times. Spectra were acquired at 785 nm.

This band presents a blue shift of approximately 10 cm^{-1} in the SERS spectrum of BPE deposited on Au NPs. These results suggest that the molecule of BPE interacts strongly with the surface of the Au NPs through the nitrogen atom corresponding to the pyridyl ring [38]. However, the bands at 1637 cm^{-1} and 1200 cm^{-1} remain unshifted.

The size distribution of the gold and silver nanoparticles was evaluated. The analysis was conducted to verify how the irradiation time during the laser ablation synthesis affected the average size of the NPs. The average particle size distributions of Au and Ag NPs synthesized by different ablation times are shown in Table 3.1. The particles at 5 min are larger (96 nm) than those obtained at 20 min. As the ablation time increases from 5 to 20 min, the size distribution experiences a significant decrease of

NP size and the average particle size is reduced to 75 nm. Similar results were obtained by Baladi [39] in the synthesis of Al nanoparticles [40, 41].

Table 3.1. Average size of Au and Ag NPs synthesized by laser ablation.

Nanoparticle Type	Irradiation Time (min)	Average Size (Z size, nm)
Au	5	96
Au	10	82
Au	15	71
Au	20	75
Ag	5	77
Ag	20	66

pH plays a very important role in the properties of synthesized NPs, including their SERS activity [42-43]. A change in the ionic strength in the medium leads to the formation of clusters of particles or even a monolayer of particles on a surface. This conglomeration of NPs leads to changes in their color analogous to the variation in color associated with altering the size or the shape of the particles. When two or more particles stick together, the absorption produced is very similar to that of a single rod-like particle with a bigger length [44]. To evaluate the SERS activity of the NPs, water at different pH values was used. The water pH was adjusted to 2.60, 4.80, 8.10 and 10.30. Irradiation time used for the synthesis was 20 min. Dependence of the pH values on color acquired by the nanoparticles was observed. Figure 3.4, contains color micrographs of Au/Ag NPs colloids synthesized at several pH values. Differences in the predominant colloidal color were found. These color changes can

be associated with the average size and the predominant shapes of the NPs in colloid suspensions.

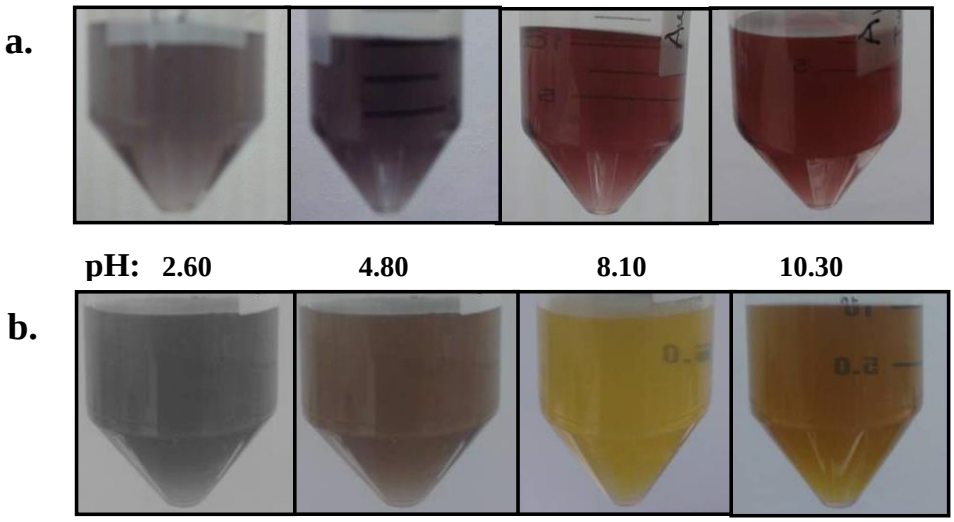

Figure 3.4. NPs suspensions at different pH values of the solvent during synthesis: (a) Au NPs suspensions; (b) Ag NPs suspensions.

Also, the UV-Vis absorption spectra for Au and Ag nanoparticles synthesized at different pH values was studied, as is showed in Figure 3.5. A broad absorption band indicates the presence of different sizes coexisting in the colloidal suspension. At acidic pH values, a low absorbance was found for both Au and Ag NP suspensions. Therefore, at pH values of 8.1 (slightly basic) and 10.3 (basic), intense absorbance were exhibited by the suspensions. No changes in the characteristic wavelength location of the plasmon resonance absorption bands were detected for the metallic NPs under study.

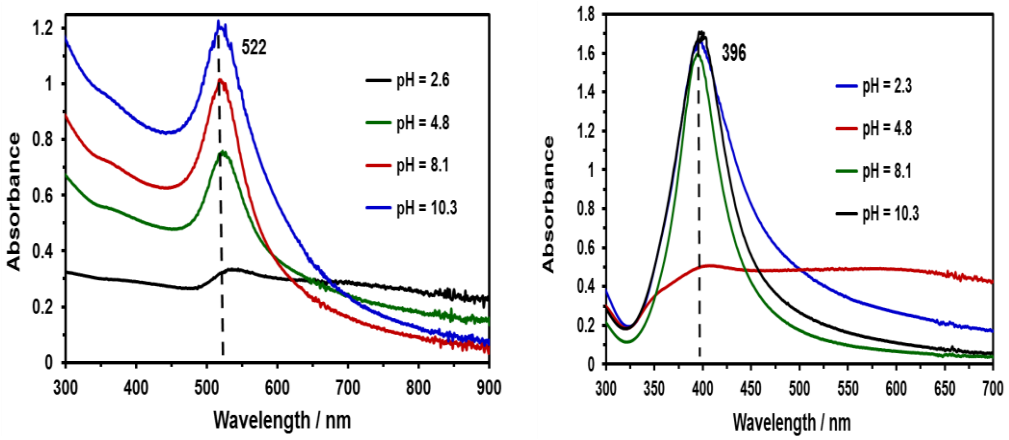

Figure 3.5. UV-Vis absorption spectra of colloids at various pH: (a.) Au NP; (b.) Ag NP.

Au/Ag NPs suspensions at different pH values were transferred onto gold-coated glass slides to prepare the SERS substrates. Then, the samples were allowed to dry, and 5.0 µL of 1.0 mM 4-ABT was deposited on the substrates. The SERS measurements were acquired using a Raman excitation source at 532 nm for the analytes deposited on Ag NPs and 785 nm for the Au NPs substrates. In Figure 3.6, results of 4-ABT on Au and Ag NPs are shown.

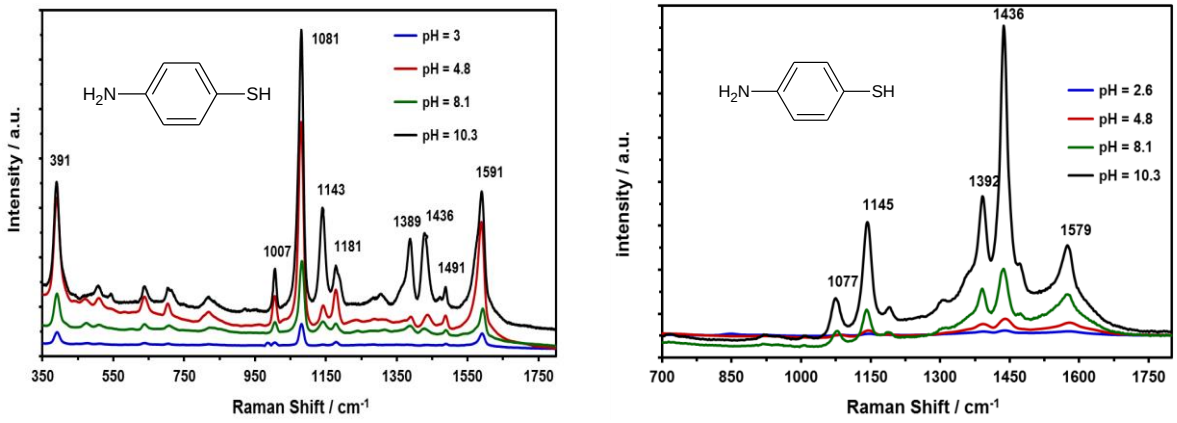

Figure 3.6. pH effect on SERS activity: (a) SERS spectra of 4-ABT on the Au NPs/Au substrate; (b) SERS spectra of 4-ABT on the Ag NPs/Au substrate.

The SERS spectra of 4-ABT on Au NPs shown in Figure 3.6 (a), are in good agreement with previous results [32]. The four strong peaks at 1591, 1436, 1389 and 1143 cm^{-1} can be assigned to ring 8b, 19b, 3 and 9b modes of 4-ABT, respectively. The peaks at Raman shifts of 1491 and 1081 cm^{-1} are due to 8a and 19a modes, respectively, that possess the a1-type of symmetry [26, 45]. For Au NPs, the best results were found at pH values of 10.30 and 4.80. Kim and collaborators found that the b2-type bands of 4-ABT are strongly affected by the solution pH [33]. Regardless of the excitation wavelength and the type of SERS substrates, the b2-type bands appeared very weak or negligible at acidic pH, while they were observed very distinctly at basic pH in Ag NPs. Our results show differences in the signals at 1143 and 1181 cm^{-1} for Au NPs at different pH values. Kim [46] attributes the disappearance of the b2-type bands at acidic pH to the protonation of the amine group, thus causing the charge transfer resonance chemical enhancement to be less likely to occur.

Likewise, the results for 4-ABT obtained for Ag NPs deposited on Au-coated glass slides presented good enhancement in the Raman signals, specifically the NP suspensions prepared at basic pH. In Figure 3.6 (b) is shown the Raman signals for 1.0 mM 4-ABT. To determine the surface enhancement factor (SEF) for 4-ABT, aliquots of 1.0×10^{-9} M were deposited on the NP substrates. The deposited sample covered an area of approximately of 0.25 cm^2. If the spot of the laser using an objective of 10× is approximately 13 μm^2, the number of 4-ABT molecules that were illuminated was calculated to be 1.4×10^5, which represents a SEF of 1.6×10^9.

The zeta potential of a system is a measure of the charge stability and controls all particle-particle interactions within a suspension. Understanding the zeta potential is of critical importance in controlling the dispersion and determining the stability of a nanoparticle suspension, i.e., to what degree aggregation will occur over time [47]. A lower level of the zeta potential results (0 to ±30 mV) in a smaller electrostatic repulsion between the particles, maximizing aggregation/flocculation. Zeta potential measurements of the as-prepared samples yielded values of −34.9 mV for the Au colloid and −20.9 mV for the Ag colloid, thus confirming the moderate stability of gold and silver nanoparticles. Similarly, the Z-potential and the Z-size were acquired for colloidal suspensions of Ag and Au NPs at different pH values. The results confirm the color differences in the colloidal suspension when the pH was adjusted to the solutions before the synthesis. The results are shown in Table 3.2.

Table 3.2. Z-potential values and the Z-size for Au NPs and Ag NPs at various pH values.

NP Type	pH	Average Size (nm)	Z Potential (mV)
Ag	4.2	96	−18.0
Ag	6.0	90	−21.8
Ag	8.3	87	−24.1
Ag	10.0	72	−26.2
Ag	10.8	70	−29.1
Au	4.3	93	−11.1
Au	6.0	75	−39.2
Au	8.3	73	−3.7
Au	10.0	47	−5.2

The values of the Z potential reflect that the stability of the Au NPs is compromised at different pH values of the synthesis of colloidal suspensions. For this reason, the suspended colloidal NPs result in low reproducibility, lower SEF values and higher LODs.

SERS is an important technique to develop applications for the detection of biological compounds [48-56]. L-His is α-amino acid with an imidazole ring functional group, which has an aromatic behavior at all pH values, because, it contains six π electrons that can form π assembling interactions represented with two equally important resonance structures [57]. Also, L-His is used to develop and maintain healthy tissues in all parts of the body, for the reason that, is the only amino acid that ionizes within the physiological pH range. L-His was selected as a biomolecule to evaluate Au/Ag NPs on Au-coated glass slides.

To determine the effect of pH on Au/Ag NPs in SERS activity for the detection of L-His, 5.0 µL of a solution of the amino acid at 1.6mM was deposited on different Au substrates with gold/silver NPs deposited. The results were compared at a pH value of nanoparticles of 4.80 and 10.30 for Au, 6.00 and 10.3 for Ag with the solid histidine spectrum. The particles obtained at acidic pH (~3) were very unstable for Au NPs. The NPs were precipitated approximately 1 h after preparation. To compare the results, in In Figure 3.7, nanoparticles deposited with analyte versus colloidal suspensions of nanoparticles are shown (see Figure 3.8). A light enhancement is observed, but the bands it's not shown a good definition in the colloidal suspension at pH 4.8. The results confirm one of the intrinsic limitations of metal colloidal nanoparticles for SERS applications, where their robustness as SERS substrates is compromised. An

important factor in the enhancement obtained through SERS is the need for aggregation to generate the necessary plasmonic conditions for the production of significant SERS. If adequate aggregation does not occur, the reproducibility of SERS on colloidal NPs is affected because the kinetics of the process can be uncontrollable once aggregation begins.

The data were compared with experiments using colloidal NPs. The Raman signals were also observed in colloidal NPs, but wasn´t good enough. A possible explanation is that the acquisition of stronger enhanced Raman signals depends on the reliability and stability of the SERS-active sites (or “hot spots”), which have a large influence on the enhancement of the Raman signal intensities.

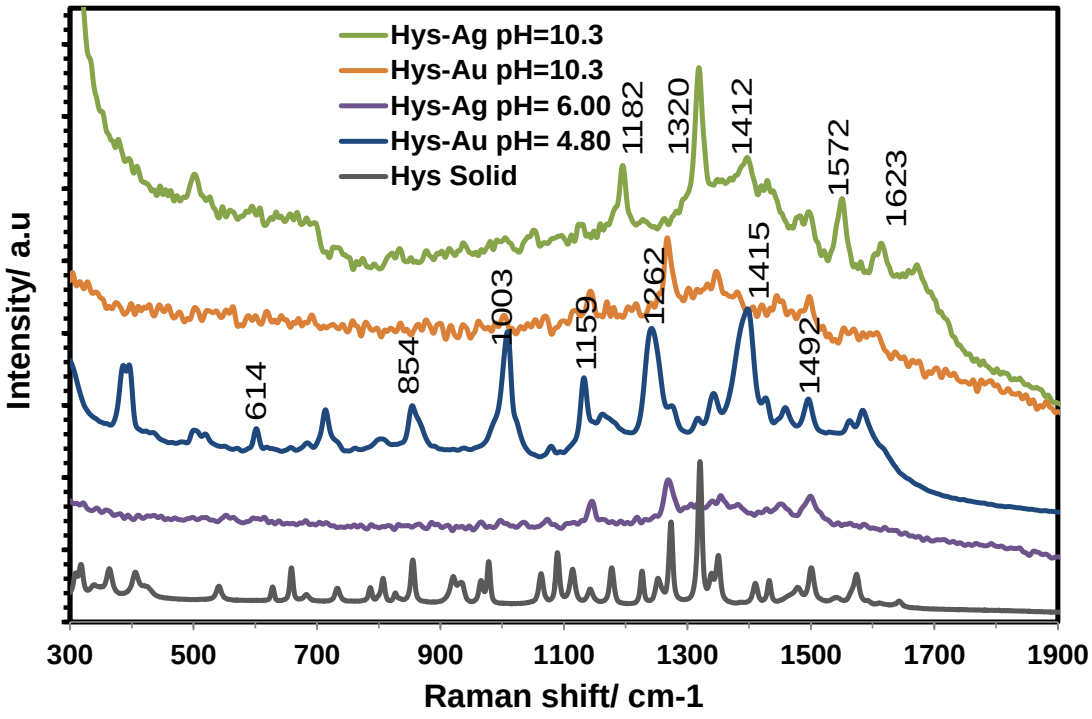

Figure 3.7. pH effect on SERS activity L-His deposited on Au/Ag NPs/Au substrate.

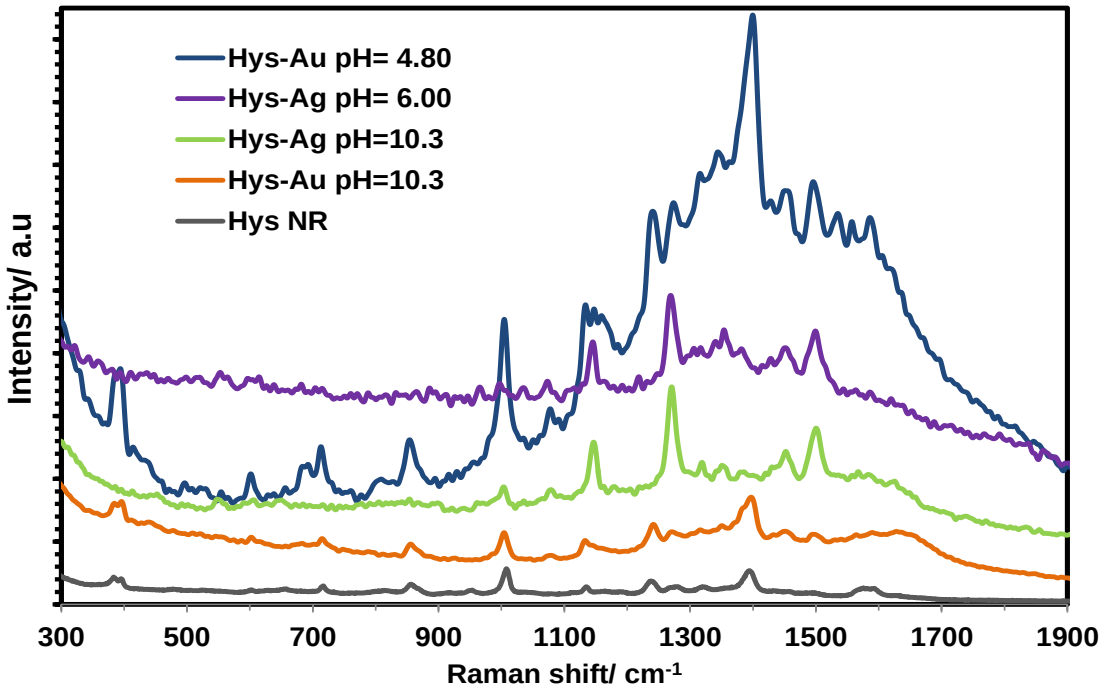

Figure 3.8. pH effect on SERS activity L-His interacting with Ag/Au colloidal suspension on Au substrate.

The enhancement in the signals obtained depends significantly on the aggregation of Ag or Au colloids and the analyte used in the analysis. The stability of metal colloids is due to the repulsive forces derived from the charged species on the surface of the colloidal particles, which assume a nonzero effective charge. When these charges are replaced with a neutral adsorbate, aggregation occurs, usually when a ligand has a greater affinity for the metal than that of the surface charged species [58].

Moreover, the number of L-His molecules that were present on the Au NPs for an area of approximately of 1.3×10^{7} μm^{2} deposited on a substrate was determined. The area (circular) or laser spot when using a 10× objective was 1.7×10^{3} μm^{2}. L-His mass contained in the interrogated area for the lowest concentration solution was 1.0×10^{-11}

g. The number of L-His molecules that were SERS excited was calculated to be 3.0×10^{14} molecules (1.0×10^{-4} M, 5 µL deposited).

3.4. Conclusions

Colloidal suspensions of Ag and Au NPs were successfully synthesized by laser ablation using water as the solvent. Colloids of different colors and sizes were obtained, depending on the time of irradiation in the synthesis and the pH of water. Excellent SERS results were found for Au and Ag NPs deposited on Au films using 4-ABT at a pH value of 10.3.

The potential application of Au and Ag nanoparticles in SERS on biological compound was evaluated. 9.4×10^{-13} g of L-His on Au NPs deposited on Au-coated glass slide was detected. The SEF obtained establishes the possibility of using the substrates prepared for the applications in the research with microorganisms and medical fields.

3.5. References

[1]. Hamouda, I.M. Current perspectives of nanoparticles in medical and dental biomaterials. *J. Biomed. Res.* (2012), 26, 143–151.

[2]. Albrecht, M.; Janke, V.; Sievers, S.; Siegner, U.; Schüler, D.; Heyen, U. Scanning force microscopy study of biogenic nanoparticles for medical applications. *J. Magn Magnc Mater.* (2005), 290–291, 269–271.

[3]. Rai, M.; Yadav, A.; Gade, A. Silver nanoparticles as a new generation of antimicrobials. *Biotechnol. Adv.* (2009), 27, 76–83.

[4]. Piao, M.J.; Kang, K.A.; Lee, I.K.; Kim, H.S.; Kim, S.; Choi, J.Y.; Choi, J.; Hyun, J.W. Silver nanoparticles induce oxidative cell damage in human liver cells through inhibition of reduced glutathione and induction of mitochondria-involved apoptosis. *Toxicol. Lett. (*2011), 201, 92–100.

[5]. Chen, X.; Schluesener, H.J. Nanosilver: A nanoproduct in medical application. *Toxicol. Lett.* (2008), 176, 1–12.

[6]. Wei, D.; Ye, Y.; Jia, X.; Yuan, C.; Qian, W. Chitosan as an active support for assembly of metal nanoparticles and application of the resultant bioconjugates in catalysis. *Carbohydr. Res.* (2010), 345, 74–81.
[7]. Lee, K.Y.; Hwang, J.; Lee, Y.W.; Kim, J.; Han, S.W. One-step synthesis of gold nanoparticles using azacryptand and their applications in SERS and catalysis. *J. Colloid Interface Sci.* (2007), 316, 476–481.
[8]. Hutchings, G.J.; Edwards, J.K. Application of Gold Nanoparticles in Catalysis. Chapter 6. *In Frontiers of Nanoscience*; Roy, L.J., Wilcoxon, J.P., Eds.; Elsevier: Amsterdam, United Kingdom, (2012); Volume 3, pp. 249–293.
[9]. Niu, Y.; Crooks, R.M. Dendrimer-encapsulated metal nanoparticles and their applications to catalysis. *Comptes Rendus Chimie.* (2003), 6, 1049–1059.
[10]. Chang, C.-C.; Yang, K.-H.; Liu, Y.-C.; Hsu, T.-C. New pathway to prepare gold nanoparticles and their applications in catalysis and surface-enhanced Raman scattering. *Colloids Surf. B.* (2012), 93, 169–173.
[11]. Yang, J.; Pan, J. Hydrothermal synthesis of silver nanoparticles by sodium alginate and their applications in surface-enhanced Raman scattering and catalysis. *Acta Mater.* (2012), 60, 4753–4758.
[12]. Eriksson, S.; Nylén, U.; Rojas, S.; Boutonnet, M. Preparation of catalysts from microemulsions and their applications in heterogeneous catalysis. *Appl. Catal. A* (2004), 265, 207–219.
[13]. Haruta, M. Catalysis and applications of gold nanoparticles. *In Studies in Surface Science and Catalysis;* Masakazu Anpo, M. O.; Hiromi, Y., Eds.; Elsevier: Amsterdam, United Kingdom, (2003); Volume 145, pp. 31-38.
[14]. Chen, X.; Zhu, H. 3.01—Catalysis by Supported Gold Nanoparticles. *In Comprehensive Nanoscience and Technology*; David, L.A., Gregory, D.S., Gary, P.W., Eds.; Academic Press: Amsterdam, United Kingdom, (2011); pp. 1–11.
[15]. El-Rafie, M.H.; Shaheen, T.I.; Mohamed, A.A.; Hebeish, A. Bio-synthesis and applications of silver nanoparticles onto cotton fabrics. *Carbohydr. Polym.* (2012), 90, 915–920.
[16]. Jung, S.-H.; Kim, K.-I.; Ryu, J.-H.; Choi, S.-H.; Kim, J.-B.; Moon, J.-H.; Jin, J.-H. Preparation of radioactive core-shell type 198Au@SiO2 nanoparticles as a radiotracer for industrial process applications. *Appl. Radiat. Isot.* (2010), 68, 1025–1029.
[17]. Yu, C.H.; Oduro, W.; Tam, K.; Tsang, E.S.C. Chapter 10. Some Applications of Nanoparticles. *In Handbook of Metal Physics*; John, A.B., Ed.; Elsevier: Amsterdam, United Kingdom, (2008); Volume 5, pp. 365–380.
[18]. Ganesh, S.; Amit, S. Perspectives on the Science and Technology of Nanoparticle Synthesis. *In Nanomaterials Handbook*; CRC Press: Boca Raton, United State, (2006).

[19]. Lawrence, D.Ä.; Ryan, R. Synthesis of Metal Colloids. *In Catalyst Preparation*; CRC Press: New York, United State, (2006); pp. 93–137.
[20]. Sergeev, G.B. 2—Synthesis and Stabilization of Nanoparticles. *In Nanochemistry;* Elsevier Science: Amsterdam, United Kingdom, (2006); pp. 7–36.
[21]. Takeshi, T. Preparation of Nanoparticles Using Laser Ablation in Liquids. *In Laser Ablation in Liquids;* Pan Stanford Publishing: Boca Raton, United State, (2012); pp. 207–268.
[22]. Haibo, Z.; Shikuan, Y.; Weiping, C. Formation of Nanoparticles under Laser Ablation of Solids in Liquids. *In Laser Ablation in Liquids;* Pan Stanford Publishing: Boca Raton, United State, (2012); pp. 327–396.
[23]. Stratakisa, E.; Shafeevb, G. Nanostructures? Formation under Laser Ablation of Solids in Liquids. *In Laser Ablation in Liquids*, Pan Stanford Publishing: Boca Raton, United State, (2012); pp. 815–854.
[24]. López-Tocón, I.; Centeno, S.P.; Otero, J.C.; Marcos, J.I. Selection rules for the charge transfer enhancement mechanism in SERS: Dependence of the intensities on the L-matrix. *J. Mol. Struct.* (2001), 565–566, 369–372.
[25]. Luo, Z.; Fang, Y. Investigation of the mechanism of influence of colloidal gold/silver substrates in nonaqueous liquids on the surface enhanced Raman spectroscopy (SERS) of fullerenes C60 (C70). *J. Colloid Interface Sci.* (2006), 301, 184–192.
[26]. Primera-Pedrozo, O.M.; Rodríguez, G.D.M.; Castellanos, J.; Felix-Rivera, H.; Resto, O.; Hernández-Rivera, S.P. Increasing surface enhanced Raman spectroscopy effect of RNA and DNA components by changing the pH of silver colloidal suspensions. *Spectrochim. Acta A.* (2012), 87, 77–85.
[27]. Hou, X.; Zhang, X.; Chen, S.; Fang, Y.; Li, N.; Zhai, X.; Liu, Y. Size-controlled synthesis of Au nanoparticles and nanowires and their application as SERS substrates. *Colloids Surf. A.* (2011), 384, 345–351.
[28]. Kundu, S.; Mandal, M.; Ghosh, S.K.; Pal, T. Photochemical deposition of SERS active silver nanoparticles on silica gel and their application as catalysts for the reduction of aromatic nitro compounds. *J. Colloid Interface Sci.* (2004), 272, 134–144.
[29]. Photopoulos, P.; Boukos, N.; Panagopoulou, M.; Meintanis, N.; Pantiskos, N.; Raptis, Y.; Tsoukalas, D. Size control of Ag nanoparticles for SERS sensing applications. *Procedia Eng.* (2011), 25, 280–283.
[30]. Vlckova, B.; Pavel, I.; Sladkova, M.; Siskova, K.; Slouf, M. Single molecule SERS: Perspectives of analytical applications. *J. Mol. Struct.* (2007), 834–836, 42–47.
[31]. Primera-Pedrozo, O.M.; Jerez-Rozo, J.I.; De La Cruz-Montoya, E.; Luna-Pineda, T.; Pacheco-Londono, L.C.; Hernandez-Rivera, S.P. Nanotechnology-based

detection of explosives and biological agents simulants. *Sens. J.* (2008), 8, 963–973.
[32]. Burda, C.; Chen, X.; Narayanan, R.; El-Sayed, M.A. Chemistry and properties of nanocrystals of different shapes. *Chem. Rev.* (2005), 105, 1025–1102.
[33]. Kim, K.; Shin, D.; Choi, J.-Y.; Kim, K.L.; Shin, K.S. Surface-enhanced Raman scattering characteristics of 4-aminobenzenethiol derivatives adsorbed on silver. *J. Phys. Chem. C.* (2011), 115, 24960–24966.
[34]. Kim, K.; Lee, H.B.; Choi, J.-Y.; Kim, K.L.; Shin, K.S. Surface-enhanced Raman scattering of 4-aminobenzenethiol in nanogaps between a planar Ag substrate and Pt nanoparticles. *J. Phys. Chemistry C.* (2011), 115, 13223–13231.
[35]. Kim, K.; Kim, K.L.; Shin, D.; Choi, J.-Y.; Shin, K.S. Surface-enhanced Raman scattering of 4-aminobenzenethiol on Ag and Au: pH dependence of b2-type bands. *J. Phys. Chem. C. (2012),* 116, 4774–4779.
[36]. Kim, K.; Kim, K.L.; Lee, H.B.; Shin, K.S. Similarity and dissimilarity in surface-enhanced Raman scattering of 4-aminobenzenethiol, 4,4′-dimercaptoazobenzene, and 4,4′-dimercaptohydrazobenzene on Ag. *J. Phys. Chem. C.* (2012), 116, 11635–11642.
[37]. Kim, K.; Yoon, J.K.; Lee, H.B.; Shin, D.; Shin, K.S. Surface-enhanced Raman scattering of 4-aminobenzenethiol in Ag sol: Relative intensity of a1- and b2-type bands invariant against aggregation of Ag nanoparticles. *Langmuir. (2011),* 27, 4526–4531.
[38]. Kim, A.; Ou, F.S.; Ohlberg, D.A.A.; Hu, M.; Williams, R.S.; Li, Z. Study of molecular trapping inside gold nanofinger arrays on surface-enhanced Raman substrates. *J. American Chem. Soc.* (2011), 133, 8234–8239.
[39]. Baladi, A.; Sarraf Mamoory, R. Investigation of different liquid media and ablation times on pulsed laser ablation synthesis of aluminum nanoparticles. *Appl. Surf. Sci.* (2010), 256, 7559–7564.
[40]. Mahfouz, R.; Cadete Santos Aires, F.J.; Brenier, A.; Jacquier, B.; Bertolini, J.C. Synthesis and physico-chemical characteristics of nanosized particles produced by laser ablation of a nickel target in water. *Appl. Surf. Sci.* (2008), 254, 5181–5190.
[41]. Tsuji, T.; Iryo, K.; Watanabe, N.; Tsuji, M. Preparation of silver nanoparticles by laser ablation in solution: Influence of laser wavelength on particle size. *Appl. Surf. Sci.* (2002), 202, 80–85.
[42]. Riabinina, D.; Zhang, J.; Chaker, M.; Margot, J.; Ma, D. Size control of gold nanoparticles synthesized by laser ablation in liquid media. *ISRN Nanotechnol.* (2012), 5.
[43]. Cañamares, M.V.; Garcia-Ramos, J.V.; Gómez-Varga, J.D.; Domingo, C.; Sanchez-Cortes, S. Comparative study of the morphology, aggregation, adherence to glass, and surface-enhanced Raman scattering activity of silver

nanoparticles prepared by chemical reduction of Ag+ using citrate and hydroxylamine. *Langmuir* (2005), 21, 8546–8553.

[44]. Schatz, S.H.a.G. Synthesis and Analysis of Silver/Gold Nanoparticles. Available online: *http://nanohub.org/topics/GeneralChemistry/File:Silvergold_module.pdf.* (accessed on 10 December 2012)

[45]. Kim, K.; Lee, H.S. Effect of Ag and Au nanoparticles on the SERS of 4-aminobenzenethiol assembled on powdered copper. *J. Phys. Chem. B.* (2005), 109, 18929–18934.

[46]. Kim, K. Surface-Enhanced Raman Scattering Characteristics of 4-Aminobenzenethiol Derivatives Adsorbed on Silver. Available online: *http://ipc.iisc.ernet.in/~umalab/icors2012/Mo_109.pdf* (accessed on 10 December 2012)

[47]. Cosgrove, T. *Colloid Science Principles, Methods and Applications;* Blackwell Publishing Ltd: Department of Chemistry, University of Bristol, Bristol, UK, (2005).

[48]. Kloglin, E. and Sequaris J., Surface Enhanced Raman Scattering (SERS) Spectroscopy of biomolecules, *In Topics in Current Chemistry*; Springer-Verlag: Berlin, (1986) 134, 1-57.

[49]. Lee, H., Suh, S, Kim, M., Raman spectroscopy of L-tryptophan-containing peptides adsorbed on a silver surface, *J. Raman Spectrosc.* (1988) 19, 491- 495.

[50]. Aliaga, A.E., Osorio-Román, I., Leyton, P., Garrido, C., Cárcamo, J., Caniulef, C., Célis, G., Díaz F., Clavijo, E., Gómez-Jeria, J.S., Campos-Vallette, M.M., Surface-enhanced Raman scattering study of L-tryptophan, *J. Raman Spectrosc.* (2009) 40, 164-169.

[51]. Chuang, C.H., Chena, Y.-T., Raman scattering of L-tryptophan enhanced by surface plasmon of silver nanoparticles: vibrational assignment and structural determination. *J. Raman Spectrosc.* (2009) 40, 150–156.

[52]. Kim, S., Kim, M., Suh, S., Surface-enhanced Raman scattering (SERS) of aromatic amino acids and their glycyl dipeptides in silver sol. *J. Raman Spectrosc.* (1987) 18, 171-175.

[53]. Nabiev, I., Efremov, R., Chumanov G., Surface-enhanced Raman scattering and its application to the study of biological molecules, *Sov. Phys. Uspekhi,* (1988) 31 (3), 241–262.

[54]. Davis, K., McGlashenf M., and Morris M., Surface-Enhanced Raman Scattering of Histamine at Silver Electrodes, *Langmuir,* (1992) 8, 1654-1658.

[55]. Lim J., Kim Y., Yeong s., Lee, S., Joo S., Spectroscopic analysis of l-histidine adsorbed on gold and silver nanoparticle surfaces investigated by surface-enhanced Raman scattering, *Spectrochimica Acta Part A* (2008) 69,286–289

[56]. Wen-Chi L., Tsong-Ru T., Hsiang-Lin H., Chyuan S.& Hai-Pang C., SERS Study of Histamine by Using Silver Film over Nanosphere Structure, *Plasmonics*, (2012) 7, 709-716.56.

[57]. Wang, L., Sun, N., Terzyan, S., Zhang, X. and Benson D.R., A Histidine/Tryptophan π-Stacking Interaction Stabilizes the Heme-Independent Folding Core of Microsomal Apocytochrome b5 Relative to that of Mitochondrial Apocytochrome b5. *Biochemistry* (2006) 46, 13750-13759.

[58]. Muniz-Miranda, M.; Pergolese, B.; Bigotto, A.; Giusti, A. Stable and efficient silver substrates for SERS spectroscopy. *J. Colloid Interface Sci.*(2007), 314, 540–544.

Chapter 4

DETECTION AND DISCRIMINATION OF MICROORGANISMS ON SUBSTRATES USING QUANTUM CASCADE LASER SPECTROSCOPY

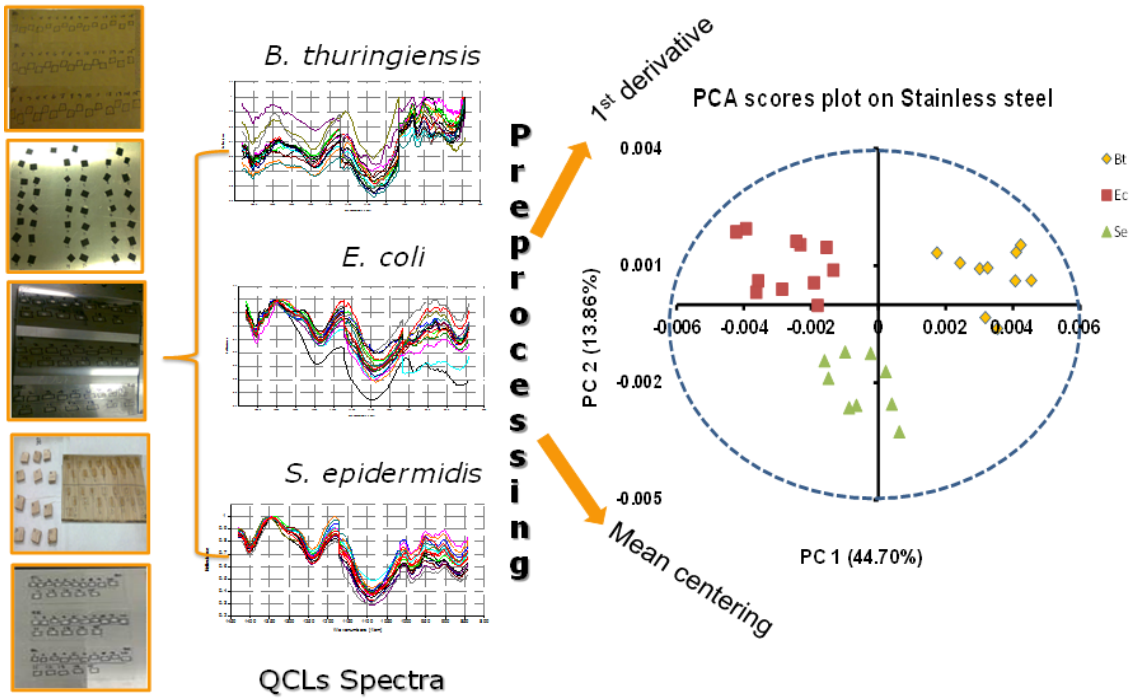

QCLS/PLS-DA detection and discrimination of microorganisms.

4.1. Introduction

Defense and security agencies, as well as the private industries, are highly interested in finding new ways to detect and identify unknown biological threats. By developing new capabilities and by expanding current experiences, food industries, environment

protection agencies, and pharmaceutical and biotechnology industries may benefit from the application of infrared sensing. Recent studies have focused on the development of rapid and accurate methods for recognizing agents that represent specific microorganisms. For example, disposable electrochemical immunosensor [1] and immobilized probes for the detection of *Escherichia coli* (*Ec*) [2] and solid phase microextraction/gas chromatography/mass spectrometry for distinguishing bacteria have been developed [3]. However, these techniques are time consuming, expensive, and involve many preparation steps and selective pre-enrichment. Although the identification and discrimination of bacterial spores with mid-infrared (MIR) technologies have been reported [4, 5], this contribution describes the first application of a tunable MIR quantum cascade laser (QCL)-based spectrometer for identification and discrimination of bacteria. The QCLs have revolutionized many areas of research and development related to applications in defense and security [6, 7].

The QCL sources are unipolar semiconductor injection lasers that are based on interband transitions in a multiple quantum-well heterostructure [8]. These lasers operate in the MIR at wavelengths starting at approximately 5 μm and expanding (in narrow or wide coverage) to 12.5 μm, which matches very well with the fundamental vibrational absorption bands of many chemical and biological species relative to the conventional diode sources, where laser emission generally matches the weaker overtones, or to oxide based thermal sources (such as the globar source), which are much less intense. The emission wavelength of a QCL depends on the thickness of the quantum well and barrier layers in the active region rather than on the band gap of the diode lasers. The QCLs operate at near room temperature, producing from milliwatts to

watts of IR radiation, both in continuous mode and pulsed laser operation. More recently, tunable QCL systems within a broad range of frequencies available for MIR experiments have become accessible [9]. In reflection mode, the same optical device is used to project the beam onto the analyte and to collect the reflected radiation.

Bacillus thuringiensis (Bt), a gram-positive bacterium that can form endospores which are highly resistant to chemical and thermal extremes in their latent state, was one of the bacteria chosen for this study [10]. The life cycle of *Bacillus* species includes vegetative cell growth that can form endospores as a defense mechanism. Endospores are highly resistant to environmental stresses including high temperatures, irradiation, strong acids, and disinfectants. In addition, endospores can tolerate extreme environments. This tolerance makes endospores suitable for transport before or during biological attack [11]. *Bt* is not harmful to humans and was chosen as a model in this study due to its similarities with *Bacillus anthracis* (anthrax), which has a high potential for use in terrorist attacks. Similarly, *Staphylococcus epidermidis (Se)* is a gram-positive cocci bacterium that is commonly associated with humans (usually with human skin) [12]. *Ec* is a member of the Enterobacteriaceae family of gram-negative bacteria. *Ec* is a thermotolerant coliform that occurs in the intestines of warm-blooded animals. Thus, *Ec* is an indicator of fecal contamination [13].

Various substrates, including cardboard (CB), glass, travel bags (TBs), wood, and stainless steel (SS), were used as support surfaces for the bacteria. Because the vibrational spectra of bacterial cells consist of signal contributions from all the cell components, these spectra reflect the overall molecular compositions of the cells. The MIR studies of Naumann et al., [14–16] were extended to identify and discriminate

between different vegetative bacteria with chemometric methods. These data were reduced to demonstrate the capability of this spectroscopic technique for identifying and discriminating between the types of bacterial cells that are considered as biological simulants [17].

4.2. Experimental setup

4.2.1. Samples preparations

Bacterial strains of *Bt* (ATCC #35646), *Ec* (ATCC #8789), and *Se* (ATCC #2228), were provided by the Microbial Biotechnology and Bioprospecting Lab at the Biology Department of the University of Puerto Rico-Mayagüez. These biological agents were selected for testing based on the previous studies, which included their resemblance to real-world biothreats and microbiological differences between the individual bacteria. Pure cultures were grown in Miller-modified Luria–Bertani (LB) agar and broth (Fisher Scientific International, Thermo Fisher Scientific, Waltham, MA). Prior to analysis, these cultures were stored at −80°C in microvials that contained 20% glycerol (cryoprotectant). After satisfactory growth of *Bt, Ec*, and *Se*, colonies were attained in agar, isolated on LB plates, and inoculated into 5 mL of LB or tryptic soy broth. These colonies were allowed to grow overnight. *Se* and *Bt* were placed in an orbital shaker at 32°C (~120 rpm) for 24 h before culturing for 72 h. *Ec* was placed in an orbital shaker at 37°C and allowed to grow for 5 h after inoculation. The subcultures were diluted (1:50) in their appropriate media and centrifuged at 5 K for 5 min at 4°C to obtain bacterial pellets.

These pellets were washed once with 20 mL of a 1% phosphate buffered saline (PBS) solution to remove the growth media. Finally, the pellets were resuspended in 4.0 mL of PBS (*Ec* and *Se*) or distilled water (*Bt*) before allowing them to grow for 72 h at 32°C and at 250 rpm. The harvested spores were stored at 4°C in distilled-deionized H_2O until the experiment was performed. Serial dilution was performed by plating the spores on LB agar to count the bacteria that were suspended in the PBS. These plates were incubated at 37°C to obtain colonies. The colonies were counted to determine the bacterial concentration in the stock suspension based on the dilution series. The following concentrations were obtained: $5.9x10^{10}/5.0x10^{3}$, $3.5x10^{9}$ and $9.5x10^{9}$ colony forming units per milliliter (CFU/mL) for *Bt* vegetative cell/endospores, *Ec* and *Se* respectively. Because the incubation time for the microorganisms must be determined from their growth curves (starting at an optical density of 0.025 at a wavelength of 600 nm), the OD600 (Biophotometer, Eppendorf North America, Hauppauge, New York) was measured before and after centrifugation.

The scanning electron microscope (SEM) images were obtained with a JEOL-JSM 6500 and a XL series 30SPhilips/ FEI to verify the size and morphology of bacterial cells. Figure 4.1 shows rod-shaped Bt and Ec with a size of between 0.5 to 1.0 × 1.4 to 3.0 µm. In addition, Se was spherically shaped with a size of 0.5 × 1.5 µm.

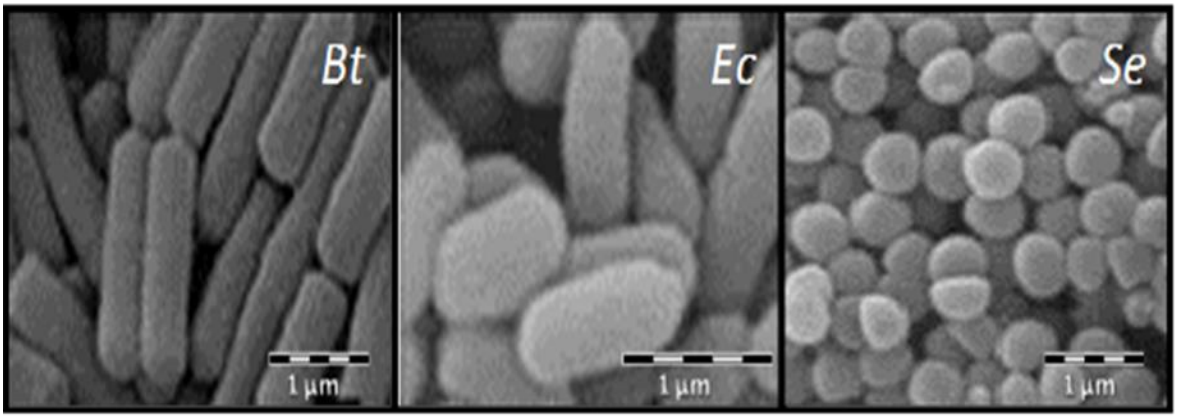

Figure 4.1. The SEM micrographics of bacteria used in this study, including *Bt*, *Ec* and *Se.* Operating voltage: 15 kV.

4.2.2. Instrumentation

A QCL-based dispersive IR spectrometer (LaserScan™, model 712, Block Engineering, LLC, Marlborough, MA) was used to acquire MIR reflectance data for the three bacterial samples on the wavenumber range of 830 to 1430 cm^{-1}. LaserScan™ uses infrared reflection spectroscopy to provide high-quality reflectance spectra from materials deposited on surfaces and from bulk substrates. The MIR laser provides the LaserScan™ with a source capable of sensitivities that are orders of magnitude larger than IR spectroscopy systems equipped with thermal sources. Added to that are the properties related to laser sources: polarized and coherent. The spectral resolution achievable by QCL sources can be very high at the cost of sacrificing tunability. However, by coupling the spectral information provided with the QCL spectroscopic system with the powerful multivariate analysis of chemometrics, highly interfering contributions from the substrates can be accounted for and separated from spectral information of bacteria.

Bacteria detection on the different substrates required a simple sample preparation procedure that consisted of depositing 10 µL of each bacterial sample suspension on the selected solid substrates (CB, TB, wood, glass, and SS) for in situ measurements [18, 19]. Biosamples were then allowed to dry to simulate real-world samples. Aluminum plates were used to support the substrates, which contained between 10 and 15 samples of each of the three analyzed bacteria that were deposited on the substrates over an area of 1 × 1 cm. Experimental setup of the QCL MIR spectroscopic system that was used to detect *Bt*, Ec, and Se on real-world substrates, including SS, glass, CB, TB, and wood, is shown in Fig. 4.2.

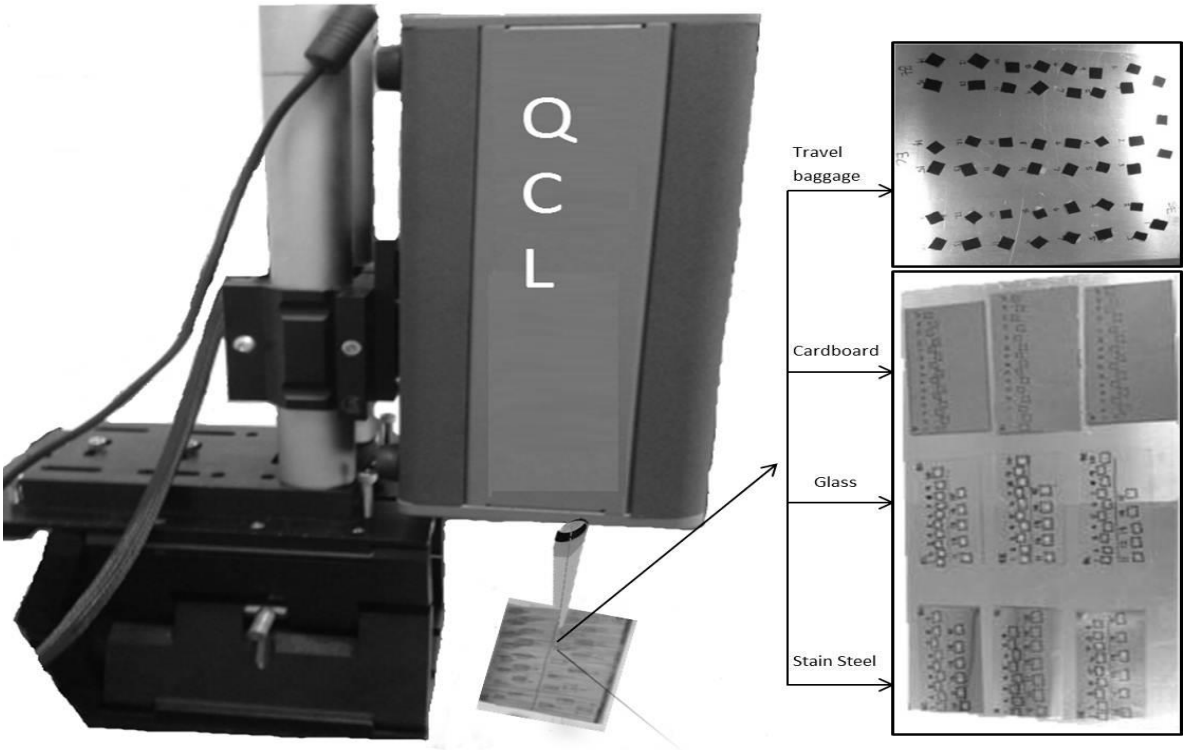

Figure 4.2. Experimental setup of the quantum cascade laser (QCL) mid-infrared (MIR) spectroscopic system that was used to detect *Bt*, *Ec* and *Se* on real-world substrates, including stainless steel (SS), glass, cardboard (CB), travel bag (TB) and wood.

Substrates with and without bacterial samples were used to measure the reflectance spectra of bacteria deposited on the substrates with the LaserScan™ (Fig. 4.2). Clean substrates were used to measure the background spectra. The QCL spectrometer had a focal point distance of 6 in. The system was sensitive to the way the material was deposited, with a light-capturing efficiency of approximately 1% for the ideal substrate. Therefore, the angle of sample placement was critical. In addition, the light from the source could be lost due to absorption or multiple reflections from the material of interest, especially for thick surfaces. Visible pointers (HeNe laser beams) were aligned with the invisible MIR radiation to form a laser spot (approximately 2 ×4 mm) on the surface. In addition, built-in algorithms were used for nearly real-time sample detection. Trace and bulk concentrations of the other substances tested were detected in the field with a minimum of 500 ng/cm^2 [20].

OPUS 6.0™ software package for data acquisition and analysis (Bruker Optics, Billerica, Massachusetts) was used for data analysis. During analysis, the spectra were normalized to be compared. For multivariate data analysis, the matrix interlinks of the individual measurements were generated in rows, and the selected wavenumber values were generated in columns. The spectral intensity of each intensity-wavenumber combination formed the elements of the matrix. Principal component analysis (PCA) regression analysis algorithm was initially used to analyze the data. The PCA is frequently used to reduce the number of variables in an experiment. With PCA, datasets with many variables can be simplified (by data reduction) to easily interpret the results. Partial least squares-discriminant analysis (PLSDA) is a multivariate method that is used to classify samples and to reduce the number of variables. For this analysis, it is

assumed that the differences between groups will dominate the total variability of the samples. The PCA and PLS-DA routines were applied using the MATLAB™ computational environment (The MathWorks, Inc., Natick, Massachusetts) coupled to the PLS-Toolbox™ v. 7.0.3 (Eigenvector Research, Inc., Wenatchee, Washington).

4.3. Results and discussion

MIR spectra of microorganisms were used to identify the molecular vibrational modes in the biosamples. These vibrational modes contain valuable information regarding the biochemical makeup of microorganisms and thus of the biomolecules of which they are composed [21]. Multivariate analyses are useful for handling large datasets and to make spectral analysis viable. Spectral analysis included tentative assignment of bands based on the reported MIR absorption frequencies characteristic of the agents that represented the tested microorganisms (*Bt, Ec,* and *Se*) and measurement of reflected intensities for applying multivariate analysis [22, 23].

Overall, 836 different MIR experiments were conducted. However, only 245 experiments are reported for simplicity. Each experiment consisted of 15 replicate spectral measurements for each bacterium for each of the substrates studied. Previous studies have used the single spectrum concept to represent replicate spectral dispersions. This method is acceptable because it yields meaningful and concrete results [24, 25]. MIR spectra of the three strains of bacteria (*Bt, Ec,* and *Se*) are illustrated in Fig. 4.3. It was difficult to differentiate the different classes of the various tested surfaces based on the raw MIR spectra data due to the high degree of band

overlapping. To overcome this problem, several pretreatments were used. The first pretreatment was spectral normalization.

Each bacterial species has a unique IR fingerprint spectrum due to the stretching and bending vibrations of its molecular bonds or protein functional groups (including nucleic acids, lipids, sugars, and lipopolysaccharides) [26], as illustrated by the reference spectra presented in Fig. 4.4. Reference spectra were obtained in absorption mode using a bench microspectrometer model IFS66/v/S (Bruker Optics, Billerica, MA).

Cell surface characteristics vary between the gram-positive and gram-negative bacteria. gram-positive bacteria have a thicker and more rigid peptidoglycan layer that makes up to 40% to 80% more of the cell wall (by weight) than in gram-negative bacteria. In addition, gram-positive bacteria contain teichoic acids that are covalently bound to peptidoglycan. In contrast, gram-negative cells do not contain teichoic acids, but contain lipoproteins that are covalently bound to the peptidoglycan in the cell walls. Gram-negative bacteria have an outer membrane outside the peptidoglycan layer that contains phospholipids in the inner layer and lipopolysaccharides in the outer layer [27].

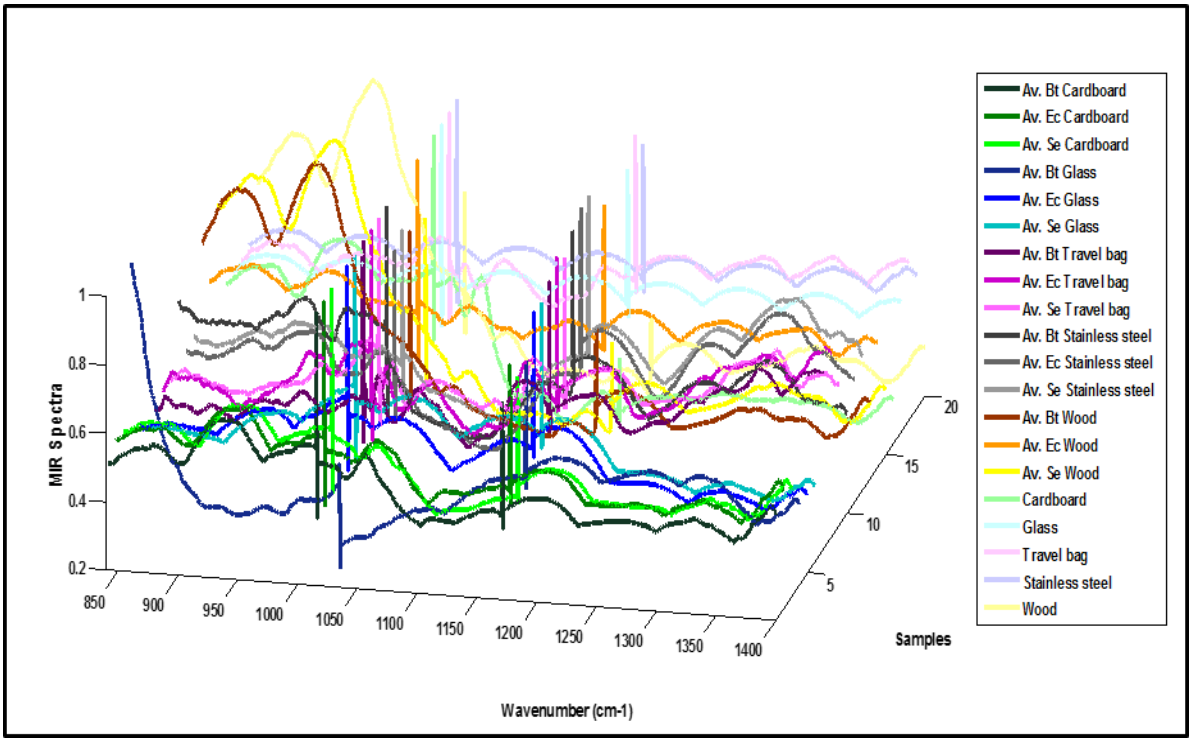

Figure 4.3. Normalized QCL spectra of bacterial suspensions.

Amino acid composition of peptide chains in the *Ec* gram-negative bacterium consists of D-alanine, D-glutamic acid, and meso-diaminopimelic acid. In contrast, the *Se* gram-positive bacterium consists of L-alanine, D-glutamine, L-lysine, and D-alanine [28]. MIR spectra of intact bacterial cells are generally complex with broad peaks due to the overlaid contributions of all the biomolecules in the bacterial cell (Fig. 4.4) [26].

Following the recommendations of Naumann [14] and Naumann et al., [15,28] the IR spectra should be analyzed for bending vibrations between 1200 and 1500 cm^{-1} to identify fatty acids, proteins, and phosphate-carrying compounds in bacteria. The region from 900 to 1200 cm^{-1} contains carbohydrate bands that result from microbial cell walls. In addition, the region between 700 and 900 cm^{-1} is a fingerprint region that contains weak but unique vibrations that are characteristic of specific bacteria [29]. Tentative

functional group assignments in these regions and their associations with the major vibration bands in the MIR spectra of each bacterium are depicted in Table 4.1.

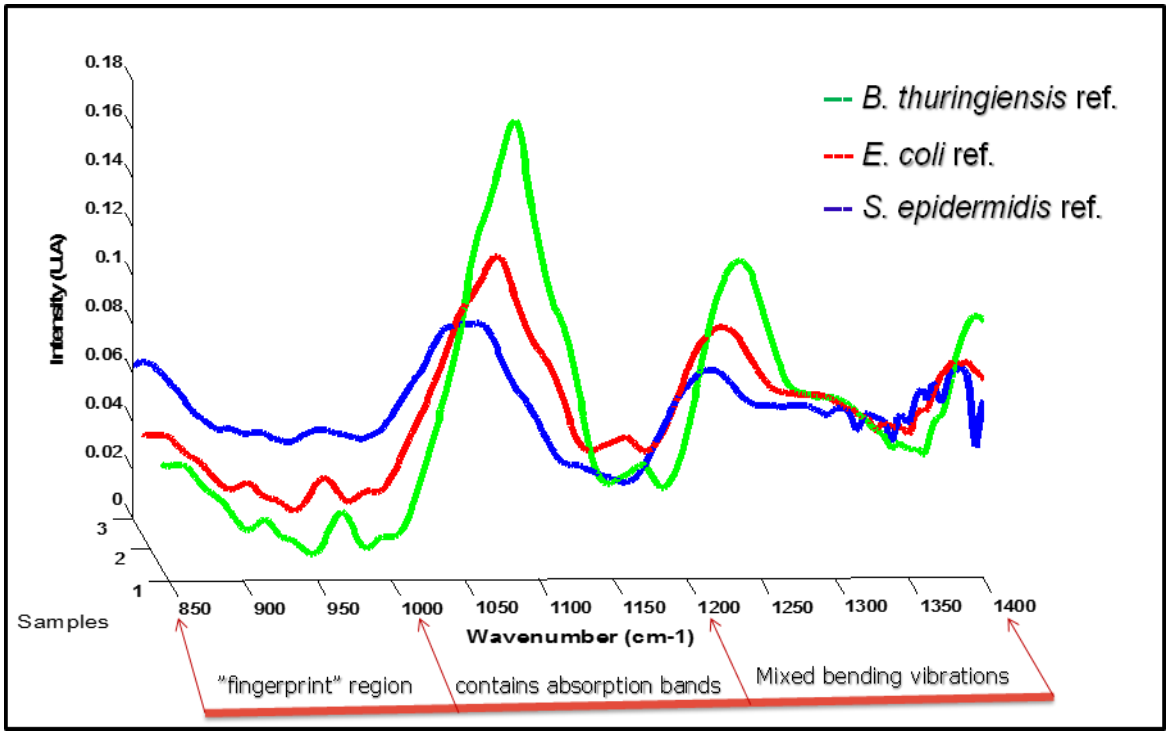

Figure 4.4. Reference MIR spectra for *Bacillus thuringiensis* (*Bt), Escherichia coli (Ec),* and *Staphylococcus epidermidis (Se)* across the studied spectral region.

The spectral information for 245 MIR spectra (and replicas) of bacteria and substrates was subjected to several preprocessing steps to reduce the number of variables, maintaining the variance between low bacterial classes.

Chemometrics models were constructed for which the datasets with many variables could be simplified by performing data reduction, making results more easily interpretable in terms of multivariate analyses models.

Table 4.1. Tentative band assignments used for bacterial identification

Bt	*Se*	*Ec*	Tentative band assignments [15, 27, 28–30]	*Bt*	*Se*	*Ec*	Tentative band assignments [15, 27, 28–30]
1426		1427	Symmetric stretching vibrations of -COO- functional groups of amino acid side chains or free fatty acids.		1087	1088	DNA PO_2- symmetric stretching
1411			Glutamic acid, CO_2- asymmetric and symmetric stretching	1082	1073		RNA PO_2- symmetric stretching
1403	1404	1402	Symmetric stretching vibrations of -COO- functional groups of amino acid side chains or free fatty acids.	1059 1031			Ribose C-O stretching, carbohydrates, RNA Ribose C-O stretching
1392	1390		C-H bending, -CH_3 stretch in fatty acids		1015	1015	DNA ribose C-O stretching and RNA ribose stretching
1387			COO stretching, Amines C-N CH_2 and CH_3 bending modes of lipids and proteins, stretching amides II	1010			Dipicolinic acid, phenylalanine
1377	1372		CH_3 symmetric bending	992	995		RNA Uracil Ring stretching; uracil ring bending
1364			Dipicolinic acid	968	964	962	DNA Ribose phosphate skeletal motion
1317		1318	Amide III protein		944		Pectin
1306	1310		CH_2 and CH_3 bending modes of lipids and proteins	929	930	931	C-OH out of plane
1294	1295	1293	Amide III	915	917	915	DNA Ribose Phosphate skeletal motion
1249			Pectin -cellulose	907	907		Pectin
1240		1241	RNA PO_2- asymmetric stretching	891	887	894	
1177	1171		Amines C-N, polysaccharides	878	875	873	Aromatic ring vibrations of phenylalanine, tyrosine, tryptophan and the various nucleotides.
1168		1167	RNA Ribose C-O stretching	871	867	866	
1151			Unsaturated fatty acids, glutamate	862	862	862	
	1104		Glycosides link	854	849	851	NH_2 wagging, tyrosine

The PCA models were represented in terms of score plots and well-defined separations between the classes of different bacteria on various substrates were not obtained. However, the PCA models represented most of the data variability.

Representative MIR-QCL spectra for each bacterium after deposition on SS substrate are shown in Fig. 4.5. Based on these spectra, the bacteria analyzed by QCL in reflectance mode resulted in unique spectral signals in the MIR region. These spectral signals were clearly observed on SS substrate, particularly in the fingerprint region. In addition, similar results were obtained for the others substrates (CB, TB, wood, and glass).

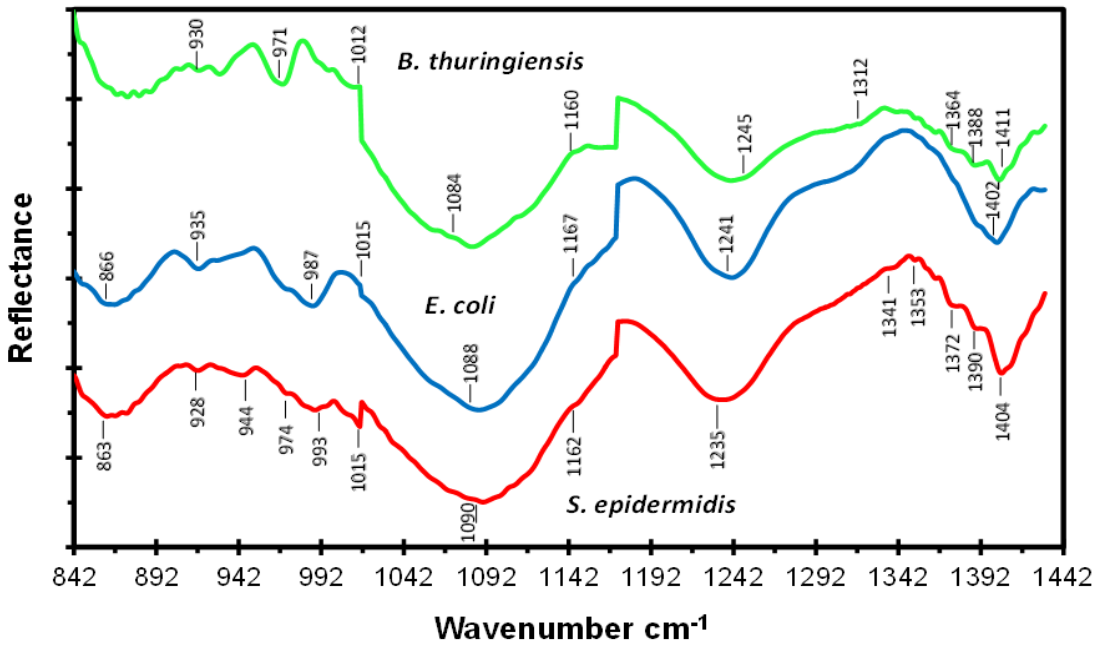

Figure 4.5. The MIR spectra of *Bacillus thuringiensis* (*Bt), Escherichia coli (Ec),* and *Staphylococcus epidermidis (Se)* at room temperature following deposition on a SS substrate.

The classification between groups of bacteria on different substrates is shown in Table 4.2, in which the bold values represent the percentages of predicted discrimination

within a group that were correctly classified. Other PCA models were built by selecting 10 to 15 MIR spectra of samples from each bacterium on each substrate (CB, TB, wood, glass, and SS, for 225 MIR spectra). Next, these spectra were preprocessed based on their first derivative (order: 2, window: 15 pt.) and mean centered for all substrates. In addition, to obtain optimal results, standard normal variate preprocessing was used for the data that were acquired for wood substrates. The data from *Bt, Ec,* and *Se* were run together in the PCA models, and the variance that was described by each PC was examined for each substrate.

Table 4.2. Classification between groups of bacteria (*Bt) Bacillus thuringiensis, (Ec) Escherichia coli,* and *(Se) Staphylococcus epidermidis* on different substrates.

		Predicted discrimination			
Actual discrimination	Group size	***Bt***	***Ec***	***Se***	**Substrates**
Bt	75	45**(60.0%)**	18(24.0%)	8(10.7%)	4(5.3%)
Ec	77	3(3.89%)	64**(83.1%)**	9(11.7%)	1(1.3%)
Se	75	14(18.7%)	3(4.0%)	50**(66.7%)**	8(10.7%)
Substrates	18	3(16.7%)	4(22.2%)	0(0.00%)	11**(61.1%)**
Percentage of cases correctly classified: **69.4%**					

Scores plot (PC-3 versus PC-1) for CB is shown in Fig. 4.6 (a). A poor separation between the different bacterium datasets is shown. PC-1 (52.84% variance) was correlated to the differences between the three bacteria. Overall, 60% of the *Bt* samples were classified as *Ec*, while 93% and 100% of the *Ec* and *Se* were correctly classified, respectively. Scores plot (PC-2 versus PC-1) on glass substrates indicated good separation between the *Bt* samples [see Fig. 4.6 (b)]. However, the *Ec* and *Se* samples

were 30% closer together, because they resulted in similar spectra when placed on glass.

This trend was also investigated for scores plot of PCs on TB (Fig. 4.7). The scores plots did not indicate class separation between the three types of bacteria on TB substrates [PC-2 versus PC-1, Fig. 4.7 (a)]. However, these plots only represent portions of the data variance (14.2% and 52.7%, respectively). For example, PC-3 versus PC-2 [Fig. 4.7 (b)] scores plot accounted for little variance (10.2% and 14.2%, respectively).

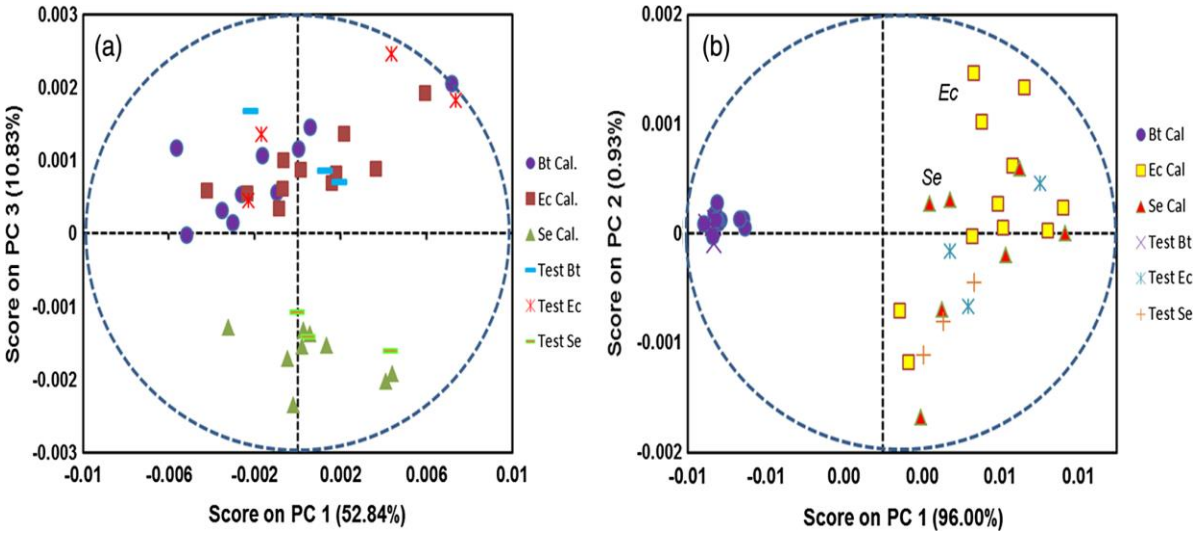

Figure 4.6. PCA for the QCL spectra of *Bacillus thuringiensis* (*Bt), Escherichia coli (Ec),* and *Staphylococcus epidermidis (Se)* deposited on (a) CB and (b) glass.

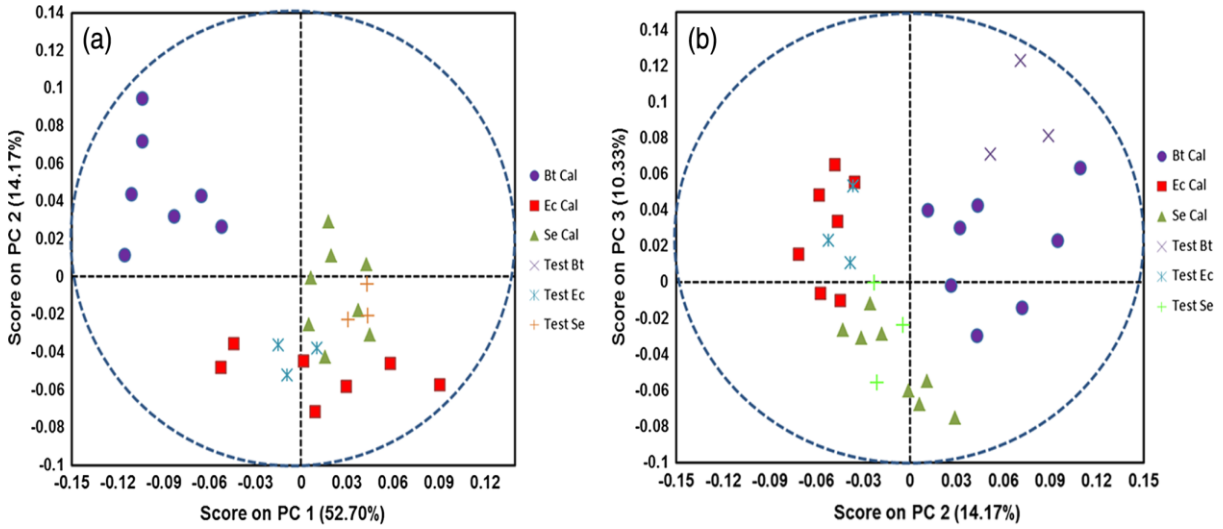

Figure 4.7. PCA for *Bacillus thuringiensis* (*Bt), Escherichia coli (Ec),* and *Staphylococcus epidermidis (Se)* on TB for (a) PC-2 versus PC-1 and (b) PC-3 versus PC-2.

The SS substrates resulted in the largest discrimination among bacterial species studied. However, scores plot (PC-2 13.9% versus PC-1 44.7%) indicated no significant variance between the three types of bacteria. *Se* samples (40.0%) were classified near *Bt* and *Ec* samples (94%) on the substrates. These results suggest that the bacteria were differentiated by their cell wall characteristics [gram-positive and gram-negative, see Fig. 4.8 (a) and Table 4.1]. Scores plots for the bacteria deposited on wood substrates required a larger number of PCs (PC-3 5.65%, PC-4 3.17%, and PC-5 2.93%) for classification. In addition, the *Ec* samples were well classified [100%, as displayed in Fig. 4.8 (b); PC-2 10.7% versus PC-1 63.4%], whereas the Se samples (53.3%) were incorrectly characterized as *Bt*. Next, *Bt* samples were confused as Ec species (74.0%). These results in turn indicate that PCA can adequately discriminate between these three types of bacteria. However, PCA, which is frequently used as an unsupervised classification method, is not statistically powerful enough to achieve class separation, because it is not effective when “within-group” variations are larger than

"between-group" variations. In this case, the use of supervised classification methods, such as PLSDA, must be considered.

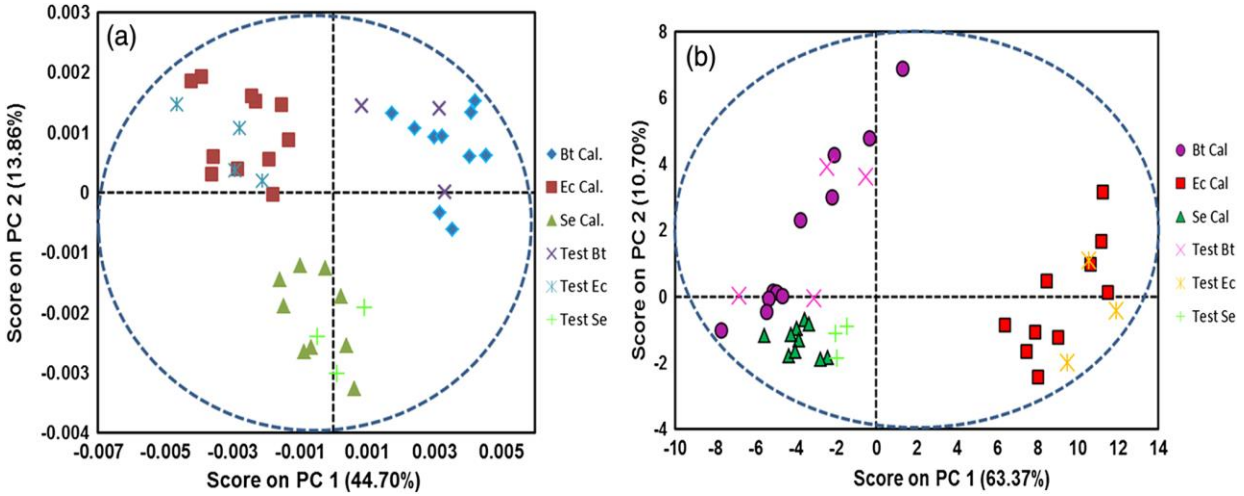

Figure 4.8. The PCA for QCL spectra of *Bacillus thuringiensis* (*Bt), Escherichia coli (Ec),* and *Staphylococcus epidermidis (Se)* deposited on (a) SS and (b) wood.

The PLS-DA was used as a chemometrics tool and as a classification method for differentiating between bacterial species (*Bt, Ec*, and *Se*) on five different substrates. In PLS-DA, sensitivity is defined as the estimated experimental percentage of correctly classified samples. In addition, specificity is defined as the estimated experimental percentage of the samples that are rejected by the other classes in the model. Thus, a perfect class model has sensitivity and specificity values of 100% [31]. Fifteen MIR sample spectra for each bacterium and surface were analyzed (225 MIR total spectra). Vibrational information was organized into two groups. Approximately 75% of the sample spectra were randomly selected as training sets for the calibration and cross-

validation (CV) models. The other 25% of the spectra were used as an external test set. To build a robust model, the spectral data were limited to the spectral ranges: 848 to 1012 cm^{-1}, 1022 to 1170 cm^{-1}, and 1173 to 1400 cm^{-1}. Next, these data were pretreated by smoothing (order: 0; window: 15 pts.) before using the first-derivative (order: 2, window: 15 pts.) preprocessing technique. A cross-validation procedure was performed by using venetian blinds with 10 splits. This procedure was used to build a classification model for 90% of the spectra. Then, the remaining 10% were assessed to determine the accuracy of the models. Smoothing and first-derivative preprocessing improved the visualization of the spectra of the bacteria. The discrimination models for each bacterium and its surface are shown in Figs. 9 to 11, which illustrate the predicted cross-validated classes for each sample (as shown in the PLS-DA plots).

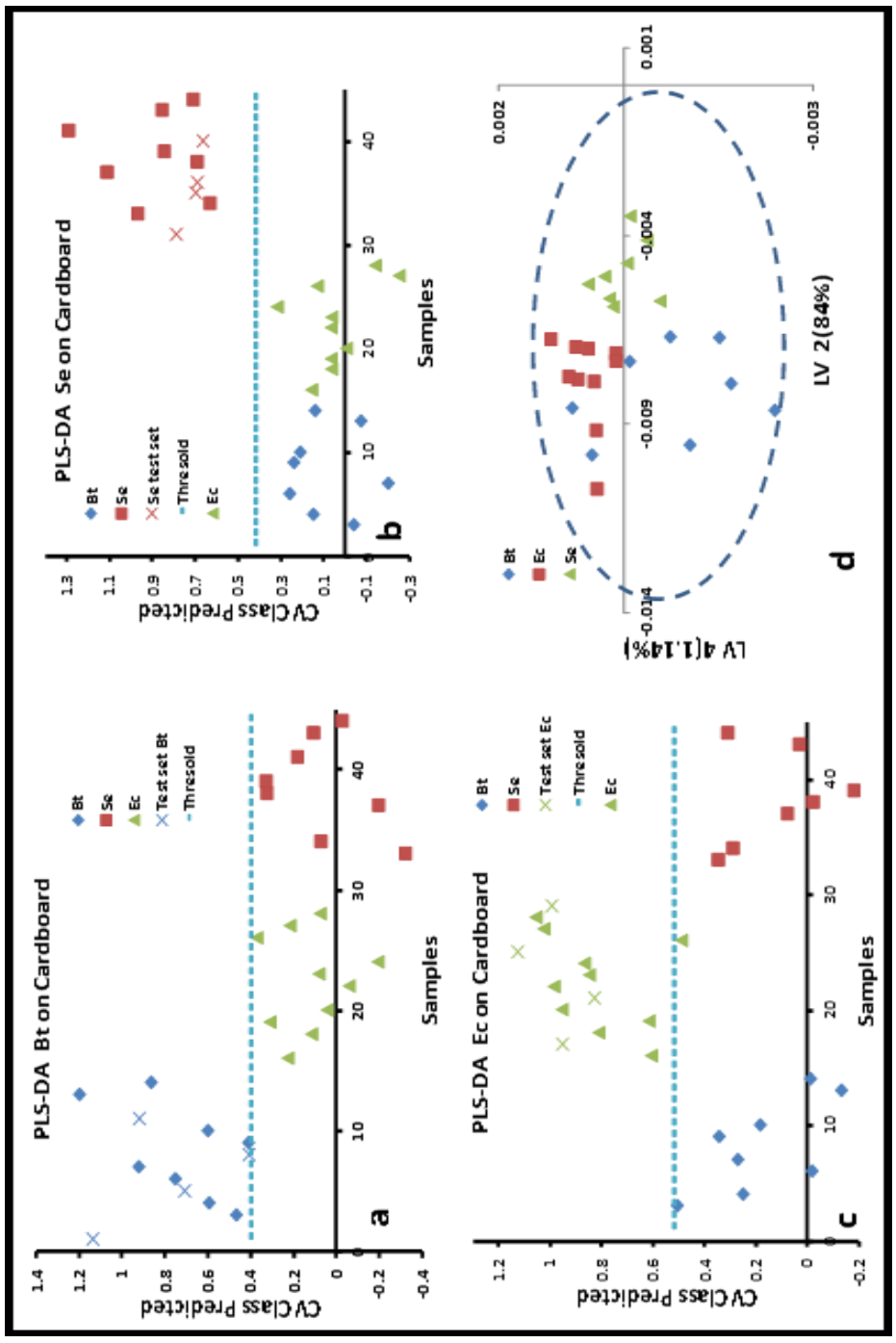

Figure 4.9. Partial least squares-discriminant analysis (PLS-DA) plots for discriminating bacteria on CB: (a) cross-validation (CV) and prediction (PRED) of *Bacillus thuringiensis* (Bt) on CB; (b) CV and PRED of *Staphylococcus epidermidis (Se)* on CB; (c) CV and PRED of *Escherichia coli (Ec)* on CB; (d) percent variation accounted for by each latent variable (LV) used in the model for each specimen on CB.

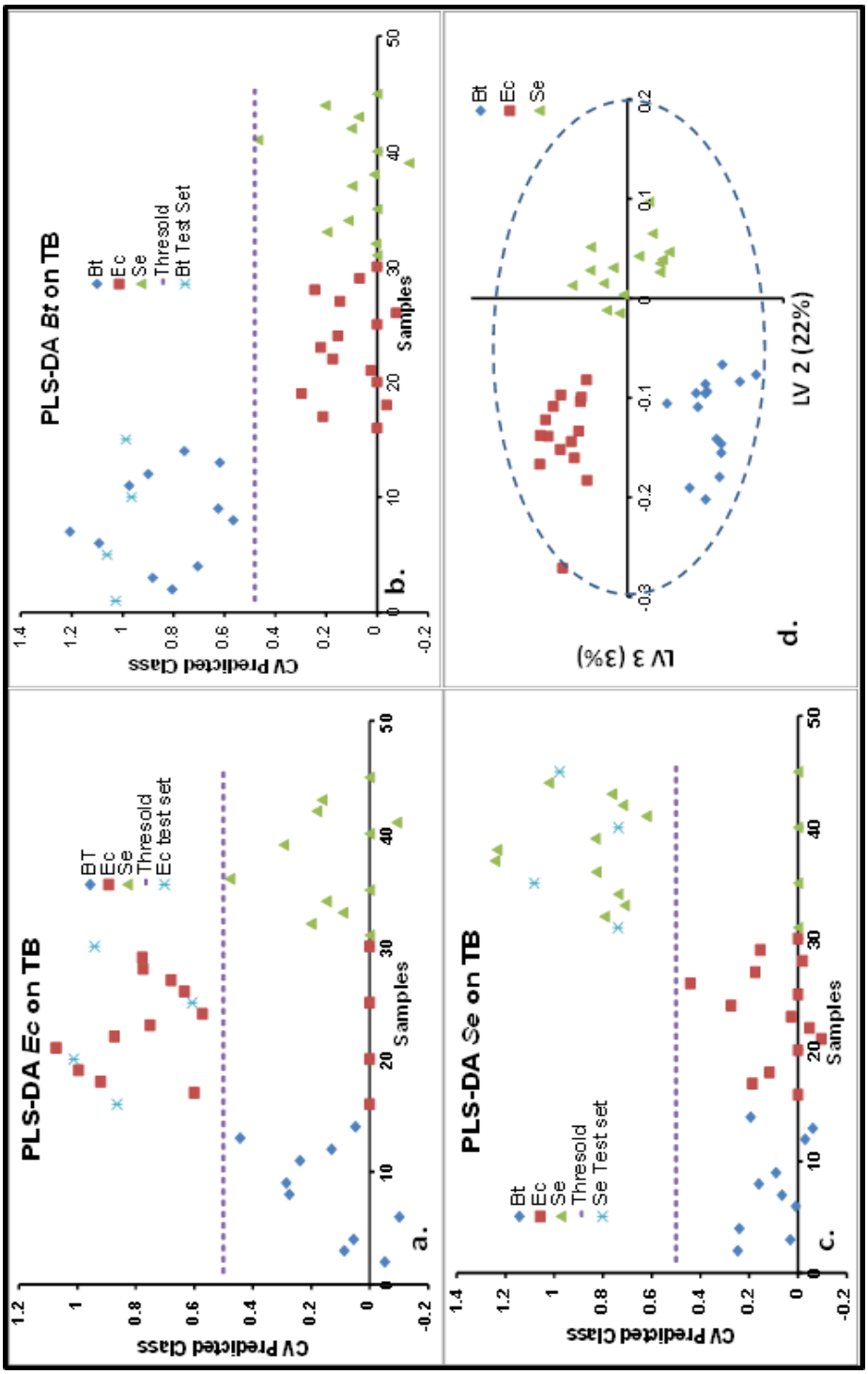

Figure 4.10. PLS-DA plots for discriminating bacteria on luggage: (a) CV and PRED of *Escherichia coli (Ec)* on TB; (b) CV and PRED of *Bacillus thuringiensis* (*Bt)* on TB; (c) CV and PRED of *Staphylococcus epidermidis (Se)* on TB; (d) percentage variation accounted for by each LV used in the model for each specimen on TB.

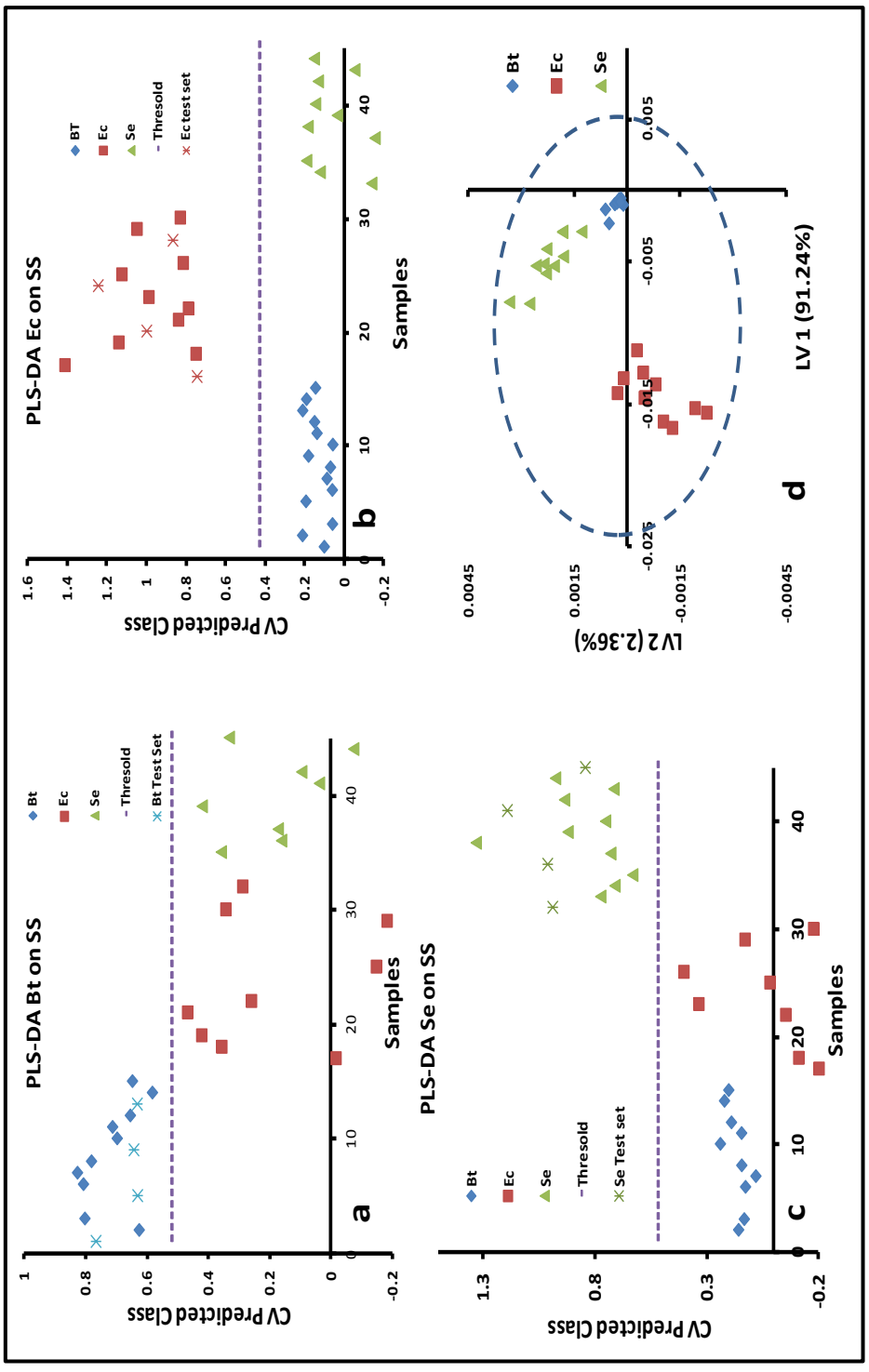

Figure 4.11. PLS-DA plots for discriminating bacteria on SS: (a) CV and PRED of *Bacillus thuringiensis* (*Bt)* on SS; (b) CV and PRED of *Escherichia coli (Ec)* on SS; (c) CV and PRED of *Staphylococcus epidermidis (Se)* on SS; (d) percentage variation accounted for by each LV used in the model for each specimen on SS.

The outlier data were determined by the evaluation of residuals versus Hotelling's T^2 plot on PLS Toolbox™ software for MATLAB®. According to the plot, the data with both high-residual variance and high leverage are outliers and can distort the model. Five percent of the calibration data were detected as outliers in calibration and cross-validation process and were removed from the analysis.

The discriminated bacterium class was located at approximately 1, while the other bacteria classes were located at approximately 0. The dashed line denotes the threshold parameter. These PLS-DA models were evaluated with several statistical parameters, including sensitivity, specificity, classification error of calibration, cross-validation (CV), and prediction (PRED) of the lowest latent variable. These values are shown in Table 4.3.

Table 4.3. The PLS-DA summary for discriminating bacteria on substrates.

PLS-DA	**Stainless steel**			**Travel baggage**			**Cardboard**			**Wood**			**Glass**		
Parameter	**Bt**	**Ec**	**Se**	**Bt**	**Ec**	**Se**	**Bt**	**Ec**	**Se**	**Bt**	**Ec**	**Se**	**Bt**	**Ec**	**Se**
Sensitivity (CV)	100	100	100	100	100	100	100	90	100	100	100	100	100	100	100
Specificity (CV)	100	100	100	96	100	96	100	100	100	100	100	100	100	100	60
Specificity (PRED)	100	100	100	100	100	100	100	100	100	100	100	100	100	100	100
Specificity (PRED)	100	100	75	100	100	88	100	100	100	100	100	100	100	100	80
Class. Err (PRED)	0.00	0.00	0.13	0.00	0.00	0.06	0.00	0.00	0.00	0.00	0.00	0.00	0.00	0.00	0.20
Num. LVs	4	4	4	4	4	4	4	4	4	5	5	5	5	5	5
RMSEC	0.32	0.19	0.25	0.22	0.25	0.20	0.27	0.27	0.20	0.24	0.13	0.22	0.19	0.09	0.22
RMSEP	0.28	0.20	0.24	0.14	0.19	0.20	0.25	0.20	0.20	0.23	0.19	0.28	0.26	0.21	0.37

Bacillus thuringiensis (*Bt), Escherichia coli (Ec),* and *Staphylococcus epidermidis (Se).*

Based on these results, all the bacteria classes were successfully classified with only four latent variables. Sensitivity and specificity values of 100% for *Bt, Ec*, and *Se* were obtained for CB, TB, SS, wood, and glass. The root mean square error of cross-validation (RMSECV) and root mean square error of prediction (RMSEP) values were below 0.30, 0.35, 0.25, 0.30, and 0.40 for all the bacteria on CB, SS, TB, wood, and glass, respectively. These statistical parameters confirm that the PLS-DA performed significantly better than PCA in discriminating between bacterial strains on the substrates investigated.

4.4. Conclusions

This study was aimed to detect and discriminate between bacteria cells on different substrates using QCL spectroscopy. The MIR diffuse reflectance spectroscopy was used on the range of 840 to 1440 cm^{-1}. In addition, PCA and PLS-DA classification models were built. Although the spectra appear very similar, slight differences occurred and revealed spectral variations. The obtained results demonstrated that the use of MIR spectroscopy (840 to 1440 cm^{-1}) with multivariate PCA and PLS-DA was useful for discriminating between bacterial strains (*Bt, Ec,* and *Se*) on various substrates. In addition, QCL spectroscopy was highly suitable for detecting microorganisms on different substrates, providing a quick response and analysis. Furthermore, this new technology can potentially be used to identify biological contaminants on surfaces and provides fast and accurate analyses for security and quality control purposes when nondestructive analytical methods are preferred. Substrate porosity clearly plays an important role in diminishing the number of microorganisms available to reflect MIR light

on the substrate surface. This aspect needs to be addressed in detail in the further studies.

In summary, QCL spectroscopy was successfully used to identify biological samples in complex matrices by using their characteristic fingerprint spectrum in the MIR. Differentiation and discrimination of microorganisms from the acquired spectra were achieved by using chemometrics tools such as PCA and PLS-DA. Overall, PLS-DA performed significantly better than PCA in the analyses of bacteria in this study.

4.5. References

[1]. G. Zhao, F. Xing, and S. Deng, “A disposable amperometric enzyme immunosensor for rapid detection of Vibrio parahaemolyticus in food based on agarose/nano-Au membrane and screen-printed electrode,” Electrochem. Commun. 9(6), 1263–1268 (2007).

[2]. V.C.H. Wu, S. Chen, and C.S. Lin, “Real-time detection of Escherichia coli O157:H7 sequences using a circulating-flow system of quartz crystal microbalance,” Biosens. Bioelectron. 22, 2967–2975 (2007).

[3]. U. Siripatrawan and B. R. Harte, “Solid phase microextraction/gas chromatography/mass spectrometry integrated with chemometrics for detection of Salmonella typhimurium contamination in a packaged fresh vegetable,” Anal. Chim. Acta 581, 63–70 (2007).

[4]. N.S. Foster, S.E. Thompson, N.B. Valentine, J.E. Amonette, T.J. Johnson. “Identification of sporulated and vegetative bacteria using statistical analysis of Fourier transform mid-infrared transmission data,” Appl. Spectrosc. 58(2), 203–211 (2004).

[5]. S.E. Thompson, N.S. Foster, T.J. Johnson, N.B. Valentine, J.E. Amonette. “Identification of bacterial spores using statistical analysis of Fourier transform infrared photoacoustic spectroscopy data,” Appl. Spectrosc. 57(8), 893–899 (2003).

[6]. F.K. Tittel, D. Richter and A. Fried, “Mid-Infrared Laser Applications in Spectroscopy”, I.T. Sorokina, K.L. Vodopyanov (Eds.): Solid-State Mid-Infrared Laser Sources, Topics Appl. Phys. 89, 445–516, (2003).

[7]. J.R. Castro, W. Ortiz, N. Galan, A. Figueroa, L.C. Pacheco and S.P. Hernandez. “Multivariate analysis in vibrational spectroscopy of highly energetic materials and

chemical warfare agents simulants," Chapter 9 in Multivariate Analysis in Management, Engineering and the Sciences, L. V. de Freitas and A. P. Barbosa-Rodriguez de Freitas, Eds., pp. 160–187, InTech, Janeza, Croatia (2013).

[8]. A. A. Kosterev and F. K. Tittel, "Chemical sensors based on quantum cascade lasers," IEEE J. Quant. Electron. 38(6), 582–591 (2002).

[9]. L. Hvozdara, N. Pennington, M. Kraft, M. Karlowatz, B. Miziakoff. "Quantum cascade lasers for mid-infrared spectroscopy," Vib. Spectrosc. 30, 53–58 (2002).

[10]. T.J. Johnson, N. B. Valentine, and S.W. Sharpe, "Mid-infrared versus far-infrared (THz) relative intensities of room-temperature Bacillus spores," Chem. Phys. Lett. 403, 152–157 (2005).

[11]. H. Félix-Rivera, R. González, G.D. Rodríguez, O.M. Primera-Pedrozo, C. Ríos-Velázquez, and S. Hernández- Rivera, "Improving SERS detection of Bacillus thuringiensis using silver nanoparticles reduced with hydroxylamine and with citrate capped borohydride," Int. J. Spectrosc. 2011, 9 (2011).

[12]. D.H. Bergey, Bergye's Manual of Systematic Bacteriology, Vols. 1–2, Lippincot Williams & Wilkins, Baltimore (1984).

[13]. C. Carlos, D.A. Marreto, R.J. Poppi, M.I. Z. Sato, L.M. M. Ottoboni, "Fourier transform infrared microspectroscopy as a bacterial source tracking tool to discriminate fecal E. coli strains," Microchem. J. 99, 15–19 (2011).

[14]. D. Naumann, "Infrared spectroscopy in microbiology," in Encyclopedia of Analytical Chemistry, R. A. Meyers, Ed., pp. 102– 131, John Wiley & Sons, Chichester (2000).

[15]. D. Naumann, C. P. Schultz, and D. Helm, "What can infrared spectroscopy tell us about the structure and composition of intact bacterial cells," in Infrared Spectroscopy of Biomolecules, H. H. Mantsch and D. Chapman, Eds., pp. 279–310, Wiley-Liss, New York (1996).

[16]. S. F. Lin, H. Schraft, and M. W. Griffiths, "Identification of Bacillus cereus by Fourier transform infrared spectroscopy (FTIR)," J. Food Prot. 61(7), 921–923 (1998).

[17]. O.M. Primera-Pedrozo, J. I. Jerez-Rozo, E De La Cruz-Montoya, T. Luna-Pineda, L. C. Pacheco-Londoño, and S. P. Hernández-Rivera "Nanotechnology-based detection of explosives and biological agents simulants," IEEE Sens. J. 8(6), 963 (2008).

[18]. O.M. Primera-Pedrozo, L.C. Pacheco-Londoño, L.F. De la Torre-Quintana, S.P. Hernandez-Rivera, R. T. Chamberlain, R. T. Lareau. "Use of fiber optic couple FT-IR in detection of explosives on surfaces," Proc. SPIE 5403, 237–245 (2004).

[19]. Y. Soto-Feliciano, O.M. Primera-Pedrozo, L.C. Pacheco-Londoño and S.P. Hernandez-Rivera. "Temperature dependence of detection limits of TNT on metallic surfaces using fiber optic coupled FTIR," Proc. SPIE 6201, 62012H (2006).

[20]. J.R. Castro-Suarez, L.C. Pacheco-Londoño, W. Ortiz-Rivera, M. Vélez-Reyes, M. Diem and S. P. Hernandez-Rivera, “Open path FTIR detection of threat chemicals in air and on surfaces,” Proc. SPIE 8012, 801209 (2011).
[21]. S.J. Barrington, H. Bird, D. Hurst, A.J. S. McIntosh, P. Spencer, S. H. Pelfrey and M.J. Baker, “Spectroscopic investigations of surface eposited biological warfare simulants,” Proc. SPIE 8358, 83580E (2012).
[22]. G. Hans-Ulrich and B. Yan, Eds., Infrared and Raman Spectroscopy of Biological Materials, Vol. 24, Practical Spectroscopy Series, Marcel Dekker, Inc., New York (2001).
[23]. J. L. Chalmers and P. R. Griffiths, Eds., Handbook of Vibrational Spectroscopy, Theory and Instrumentation, Vol. 1, John Wiley & Sons Ltd., Chichester (2002).
[24]. H. C. Van der Mei, D. Naumann, and H. J. Busscher, “Grouping of oral streptococcal species using Fourier-transform infrared spectroscopy in comparison with classical microbiological identification,” Arch. Oral Biol. 38, 1013–1019 (1993).
[25]. A.C. Samuels A.P. Snyder, D.S. Amant, D.K. Emge, J. Minter, M. Campbell, A. tripathi. “Classification of select category A and B bacteria by Fourier transform infrared spectroscopy,” Proc. SPIE 6954, 695413 (2008).
[26]. R. Davis and L.J. Mauer, “Fourier transform infrared (FT-IR) spectroscopy: a rapid tool for detection and analysis of foodborne pathogenic bacteria,” Appl. Microbiol. 2(1), 1582–1594 (2010).
[27]. M.J. Willey, L.M. Sherwood, and C.J. Woolverton, Prescott, Harley and Klien’s Microbiology, 7th ed., McGraw-Hill Companies, New York (2008).
[28]. D. Naumann, D. Helm, and H. Labischinski, “Microbiological characterizations by FT-IR spectroscopy,” Nature 351, 81–82 (1991).
[29]. D. Helm, H. Labischinski, and D. Naumann, “Elaboration of a procedure for identification of bacteria using Fourier transform IR spectral libraries: a stepwise correlation approach,” J. Microbiol. Methods 14, 127–142 (1991).
[30]. D. Naumann, “FT-IR and FT-Raman spectroscopy in biomedical research,” in Chapter 9 in Infrared and Raman Spectroscopy of Biological Materials, H.-U. Gremlich and B. Yan, Eds., pp. 323– 378, Marcel Dekker, New York (2001).
[31]. M. Forina, C. Armanino, R. Leard, G. Drava, “A class modeling technique based on potential functions,” J. Chemometr. 5, 435–453 (1991).

Chapter 5

SPECTROSCOPIC DETECTION OF BACTERIA USING TRANSMISSION MODE QCLS

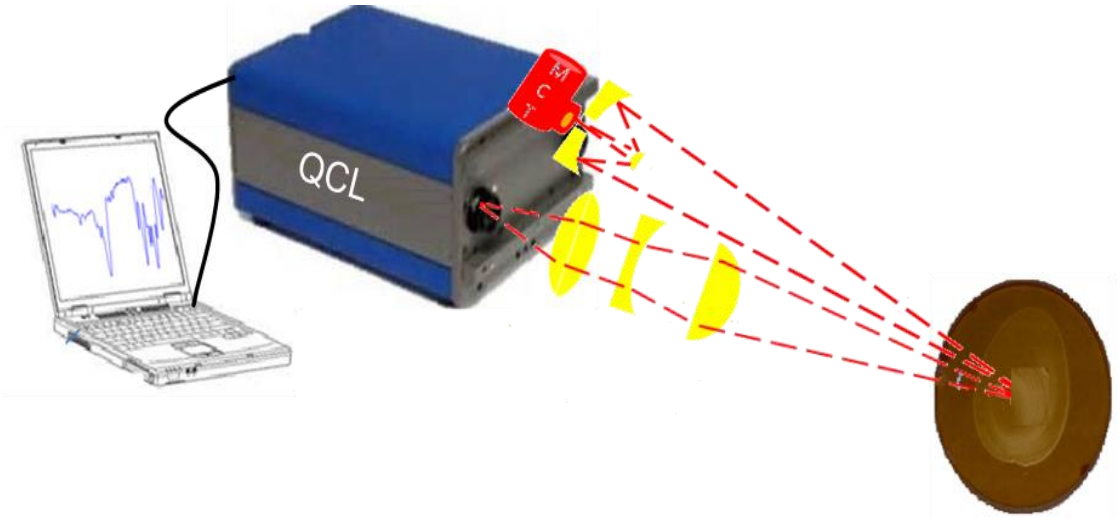

Transmission mode QCLS of microorganisms.

5.1. Introduction

Biological contamination represents a hazardous threat for food-related industries and plays an important role in pharmaceutical and biotechnology clean-room production environments. In health related fields, fast identification of microorganisms is necessary, because the time required for the identification of bacteria and viruses is an important determinant of infection-related mortality rates of hospitalized patients. The development of new techniques for the identification of microorganisms, which include molecular methods, such as mass spectrometry, electrospray ionization and matrix-

assisted laser desorption ionization, Fourier transform infrared (FT-IR) spectroscopy, Raman spectroscopy and surface enhanced Raman scattering (SERS) has been addressed in several related publications [1-6]. Vibrational spectroscopy, in particular, has gained considerable attention because generally speaking, there is no need to add chemical dyes or labels for identification provides a definitive means for identifying the species involved and is able to distinguish between target microorganisms and the substrates they are adhered to. In principle, any technique that can be used to obtain vibrational data from substrates (IR, Raman, etc.) can be applied to the study of microorganisms. In addition, there are a number of techniques which have been specifically developed to study the vibrations of molecular species at interfaces based on IR spectroscopy in several of its modalities, including mid-IR (MIR) absorption/reflection in which the vibrational spectrum of a molecule is considered to be a unique physical property. The characteristics of the absorbed/reflected light depend on the molecules found within the sample and the environment in which the molecules are found. However, simplicity of sample preparation and speed of analysis are important advantages when vibrational methods are compared to classical microbial identifications tools [7]. Other advantages of vibrational spectroscopy are that it is a rapid, specific, and a noninvasive analytical method.

Several methods can be used for biological analyses of culture grown colonies to differentiate bacterial spores from other bacteria and from each other. Some of these require special equipment which is not present in an average biological laboratory, whereas others rely on sophisticated electronic equipment and techniques. These types of analyses are usually time consuming and labor intensive, and require expertise in

sample preparation, as well as delay in identification due to the fact that spores, for example, have to be germinated and grown in culture media to sufficient cell numbers until they can be measured. In contrast to these traditional techniques, optical spectroscopy holds promise as a rapid, label-free analytical strategy, which is potentially labor free and time saving, and requires a minimum amount of training. In particular, if appropriate data processing, particularly in the event of exposure to pathogen microorganisms is detected within the first few days, the majority of victims can be treated successfully [5]. Cultures of microorganisms can be grown on any medium that is appropriate for their isolation and cultivation. Identification and characterization of bacteria starts by inspecting the colony morphology when the cells have been cultured in solid media, followed by microscopic analysis of gram-stained preparations [8].

As vibrational spectra of bacterial cells consist of signal contributions of all components in the cells, they reflect their overall molecular composition. Thus, the aim of the present research was to compare measured FT-IR spectra with transmission mode spectra obtained with quantum cascade laser spectroscopy (QCLS) operating in the MIR region, in order to identify and discriminate vegetative bacteria by applying established multivariate techniques to the spectra obtained. Based on the above considerations, this work addressed the demonstration of the capability of this spectroscopic technique in identification and discrimination of bacterial cells between strains such as *Bacillus thuringiensis (Bt), Escherichia coli (Ec)* and *Staphylococcus epidermidis (Se)*. Research was also aimed at demonstrating that the technique is suitable for detection of microorganisms on MIR transparent substrates.

5.2. Materials and methods

5.2.1. Materials

Zinc selenide (ZnSe) discs obtained from Specac, Inc. (Swedesboro, NJ, USA) were used as support material for transferring samples of bacteria. ZnSe is chemically inert, non-hygroscopic and is very effective in many infrared optical applications due to its extremely low bulk losses of IR light by absorption, high resistance to thermal shock and stability in virtually all environments. It can be easily machined into IR optical devices and is transparent in a wide spectral range from the yellow region (visible) to the far IR.

5.2.2. Preparation of bacterial samples.

Bacterial strains of Bt (ATCC # 35646), Ec (ATCC # 8789), and Se (ATCC # 2228), were provided by the Microbial Biotechnology and Bioprospecting Lab (Biology Department, University of Puerto Rico-Mayagüez, Mayagüez, PR, USA). Samples were prepared following the protocol reported by Padilla et al., [9]. In brief, pure cultures were grown using Miller modified Luria-Bertani (LB) agar and broth (Thermo-Fisher Scientific, Waltham, MA, USA). After satisfactory growths were achieved in agar, colonies of *Bt, Ec* and *Se* were isolated on LB plates and inoculated into 5.0 mL LB broth or tryptic soy broth (TSB) and allowed to grow overnight. *Se* and *Bt* were placed in an orbital shaker at 32 °C (~120 rpm) for 24 h and cultured for 72 h. *Ec* was placed in an orbital shaker at 37 °C until growth of 5 h post inoculation. Sub-cultures were diluted 1:50 in appropriate media and centrifuged at 5K x g for 5 min at 4 °C until pellet formation. Pellets of bacteria were washed once with 20 mL of 1% phosphate buffered saline solution (PBS) to remove growth media. The pellets were resuspended in 4.0 mL

of PBS (*Ec* and *Se*) or distilled water (*Bt*) before allowing them to grow for 72 h at 32°C and at 250 rpm to induce spores production. Harvested spores were stored at 4 °C in distilled, deionized H_2O until spectroscopic measurements were made. Serial dilution followed by plating on LB agar in order to count bacteria suspended in PBS. Plates were incubated at 37 °C for ~24 h in order to form colonies. Concentration of the stock suspension of bacteria was determined by back calculating the dilution series.

5.2.3. Experimental setup

A MIR spectrometer (LaserScope™, Block Engineering, LLC, Marlborough, MA, USA) based on QCL technology, was used for data acquisition in the MIR: 875-1405 cm^{-1} of the bacterial suspension samples. QCL are different from traditional semiconductor laser diodes, which use p-n junctions for light emission. Instead, QCLs have multiple active regions, which are composed of a multilayered semiconductor material structure, specially designed to have the appropriate electronic bands [10]. Figure 5.1 shows a schematic diagram of the QCL spectrometer set up for transmission/absorption measurements, rather than the more common reflectance mode setup.

A key feature of the QCL spectrometer is the high spectral radiance or brightness of the QCL source, which results in high signal to noise ratios (SNRs) and excellent quality data from samples compared to FT-IR equipped with conventional thermal sources particularly when analyzing thick, highly diffuse, or very small samples. However, FT-IR spectrometers are important in obtaining reference spectra of bacterial samples. A bench FT-IR interferometer, model IFS 66v/S FT-IR (Bruker Optics, Billerica, MA, USA)

was used to characterize the microorganisms of interest and to provide reference spectra to assist in spectral assignment of bacteria studied.

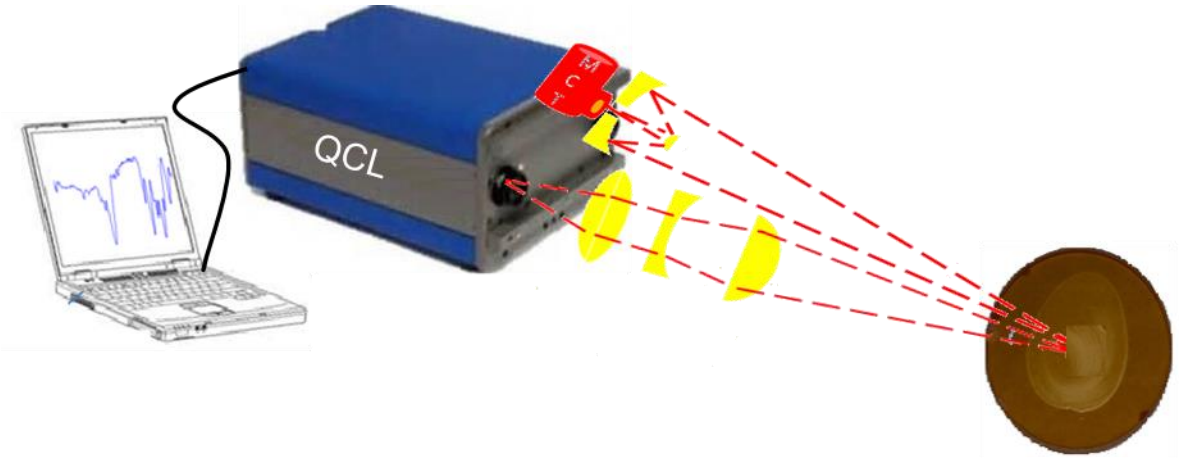

Figure 5.1. Transmission mode QCLS setup.

5.2.4. Data acquisition and analysis

Bacterial sample of 10 µL each with concentrations at $5.9x10^8$/$5.0x10^1$, $3.5x10^7$ and $9.5x10^7$ colony forming units per milliliter (CFU/mL) for *Bt* vegetative cell/endospores, *Ec* and *Se* respectively, were deposited on ZnSe discs for MIR transmission measurements. Samples were dried at 40 °C in an incubator for 5-10 min prior to analysis. Four replicas of each kind bacteria sample were analyzed.

OPUS™ 6.0 spectroscopic suite (Bruker Optics) was used to analyze the data obtained. During the analysis performed, the spectra were normalized in order to allow a proper comparison of the spectra. Partial least squares combined with linear discriminant analysis (PLS-DA) was used for classification of samples by reducing the number of variables and determining if group differences will dominate the total variability of the samples. PLS-DA is a supervised discriminant analysis methodology derived from PLS

regression algorithm. PLS not only considers the variation in the original multi-dimensional dataset generated by analytical measurement (e.g., MIR spectra), but also simultaneously takes into account the variation in the original multidimensional value dataset (e.g., concentration). This algorithm was applied in the MATLAB™ computational environment (The MathWorks, Inc., Natick, MA, USA), using the PLS-Toolbox, v. 7.0.3 (Eigenvector Research, Inc., Wenatchee, WA, USA).

5.3. Results and discussion

5.3.1. FT-IR Detection of microorganisms

Conventional micro FT-IR in transmission mode was employed as a reference spectroscopic technique for establishing vibrational signatures of bacteria utilized in this study and is shown in Figure 5.2.

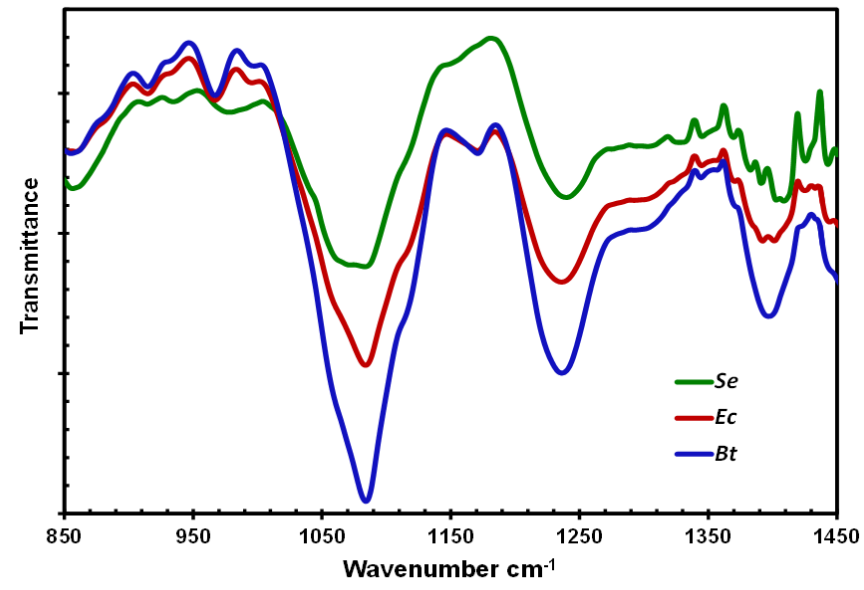

Figure 5.2. MIR spectra of bacteria deposited on ZnSe discs by FT-IR.

5.3.2. QCLS Detection and discrimination

MIR spectra of bacteria acquired on the QCL spectroscopic system in the spectral region from 875 to 1400 are illustrated in Figure 5.3. It is possible to observe the different vibrational spectroscopic signatures of biological components of bacteria clearly. There is difference in the appearance of the QCL spectra in the region between 900 and 1200 cm^{-1} in which P–O–C and C–O–C stretches of oligo- and polysaccharides occur [11, 12]. However it is more practical to use chemometric tools to have a better spectral discrimination of bacteria.

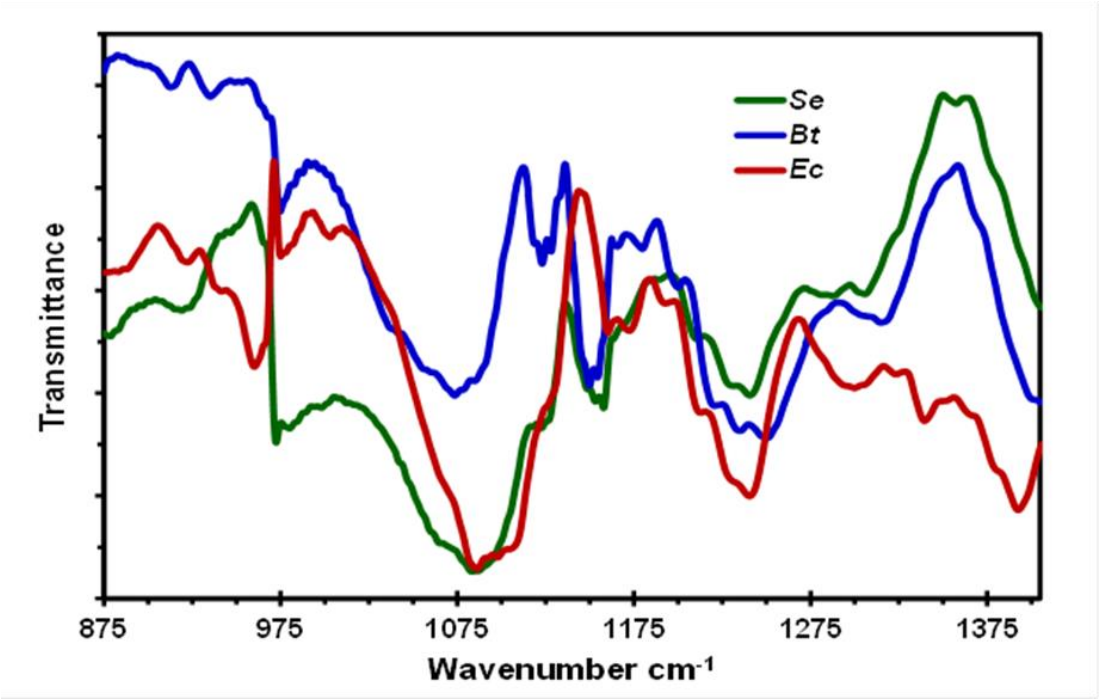

Figure 5.3. MIR spectra of bacteria deposited on ZnSe discs by QCLS.

IR spectra were analyzed for identification of bacteria for bending vibrations of fatty acid, proteins, phosphate containing compounds and carbohydrates bands of the

microbial cell wall [7]. Tentative band assignments used in bacterial identification of functional groups associated with major vibrational bands in the MIR following Padilla-Jimenez, et al., [13] are shown in Figs. 5.4, 5.5 and 5.6. Spectra in these figures display representative QCLS spectra in transmittance mode and in reflectance mode for each bacterium and a comparison with corresponding reference FT-IR spectra. A QCL based MIR dispersive spectrometer: LaserScan™, model 710 (Block Engineering) operating in reflectance mode was used to measure the reflectance spectra of the bacterial species. The main differences found between the two QCLS modes arise from spectral artifacts caused from the gap junction between two adjacent QCL laser diodes that affected even more the absorption/transmission QCLS (LaserScope) as can be observed in Figs. 5.4 to 5.6.

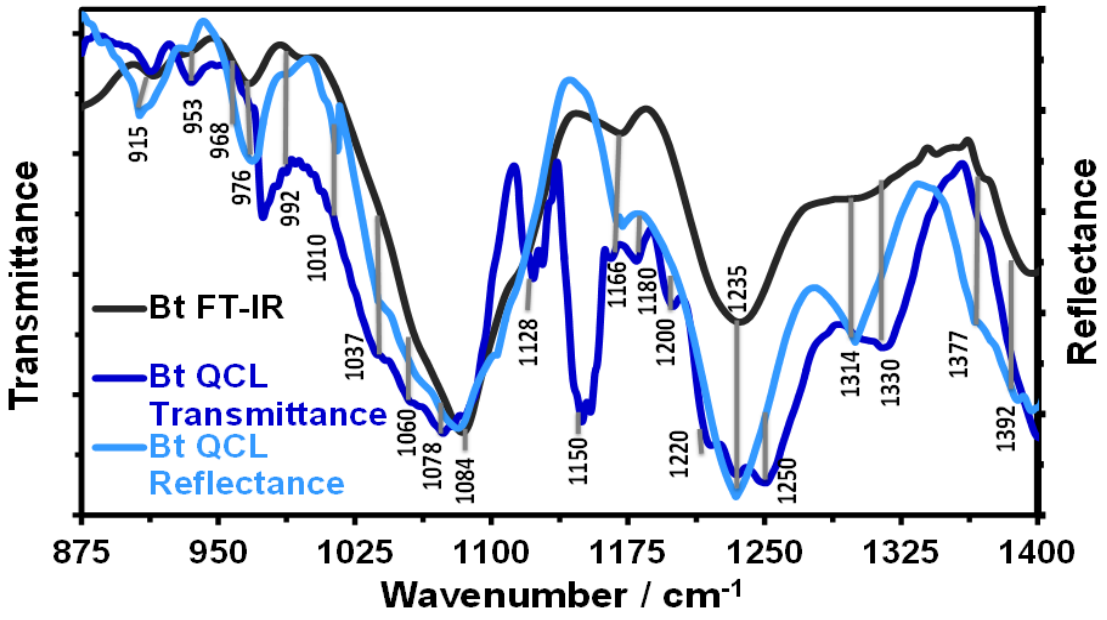

Figure 5.4. Comparison between *Bt* spectra QCLS in transmittance mode and in reflectance mode with FT-IR.

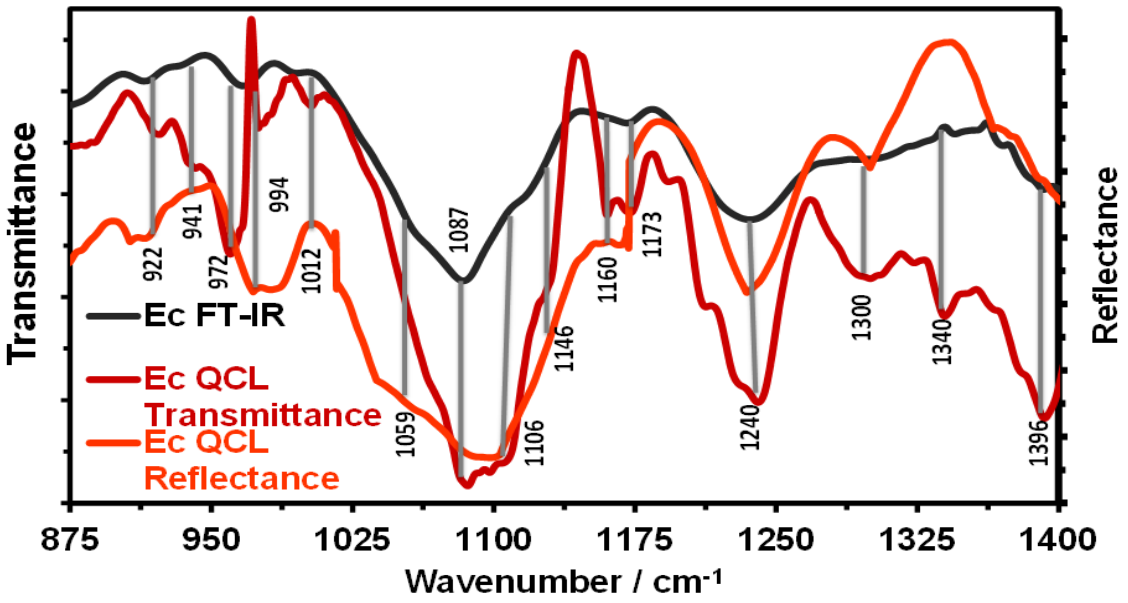

Figure 5.5. Comparison between *Ec* spectra QCLS in transmittance mode and in reflectance mode with FT-IR.

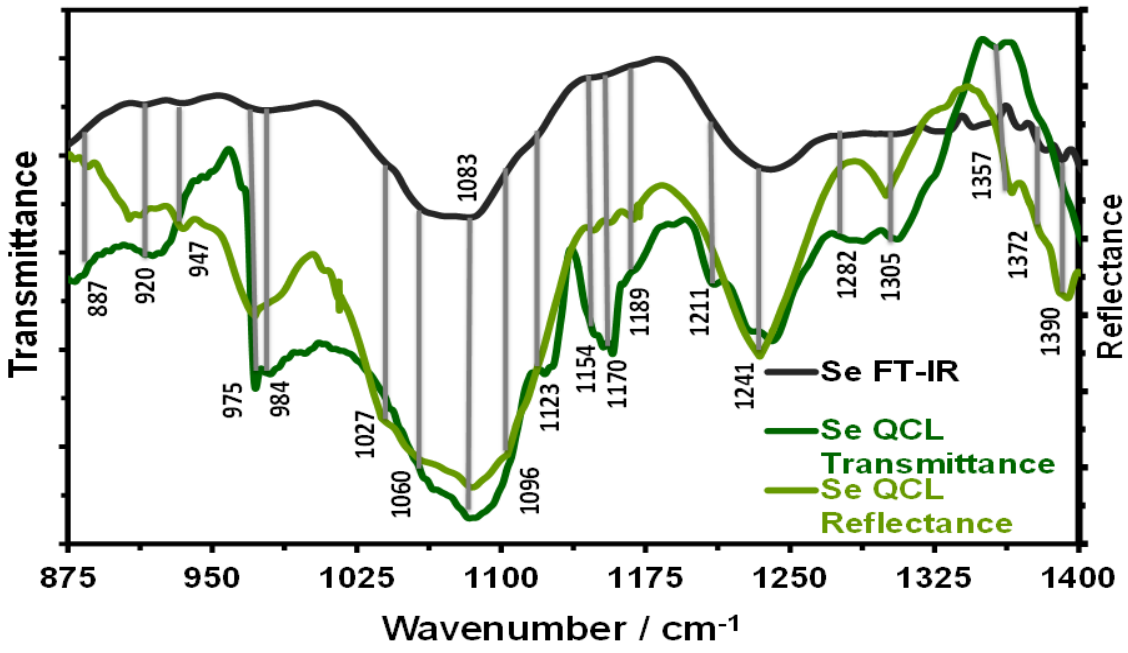

Figure 5.6. Comparison between *Se* spectra QCLS in transmittance mode and in reflectance mode with FT-IR

Two bacteria are gram-positive and one is gram-negative, according to cell membrane characteristics. Gram-positive bacteria contain teichoic acids that are covalently bound to the peptidoglycan whereas; gram-negative cells do not contain teichoic acids. One of the major components of the outer membrane of gram-negative bacteria is lipopolysaccharide [14]. Ribitol is a significant component of gram (+) bacterial membranes, for this reason in the MIR spectra measured on bacteria the characteristic bands of ribitol were identified. Vibrational modes at 1315, 1180, 1128, 1060, 1037, 953, 915, 889 cm^{-1} for *Bt* and 1357, 1282, 1211, 1189, 1123, 1025, 947, 915, 897 cm^{-1} for *Se* were observed that correspond to contributions of this component in a bacterial cell. The P=O asymmetric stretch of phosphodiesters in phospholipids on gram-negative bacteria was detected at 1240 and 1086 cm^{-1}. The notable peaks that distinguish vegetative cell forming endospores for bacillus were not observed.

5.3.3. PLS-DA multivariate analysis

Figure. 5.7, shows QCL spectra of bacteria from the three strains studied: *Bt, Ec* and *Se*. It was difficult to find differences in the raw QCL spectra between the different classes of bacteria at first sight. To prepare for applying multivariate analysis, data pre-treatments were applied. In particular, normalization and smoothing were used. PLS-DA was employed as chemometric tool as classification method to differentiate bacterial species.

Thirty QCL spectra of samples of each bacterium were obtained for a total of 90 total spectra. PLS-DA model was built on vibrational information in spectral region of 875-1400 cm^{-1}. The spectral data were normalized and pretreated employing a second-order

derivative (Savitzky-Golay) and improving the classification performance by reducing model complexity and achieving 100% of sensitivity and specificity for all bacteria. These values and other PLS-DA quantitative parameters such as root mean square error of cross validation (RMSECV) and root mean square error of prediction (RMSEP) with the lowest latent variable. These values are shown in Table 5.1, where important parameters such as, sensitivity and specificity are employed in PLS-DA. Sensitivity is defined as the estimated experimental percentage of correctly classified samples. Moreover, specificity is defined as the estimated experimental percentage of the samples that are rejected by the other classes in the model. Thus, a perfect class model has sensitivity and specificity values of 100 % [15].

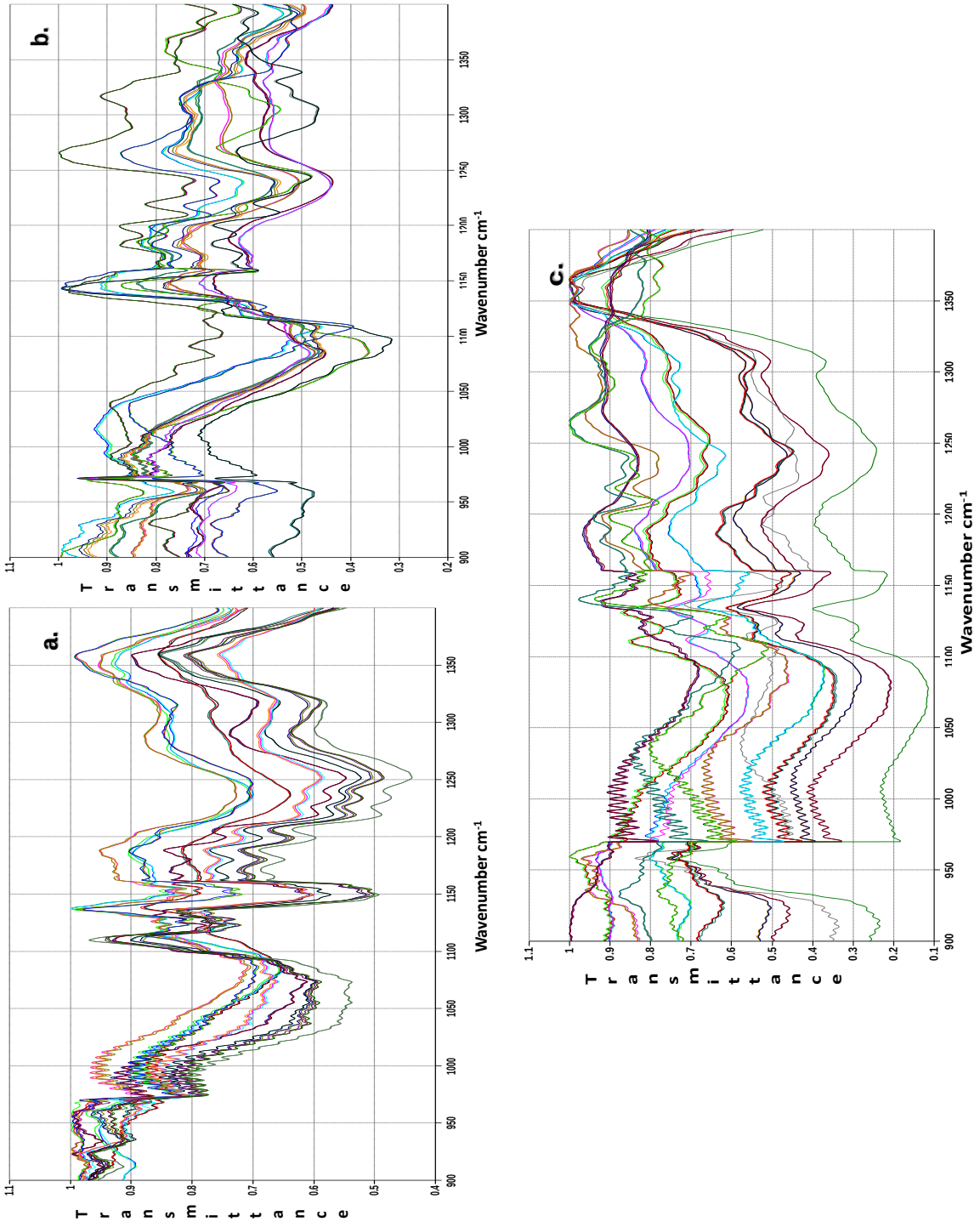

Figure 5.7. QCL raw spectra normalized of bacteria showing reproducibility of MIR signatures: **a.** *Bacillus thuringiensis* (*Bt);* **b.** *Escherichia coli (Ec)*; **c.** *Staphylococcus epidermidis (Se).*

Table 5.1. QCL PLS-DA summary for the discrimination of bacteria (*Bt) Bacillus thuringiensis, (Ec) Escherichia coli,* and *(Se) Staphylococcus epidermidis* on ZnSe.

PLS-DA Parameter	*Bt*	*Ec*	*Se*
Specificity (CV)	100	100	100
Sensitivity (PRED)	100	100	100
Specificity (PRED)	100	100	100
Class. Err (PRED):	0	0	0
Num. LVs	4	4	4
RMSECV	0.158	0.139	0.169
RMSEP	0.138	0.136	0.162

Spectroscopic data were separated two groups. Approximately 70% of the sample spectra were randomly selected as training set for the calibration and cross-validation (CV) models. The remaining 30% of the spectra were used as an external test set employing all the spectral range. Models were built by a cross-validation procedure performed by using venetian blinds with 10 splits. This procedure was used to build a classification model for 90% of the spectra. Then, the remaining 10% were assessed to determine the accuracy of the models. The discrimination models for each bacterium on ZnSe cell are shown in Figure 5.8, which illustrate the predicted cross-validated classes for each sample (as shown in the PLS-DA plots). Based on these results, all the bacteria classes were successfully classified with only four latent variables (LV). Sensitivity and specificity values of 100% for each bacterium and RMSECV and RMSEP values were below 0.2 for all the bacteria. These results corroborate that PLS-

DA was highly efficient in discriminating between bacterial strains on ZnSe employing QCLS.

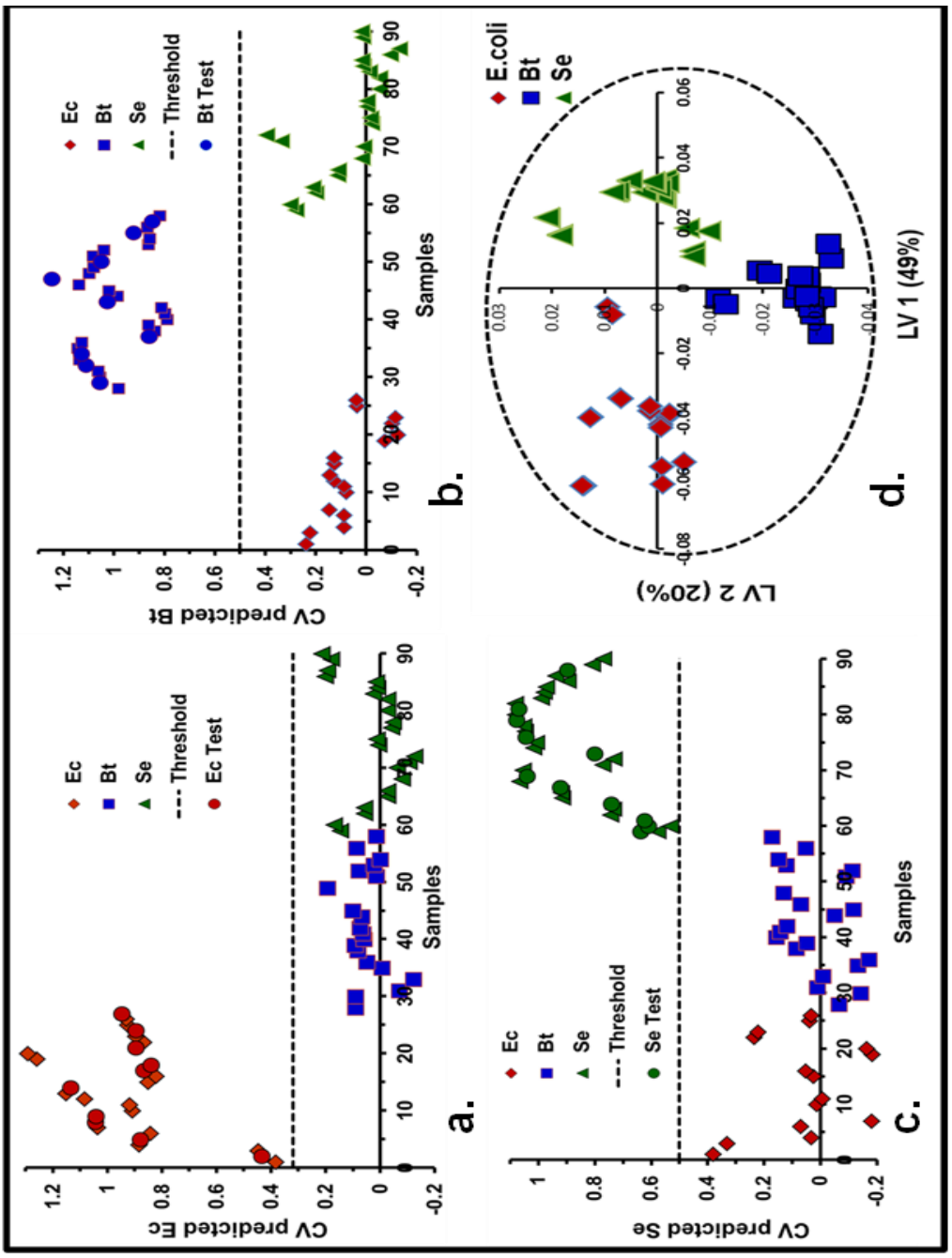

Figure 5.8. PLS-DA plots for discriminating bacteria on ZnSe discs: **(a).** cross-validation (CV) predicted of *Escherichia coli (Ec)*; **(b).** CV predicted of *Bacillus thuringiensis* (Bt); **(c).** CV predicted of *Staphylococcus epidermidis (Se)*; **(d).** Percent variation accounted for by each latent variable (LV) used in the model for each specimen.

5.4. Conclusions

Results obtained demonstrate that transmission mode QCLS, in the range of 875-1400 cm^{-1} produced high quality spectral information of bacterial species studied: *Bt*, *Ec* and *Se*. Results achieved are in excellent agreement with previously published QCL spectra obtained in reflectance mode and with reference spectra obtained in transmittance mode in the micro compartment of a bench FT-IR interferometer.

When transmittance mode QCL spectra were coupled to multivariate analysis (PLS-DA) a highly effective discrimination between bacterial strains deposited on ZnSe discs: *Bt, Ec,* and *Se* was achieved. PLS-DA classified correctly all bacterial samples using only four LV. Sensitivity and specificity values were 100% with very low values for RMSECV and RMSEP. The development of this new methodology for analysis of bacteria using transmittance mode QCLS provides a fast and accurate analysis in the detection of microorganisms accompanied to a great potential for discrimination between different and similar strains microorganisms as was demonstrated in this study.

5.5. References

[1] C.L. Wilkins, J.O. Lay, “Identification of Microorganisms by Mass Spectrometry”, Nature Reviews Microbiology. 2010. 8, 74-82.

[2] M.G. Kedney, K.B. Strunk, L.M. Giaquinto, J.A. Wagner, S. Pollack and W.A. Patton. “Identification of Bacteria Using Matrix-Assisted Laser Desorption Ionization Time-of-Flight Mass Spectrometry”. Biochemistry and Molecular Biology Education. 2007. 35 (6), 425–433.

[3] B.L. Van Baar. “Characterization of bacteria by matrix assisted laser desorption/ionization and electrospray mass spectrometry”. FEMS Microbiol. Rev. 2000. 24, 193–219.

[4] P.D. Nichols, J.M. Henson, J.B. Guckert, D.J. Nivens and D. C. White. “Fourier transform-infrared spectroscopic methods for microbial ecology: analysis of bacteria, bacteriapolymer mixtures and biofilms”. Journal of Microbiological Methods. 1985. 4, 79-94.

[5] S. Farquharson, L. Grigely, V. Khitrov, W. Smith, J.F. Sperry and G. Fenerty. “Detecting *Bacillus cereus* spores on a mail sorting system using Raman spectroscopy”. J. Raman Spectrosc. 2004. 35, 82–86.

[6] H. Félix-Rivera, R. González, G.D. Rodríguez, O.M. Primera-Pedrozo, C. Ríos-Velázquez and S.P. Hernández-Rivera. “Improving SERS Detection of *Bacillus thuringiensis* using Silver Nanoparticles Reduced with Hydroxylamine and with Citrate Capped Borohydride, Int. J. Spectrosc. 2011. 9.

[7] R. Davis and, L.J. Mauer. “Fourier transform infrared (FT-IR) spectroscopy: A rapid tool for detection and analysis of foodborne pathogenic bacteria”. Applied Microbiology. 2010. 2 (1), 1582-1594.

[8] P. Rösch, M. Harz, M. Schmitt and J. Popp. “Raman spectroscopic identification of single yeast cells”. Journal of Raman Spectroscopy. 2005. 36 (5), 377–379.

[9] A.C. Padilla-Jiménez, W. Ortiz-Rivera, J.R. Castro-Suarez, C. Ríos-Velázquez, I. Vázquez-Ayala and S.P. Hernández-Rivera. “Microorganisms detection on substrates using quantum QCL spectroscopy". Proc. SPIE 8710, Chemical, Biological, Radiological, Nuclear, and Explosives (CBRNE) Sensing XIV. 2013.

[10] D. Hofstetter and J. Faist. “High performance quantum cascade lasers and their applications”. Top Appl Phys. 2003. 89, 61-96.

[11] D. Naumann. “Infrared spectroscopy in Microbiology”, Meyers, R. A. (Ed.), Encyclopedia of Analytical Chemistry, John Wiley & Sons, Chichester, UK. 2000. 102-131.

[12] D. Naumann, C.P. Schultz, D. Helm. “What can infrared spectroscopy tell us about the structure and composition of intact bacterial cells” in: Mantsch, H. H., Chapman, D. (Eds.), Infrared Spectroscopy of Biomolecules. Wiley-Liss, New York. 1996. 279-310.

[13] A.C. Padilla-Jiménez, W. Ortiz-Rivera, C. Ríos-Velázquez, I. Vázquez-Ayala and S.P. Hernández-Rivera. “Detection and discrimination of microorganisms on various substrates with quantum cascade laser spectroscopy”. J. Opt. Eng. 2014. 53(6), 061611-10. DOI: 10.1117/1.OE.53.6.061611.

[14] D. Naumann. “FT-IR and FT-Raman Spectroscopy in Biomedical Research”, in Infrared and Raman Spectroscopy of Biological Materials, H.-U. Gremlich and B. Yan, Eds. Marcel Dekker, New York, Chap. 9. 2001. 323-378.

[15] M. Forina et al., “A class modeling technique based on potential functions,” J. Chemometr. 1991. 5, 435–453.

Chapter 6

SPECTROSCOPIC DETECTION OF BACTERIA IN PHARMACEUTICAL INDUSTRIES

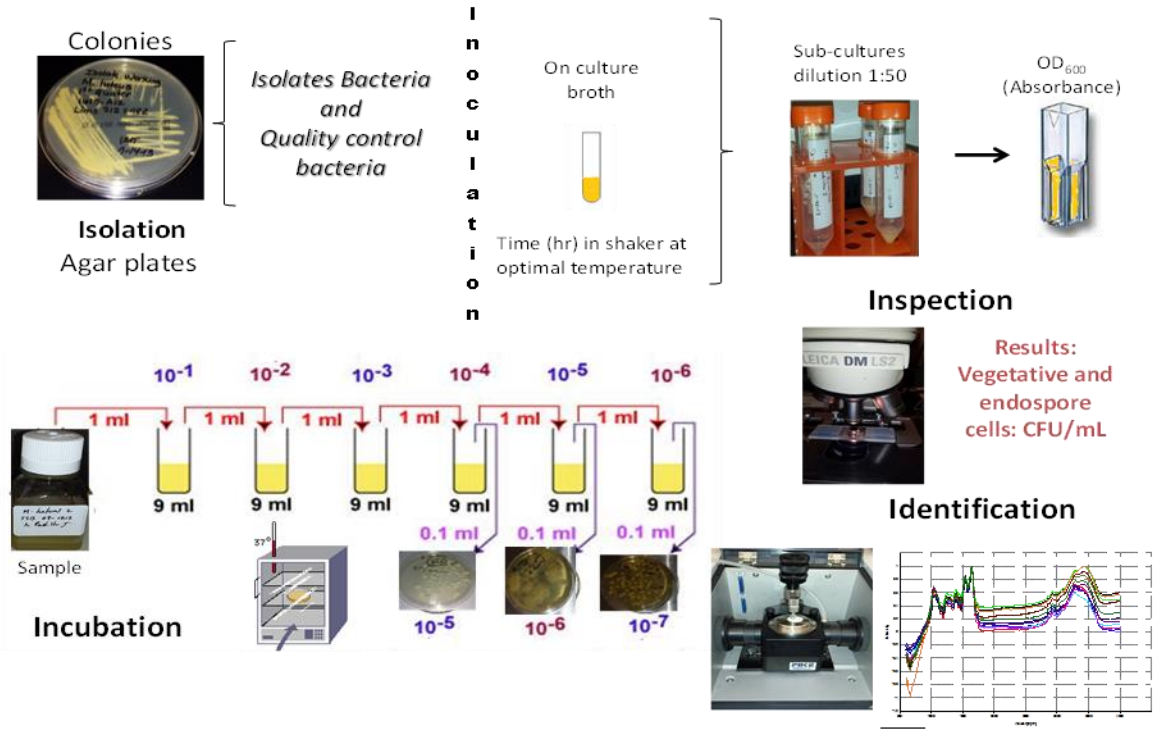

Pharmaceutical and biotechnology industries applications of QCLS.

6.1. Introduction

In industrial applications of quality control (QC) and quality assurance (QA) an identification (ID) test is typically performed on a substance to confirm or verify its identity or a component's identity. ID tests usually require a physical and/or chemical manipulation of the sample (e.g. dissolving, addition of reagents, filtering, interaction with light, etc.). For ID tests, a complete description of observations and results must be

included in the test record. For these applications, the need to develop methods for detecting and quantifying biological threat agents is a top priority for the food technology and pharmaceutical and biotechnology industries. Structure and chemical composition of microorganisms, cells and tissues, affected by environmental factors are subject to changes at the molecular level. Optical spectroscopy offer means to study these changes. It can be used to measure composition of cells and tissues based on their characteristic spectral properties. This involves visible, ultraviolet, or infrared light, alone or in combination, and is part of main topics in biomedical optics. It deals with how light is absorbed or scattered due to the changes in chemical composition and structure in the biological matrix.

Vibrational spectroscopy provides the most definitive means of identifying the species generated upon molecular adsorption and the species generated by biochemical reactions, because when light hits a sample, molecules in the sample are excited and stimulated to vibrate. These vibrations exactly are being measured in vibrational spectroscopy. Mid infrared (MIR) spectroscopy is an extremely reliable and well recognized fingerprinting method. Fourier transform infrared (FT-IR) spectroscopy in the MIR (4000-350 cm^{-1}) has been used to identify and differentiate microorganisms on various species and strains level based upon spectral features. The combination of attenuated total reflectance (ATR) of infrared spectrometer has revolutionized solid and liquid sample analyses in current years because, it contests the peak challenging aspects of infrared analyses, namely sample preparation and spectral reproducibility. Quantum Cascade Laser spectroscopy (QCLS) is another technique that has features such as: wide contiguous mid-IR tuning, integrated “one-box” design, high spectral

radiance, small spot size, collimated laser beam, thermo-electrically cooled MCT and optimized for standoff analysis. Also, it has some advantages as: numerous chemical/bio applications, small footprint, ready to go in minutes, sensitive, high quality results, eye-safe, long path measurements, superior spatial resolution. These two techniques were selected to carry out this work. A handheld system developed for portable field applications and used in pharmaceutical plant cleaning validation and surface contamination detection was used.

The microbiological quality of a pharmaceutical product may represent contamination from raw materials, manufacturing equipment, environment, personnel and containers. Contamination by microorganisms is a major problem in biotechnology laboratories. Bacteria, mycoplasma, viruses, yeast, and fungal spores may be introduced via people working in the lab, the atmosphere, work surfaces, solutions, etc. The classified part of a facility that includes the aseptic processing room and ancillary clean rooms in which air supply, materials, and equipment are regulated to control microbial and particle contamination is named Aseptic Manufacturing Area. Aseptic technique is a combination of procedures designed to reduce the probability of infection by microorganisms. It is essential to establish a strict code of practice and adhere to it, particularly if several people share the same workspace. QA and manufacturing controls should be such that organisms capable of proliferating and contaminate the products are within acceptable limits. The microbial limits and batch testing regimes set for the various categories of products should reflect the types of contamination most likely to be introduced during manufacture.

The types of organisms selected in this project suggest that the main source of contamination of these products could be from the processing unit. Bacillus species are ubiquitous and considered harmless into environment on the pharma industries. However, a non-pathogenic organism in an immunocompetent individual may be a pathogen in an immunocompromised individual. However, someone who is immunocompromised will usually get sick more often, stay sick longer, and be more vulnerable to different types of infections with these bacteria types. Their presence in product suggests poor environmental hygiene during processing or badly contaminated or adulterated raw materials [1]. The extent of microbial contamination depends on a number of factors such as availability of nutrients, presence of microorganisms; oxygen, etc. and the factors that include the type and degree of microbial contamination, root of administration and state of the patients' immune system [2].

The objective of this work is to acquire mid infrared (MIR) spectral signatures of the bacteria found in air and on surfaces, collected at specified places on a random sampling of the aseptic manufacturing area at the host Pharmaceutical Industry. MIR spectroscopy detection based on ATR and QCLS was used to detect and discriminate between bacteria. Also, applying established chemometrics multivariate techniques such as PCA for spectra obtained the data could be reduced to demonstrate the capability of these spectroscopic techniques in the characterization/discrimination of bacterial cells between types of species considered as contaminants associated with pharmaceutical industry. All that has been stated before is to develop a technique that would reduce significantly the time of regularly applied procedures to reduce

contamination by microorganisms and that are carried out in the pharma and biotech industries.

6.2. Experimental section

6.2.1. Selection of microorganism collected in environmental monitoring

Microbial Environmental Control (MEC) sampling and testing is performed in order to ensure that the amount of bacteria found in air, and on surfaces in the manufacturing areas do not exceed acceptable levels. The samples from air (viable and non-viable) and surfaces were collected on the places randomly. For microbial Identification of Environmental Monitoring (EM) Isolates, must be evaluated with EM plates and strips that indicate excursions. For over actions and alerts, from non-critical and critical areas, performing a full ID on each isolate type identified according to the guide for identification of bacterial isolate using an Applied BioSystems Inc. (ABI) Prism 3100 Genetic Analyzer. The centrifugal air samplers were used to collect a viable air sample in the lab room. This equipment is placed in the horizontal position, 2 feet off the floor when sampling a room and screwed onto a tripod stand at working height. Detection and enumeration of microorganisms present on surface sampling programs were collected using BBL™ RODAC™ (replicate organism detection and counting) plates method using the following steps:

- Aseptically removed the BBL™ RODAC™ plates from the cover that contain BBL™ Trypticase™ Soy Agar with Lecithin and Polysorbate 80.
- Firmly pressed the agar surface against the test area without splitting the agar.

- Removed the RODAC™ plate and replaced the cover without touching the surface or sides of the RODAC™ plate.
- Sprayed the test area with alcohol and wiped it with a sterile Tex wipe
- Transferred samples to the lab.
- Incubated samples (30-35) ^{o}C for a min of 2, 3 or 4 d, after which the microbial counts were determined, and the test results were reported to the manufacturing areas supervisor.

6.2.2. Preliminary screening of microbial isolates

The first step after the screening for microorganisms was to perform a Gram stain on each microbial isolate, to begin its identification. Morphological (microscopically) studies of bacteria were done on fixed and stained preparations. Organic dyes were used to stain cells increasing their contrast so that they can be more readily seen under the microscope. Commonly used dyes are positively charged, which combine strongly with the negatively-charged cell surfaces. One of the most important staining procedures in bacteriology is the Gram stain, which is called a differential stain because it separates bacteria into gram-positive and gram-negative cells and should be used only to provide taxonomic information.

The essential difference between gram-positive and gram-negative cells is their ability to retain the crystal violet-iodine complex after they have been treated with a solvent. Gram reactivity is not an absolute characterization and it is influenced by several factors. The age of a culture affects its degree of gram positivity. In general, cells from young, actively growing cultures retain the crystal violet-iodine complex more avidly

than cells from older cultures. Although the optimum age for staining may vary from species to species, it is general practice to examine 18-24 h cultures. Different species of bacteria may not be equally sensitive to the deleterious effects of heat fixation, but overheating bacterial species characteristically stain unevenly and may appear gram variable or gram-negative with gram-positive stippling [3].

Endospores are relatively resistant to physical and chemical agents and are not easily stained. In routine staining procedures, such as the Gram stain, they may appear as unstained retractile bodies. Heat or acid is usually required to promote penetration of the stain into the endospores [4]. Once stained, they are quite resistant to discoloration. Endospore staining methods to be employed include a two-step method: malachite green (primary stain) and safranin (counter stain). The fixed bacterial smear is stained with 7.6% aqueous malachite green solution for 10 min, rinsed, and counter stained with a 0.25% aqueous safranin solution for 15 s, rinsed, and blotted dry. This procedure stains the endospores bright green and vegetative cells are brownish red to pink.

6.2.3. Nucleic acid based (genotypic) microbial methods

The ABI PRISM® 3100 Genetic Analyzer used with the FAST MicroSeq assay is an automated, high-throughput, capillary electrophoresis system with a CCD camera used for analyzing fluorescently labeled DNA fragments: identification and classification of bacteria by the DNA sequence of their 16S rRNA gene. This molecular target has served as an important tool for determining phylogenetic relationships between bacteria. The method requires reagents and instrumentation for amplification and sequencing, a database of known sequences, and software for sequence editing and database

comparison [5]. In clinical and pharmaceutical microbiology, molecular identification based on 16S rDNA sequencing is applied fundamentally to bacteria whose identification by means of other types of techniques fails, is difficult, or is too time consuming. Amplification of the gene to be sequenced uses preferably DNA extracted from a pure bacterial culture, but can be achieved also directly from a microbial isolates. Not all strains of the same species have identical 16S rDNA sequences. The comparison of the 16S rRNA gene sequences allows differentiation between organisms at the genus level across all major phyla of bacteria, in addition to classifying strains at multiple levels, including the species and subspecies level [6]. The MicroSeq 500 16S rDNA Polymerase Chain Reaction (PCR) and sequencing kits, provide the reagents necessary to sequence the ribosomal DNA of unknown isolates. For bacterial identification, the first 500 base pairs of the 16S rRNA gene are sequenced. The resulting DNA (deoxyribonucleic acid) sequence is analyzed and compared to the library of bacterial sequences using MicroSeq Analysis Software.

The steps in the MicroSeq procedure were:

- DNA extraction from a bacterial culture. The bacterial cells were lysed by suspending in commercial system (e.g., PrepMan DNA extraction ultra-reagent; ABI) and heating. The suspension should have been at least modestly turbid but not so dense as to be opaque. Sometimes more than one colony was required to achieve the desired density.
- PCR Amplification of 16S rRNA gene. The 16S rRNA gene target was amplified from the bacterial genomic DNA prep by the polymerase chain reaction (PCR) using FAST MicroSeq reagents and a thermal cycler. The PCR products were

purified to remove excess primers and nucleotides. Several good commercial kits are available for this task [e.g., ExoSAP-IT® reagent, Microcon-100 Microconcentrator columns (Millipore)]. Presence of the desired PCR product was confirmed by gel electrophoresis.

- "Cycle Sequencing" reaction for incorporation of fluorescent dyes into the amplified 16S rDNA sequence. The 16S rRNA sequence amplified in the previous step was labeled with fluorescent dyes in the MicroSeq kit through a second PCR step in the thermal cycler. For each bacterial isolate (PCR amplification product), both forward and reverse sequences were used as the template in separate reactions in which only the forward or reverse primer was used. This step was followed by a clean-up reaction to remove unreacted dyes with small gel-filtration spin columns. As each of the four added labeled terminator bases had different fluorescent dye, each of which absorbed at a different wavelength, the terminal base of each fragment could be determined by a fluorimeter.
- DNA sequence determination on the 3100 Genetic Analyzer. The products were purified to remove unincorporated dye terminators, and the length of each was determined using capillary electrophoresis (e.g., ABI PRISM 3100 genetic analyzer with 16 capillaries). The two strands of the DNA were sequenced separately, generating both forward and reverse (complementary) sequences. An electropherogram, a tracing of the detection of the separated fragments as they elute from the column in which each base was represented by a different color.
- Data processing and identification reports. The generated DNA sequences were usually assembled by aligning the forward and reverse sequences. The DNA

sequence data of the unknown isolate were processed and then compared for the closet match with a database library by using analysis software. Reports are generated.

6.2.4. Growth promotion of microbial isolates

The first step in microbial analysis is labeling all samples for each microorganisms isolated to the origin, location, date and time of sampling. Phenotypic methods utilize expressed gene products to distinguish among different microorganisms. Generally these require a large number of cells in pure culture. Viable count enumeration (VCE) and absorbance measurement are commonly two methods used to monitor growth of bacteria. Monitoring bacterial growth by VCE includes long incubation times, inability of most environmental microorganisms to grow on artificial media, specific growth requirements of many microorganisms, unintentional selectiveness of culture methods, and need to full phenotypic properties of recently isolated stressed microorganisms by subculture from primary isolation, selective or diagnostic media prior to microbial identification. Also, when bacteria are grown on defined and reproducible media, the fatty acid composition of their membranes is consistently expressed as a phenotypic characteristic. Use of these methods will not likely be required and rather expensive, but it remains the method of reference. Methods based on absorbance measurements constitute a second set of methods based on the direct proportionality between the optical density (OD) of a liquid medium and the concentration of bacteria. OD techniques are rapid, convenient, non-destructive, inexpensive and relatively easy to automate. However, many difficulties are inherent to these techniques. The main

problem encountered is the limited range of validity since the detection threshold typically corresponds to a bacterial concentration larger than, 10^6 bacteria/mL [7].

6.2.5. Bacterial strain and growth conditions

Bacterial cells used in this study were obtained from environmental monitoring (EM) program established for all controlled facilities such as aseptic manufacturing area and aseptic processing room. These are the classified part of a facility that includes the aseptic processing room and ancillary clean rooms, in which air supply, materials, and equipment are regulated to control microbial and particle contamination at Pharmaceutical Industries. Six bacterial strains were isolated and studied: *Bacillus subtilis (Bs), Bacillus pumilus (Bp), Bacillus lincheniformis (Bl), Micrococcus luteus (Ml), Staphylococcus epidermidis (Se) and Acinetobacter genomospecies 3 (Ag3)*, which were selected based upon the frequency in which the environmental isolate has been isolated from the manufacturing area and identified using 16S rDNA sequencing according to a guide for identification of bacterial isolate using the (ABI) Applied BioSystem Prism 3100 Genetic Analyzer. Also four qualified inoculum microorganisms as certified quality control (QuantiCults® Plus microorganisms): *Staphylococcus aureus* (*Sa*) ATCC 6538, *Pseudomonas aeruginosa (Pa)* ATCC #9027, *Bacillus subtilis (Bs)*ATCC #6633 and *Escherichia coli (Ec)* ATCC #8739, in wich, QuantiCult® Plus contains <100 CFU/0.1mL were used. QuantiCult Plus® Cell Suspensions contain multiple aliquots and should be rehydrated using the 1.2 mL rehydrating fluid. All qualified bacterial cells were grown in 10 mL of TSB overnight with constant shake to 32.5^{o}C. After, each bacterial culture was diluted in 100 mL of tryptic soy broth (TSB)

with OD600 0.0100-0.0168 range. The optical density was taken each hour during 15 h. Aseptically were pipetted 100 μL of QuantiCult Plus onto each tryptic soy agar (TSA) standard plate surface. Allowing medium to dry completely before inverting and placed into the incubator at 30°C to 35°C during three days, because these are the conditions that microorganism growth on pharmaceutical industry following USP (United Stated Pharmacopeia) guidelines. Each selected environmental isolates was cultured and incubated at 30°C to 35°C between 18 and 24 h. A well-isolated single colony of each strain was then aseptically collected with a sterile loop and suspended in 10 mL of sterile TSB and left to grow overnight in a rotatory shaker at 32± 2 ºC and (~120 ± 5 rpm). After this time incubation, the samples were diluted with sterile growth medium, taken one mL of nutrient broth of each strain inoculated and added into 50.0 mL TSB and incubated at 32.5^{o}C in a rotatory shaker for 16 h in a 250 mL square media bottle of PETG (polyethylene terephthalate glycol; Eastman Chemical, SK Chemicals) to yield a cell count initial concentration of bacteria in the range 1.5 x 10^5 to 3.0 × 10^9 CFU/mL, approximately. In order to establish bacterial growth rates as well as to set up new cultures with known cell counts, the bacterial cultures were immediately measured in duplicate by serial decimal dilutions followed spread plating and by measuring the optical density using Varian Cary 100 (series UV-Vis spectrophotometer, Agilent Technologies, USA) at wavelength of 580, 600 and 660 nm. Aliquots of samples were withdrawn at time-defined intervals during culture growth and submitted to analysis for determination of the absorbance. 1.0 mL of medium from agitated flask cultures into disposable semi-micro cuvettes assorted by one cavity number (Platibrand, Postfach 1155 97861 Wertheim, Germany) was dispensed. Also, each dilution was inoculated in

TSA plate by spreading methods. A total of 16 growth curves were generated in duplicates by using both viable counts and absorbance measurements. After 96 h incubation at 32.5 ± 2 ^{o}C, on appropriate plate (30-300 colonies), were chosen, and the number of CFU/mL was determined of the original culture for each microorganisms isolates.

For the FTIR and QCLs measurements, 30 mL broth of each strain was transferred to a 50 mL sterile centrifuge tube. The tubes were then centrifuged at room temperature for 15 min at 3750 rpm (Beckman Coulter Allegra 6R Refrigerated Centrifuge (Thermo IEC, San Jose, CA) to harvest bacterial cells. To reduce the effect of media components and bacterial metabolites, the resultant pellets were suspended in 10 mL sterile 0.85% saline solutions and centrifuged again; this step was repeated twice. The supernatants were removed and the remaining wet pellets were resuspended in 300 µL sterile 0.85% saline solution and vigorously mixed to obtain a homogeneous cell distribution. A 150 µL of each bacterial suspension was uniformly applied to a 0.2-µm pore size aluminum oxide membrane filter (25 mm OD; Anodisc™, Whatman, Inc., Clifton, NJ). Under aseptic conditions, the filters were then air-dried at room temperature (22^{o}C) for 30 min under a laminar flow hood. This procedure yielded a filter with a relatively uniform coating of dried bacterial cells. The Anodisc™ membrane filter was used because it does not contribute significantly to the bacterial spectra and it gives a smooth and a flat surface for bacterial cell adhesion [8, 9].

6.2.6. FT-IR measurements of bacteria isolates

A Thermo-Nicolet FT-IR spectrometer, Model Avatar 470 (Thermo-Electron, Inc., San Jose, CA, USA) equipped with OMNIC™ software was used for samples microbial isolates (*B. subtilis, B. pumilus, B. licheniformis, M. luteus, S. epidermidis and A. genomospecies 3*). Also, an IRPrestige-21 IR Affinity FT-IR, 8000 series (Shimadzu Corporation, Kyoto, Japan) was used. A MIRacle™ ATR (Pike Technologies, Madison, WI, USA) accessory was used with the IRPrestige-21 spectrometer. The MIRacle™ ATR has a single reflection sampling plate with ZnSe crystal and a high pressure clamp system for sample compression. When the ATR accessory was plugged in it was be recognized automatically and controlled by means of the IR-Solution™ software.

The aluminum oxide membrane filter coated with a uniform and thin layer of bacterial cells was placed in direct contact with the diamond crystal cell of attenuated total reflectance (ATR) detector [see Figure 6.1 (a)]. Infrared spectra were recorded from 4000 to 600 cm^{-1} at a resolution of 2 cm^{-1}. Each spectrum was acquired by adding together 64 interferograms. Six and ten spectra were acquired at room temperature (20 ^{o}C) for each sample at different locations on the aluminum oxide filter. Triplicate experiments were conducted and 70% spectra were used for establishment of chemometric models and 30% spectra were used for model validation. To comparison spectra, one colony of each bacterium with loop was taken and placed on ZnSe disc, as shown Figure 6.1 (b).

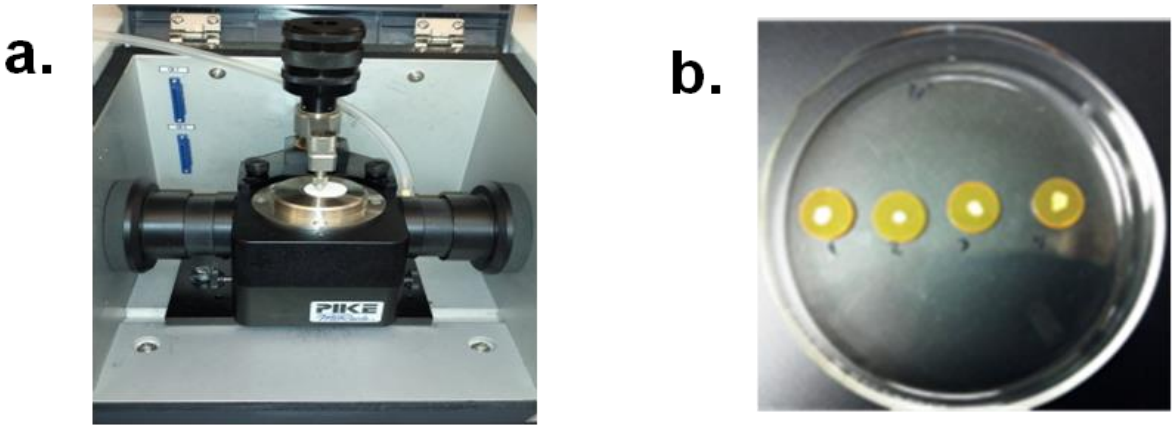

Figure 6.1. (a) Bacterium sample on aluminum oxide membrane filter placed on MIRacle™ ATR accessory; **(b)** *Se* deposited on ZnSe discs ready for spectroscopic analysis.

6.2.7. QCLS measurement of bacteria isolates

A LaserScan™, model 712 (Block Engineering, Inc., Marlborough, MA, USA) was used It used a 200 kHz laser pulse modulation. Spectral information coverage was 1600-990 cm^{-1} of the bacterial suspension samples.

6.2.8. Multivariate data analysis

For multivariate data analysis, a matrix interlinking the individual measurements as rows and the selected wavenumber values as columns could be generated. The spectral intensity for each measurement-wavenumber combination comprised the matrix elements. PCA was performed in the MATLAB computational environment (The MathWorks, Inc., Natick, MA, 01760 USA), using the PLS-toolbox (Eigenvector Research, Inc., Wenatchee, WA, USA, version 7.0.3).

6.3. Results and discussion

6.3.1. Growth curves

In order to obtain detailed information on the microorganisms' growth behavior and bacterial life cycles, OD measurements were collected at wavelength 580, 600 and 660 nm every hour during a period of sixteen (16) hours using 1 mL of the growing bacterial suspension. Operating at 600 nm is the traditional wavelength for cell growth. However, when other wavelengths are used a very similar shaped curve is observed. Theoretically, a whole variety of wavelengths could be used to measure cell growth.

The model constructed for this research is based on the supposition that there is direct proportionality between absorbance measurements obtained by OD (xOD) and VCE (xVCE): xOD(t) = kxVCE(t). As OD and VCE growth data were obtained simultaneously from the same bacterial cultures, a model to both types of data could be fitted. Fits of models to the log-transformed data were performed by nonlinear regression using Statgraphics™ that uses the Levenberg-Marquardt algorithm. This is a search method to minimize the sum of the squares of the differences between the predicted and measured values. The program automatically calculates starting values by searching for the steepest ascent of the curve between four data points (estimation of μ_{max}) by intersecting this line with the x axis (estimation of λ) and by taking the final datum point as estimation for the asymptote. The algorithm then calculates the set of parameters with the lowest residual sum of squares (RSS) and their 95% confidence intervals. Then the data were fitted by the logistic model using the equation, which is written as:

$$\frac{a}{1+e^{(-kt+b)}} \qquad \textbf{6.1}$$

Where parameters a, k and b were evaluated.

On the constructed growth curves, can be distinguish 4 phases characteristic for growth of each bacteria [10]:

I. *Lag phase:* during lag phase, bacteria are adapting to new conditions. The population remains temporarily unchanged. Although there is no apparent cell division occurring, the cells may be growing in volume or mass, synthesizing enzymes, proteins, RNA, etc., and increasing in metabolic activity The length of the lag phase is dependent on some factors: age of culture inoculum, size of inoculum and environment. Can go on for several hours, or many days, depending on the particular bacteria.

II. *Exponential growth phase:* quantity of growing bacteria doubling time of the bacterial population, regularly 2^n. The cells divide at a constant rate depending upon the composition of the growth medium and the conditions of incubation. The rate of exponential growth of a bacterial culture is expressed as generation time.

III. *Stationary phase:* is characterized by absence of increase of quantity of bacteria, because, exponential growth cannot be continued forever in a batch culture (e.g. a closed system such as a test tube or flask). Population growth is limited by one of three factors: exhaustion of available nutrients; accumulation of inhibitory metabolites or end products; and exhaustion of space, in this case called a lack of "biological space". Although there is growth during this phase, quantity of growing and dying bacteria is approximately the same.

IV. *Death phase:* If incubation continues after the population reaches stationary phase, a death phase follows, in which the viable cell population declines. During the death phase, the number of viable cells decreases geometrically, essentially the reverse of growth during the log phase.

All the models logistic of bacteria visually gave reasonably good fits of the data as is shown in Figure 6.2 and 6.3., because survival, reproduction, proliferation and differentiation of cells in an environment depend on two critical factors: culture medium and substrate for growth. The other growth curves are shown Appendix A.

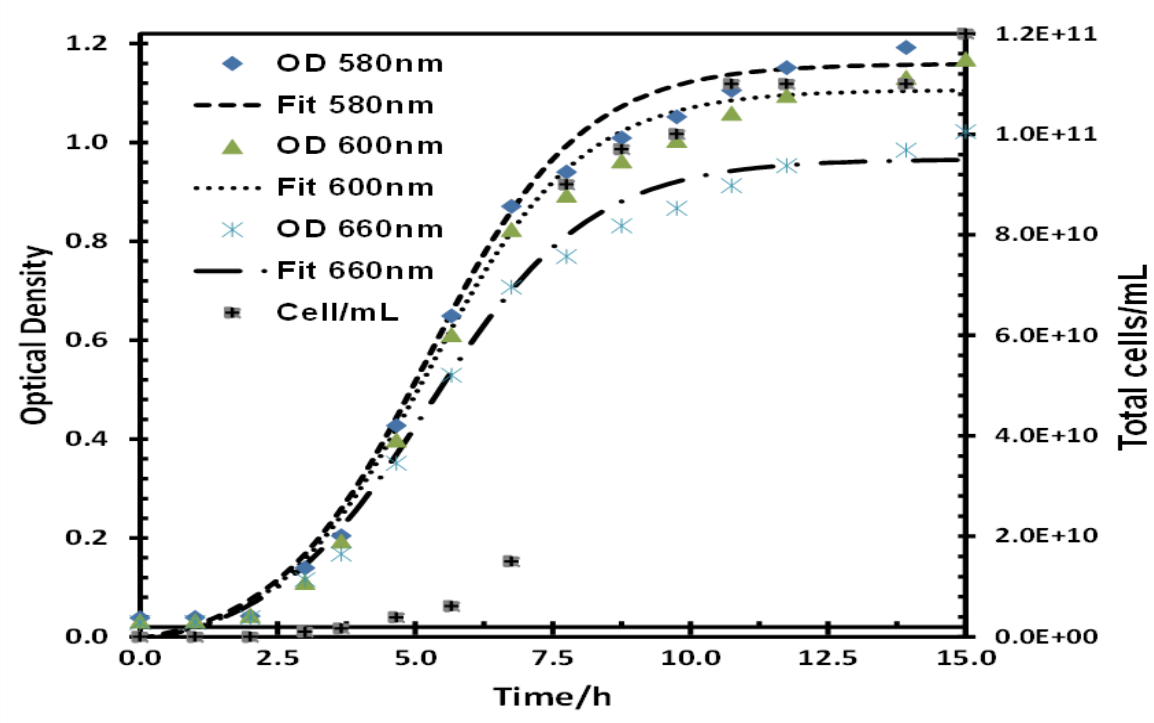

Figure 6.2. Growth curve of *S. aureus* ATCC# 6538 at 32.5°C±2 fitted with the logistic model.

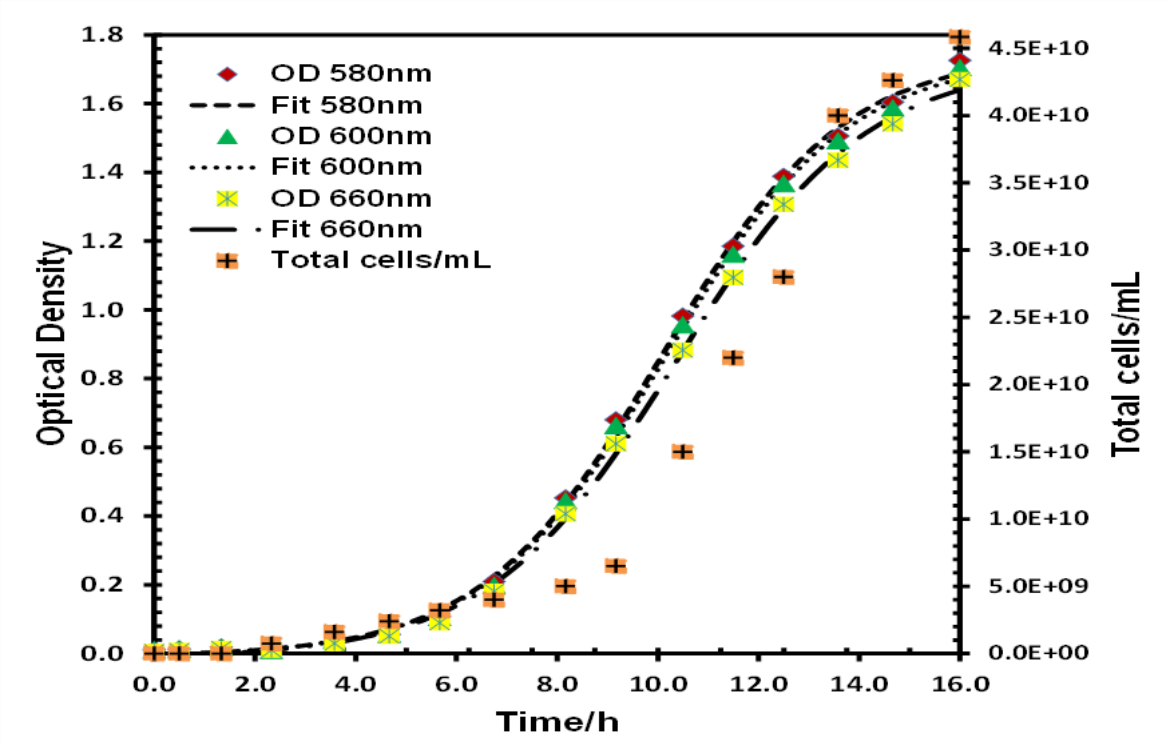

Figure 6.3. Growth curve of isolate *M. luteus* at 32.5°C ± 2 fitted with the logistic model.

The aim of the methodology proposed in this work, is to minimize the time of the procedures that are been used in the pharma industries at this moment for the identification of isolates bacteria. It is necessary the full characterization of the microorganisms, for this reason modeling bacterial growth curves were performed. There is a variation in composition and distribution of bacterial biochemical structure including cell wall and cell membrane structural lipids (phospholipids and lipopolysaccharides), cellular proteins and enzymes, nucleic acids, and polysaccharides this should be reflected in spectral features at each growth stage.

6.3.2. Mid-Infrared spectroscopy

The purpose of the spectroscopic measurements was to evaluate the FT-IR spectral signatures of bacterial cells to determine if variations in composition and distribution of

the biochemical components of bacterial cells can be distinguished using this spectroscopic technique. FT-IR spectra between 4000–600 cm^{-1} include stretching vibrations and deformation of C–H, C=O, N–H, P=O, and C–O–C and which reflect the differences in the biochemical composition of microbial cells i.e., DNA, proteins, polysaccharides and fatty acids [11, 12].

The total reflection occurs on the boundary surface of two media with different optical densities in ATR-IR spectroscopy. If IR radiation in an ATR crystal with a higher refraction index (n_1) strikes obliquely on the boundary surface of an optically thinner medium (n_2), the IR radiation is reflected back into the crystal if the angle of incidence exceeds the angle of the total reflection. A portion of the electromagnetic energy penetrates into the sample (the optically thinner medium) to a slight extent. If the penetrating IR radiation is absorbed by the sample, then a characteristic spectrum is provided for identification. Spectra of all isolates bacterial suspensions and quality controls acquired are shown in Figure 6.4., in the region of 1600 to 1000 cm^{-1}. These original spectra show almost identical patterns for all bacterial samples with strong absorption bands. FT-IR spectroscopy was used to characterize these changes through spectral features analysis of various functional chemical groups and polar bonds that reflect the biochemical composition of the cellular constituents. The MIR spectra of intact bacterial cells are generally complex with broad peaks due to the overlaid contributions of all the biomolecules in the bacterial cell (see Figure 6.4) [13].

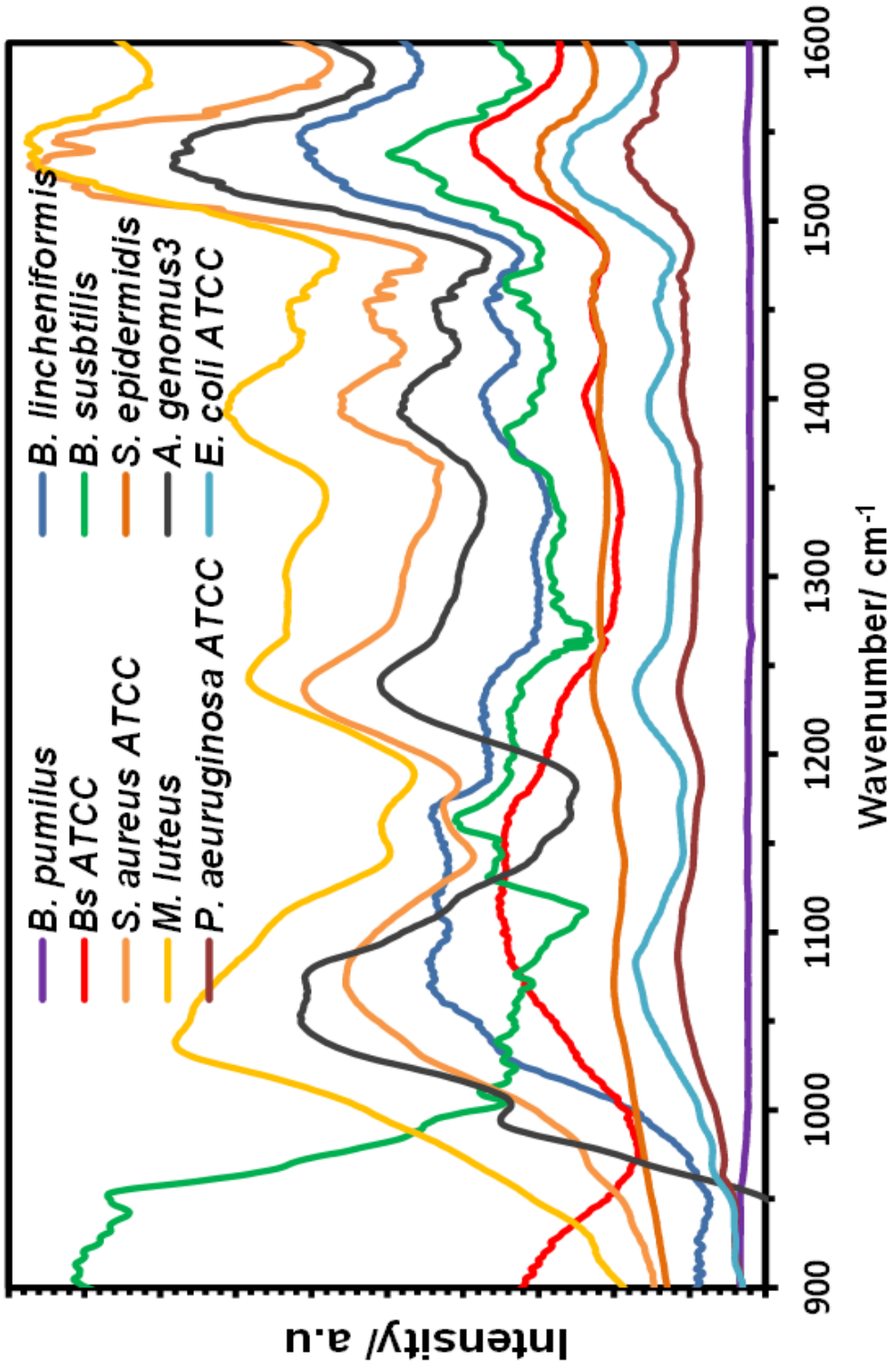

Figure 6.4. FT-IR spectra of bacteria deposited on Anodisc™ aluminum oxide filter.

A total of 300 bacterial samples on different substrates (Au coated glass, aluminum, stainless steel, ZnSe and Anodisc™), were prepared and analyzed to determine if the QCLS spectrometer could provide better analytical results than have been achieved using other spectroscopic techniques. Specifically, the purposes of this sample assessment were to compare the variability of the spectra within each bacteria type and the spectral differences among the bacteria strain. It was determined that the spectra cannot be readily differentiated using simple spectral feature analysis, but that a full-spectrum algorithm may be able to discriminate them based on overall feature variability. All samples were analyzed using a commercial QCLS infrared spectrometer operating from 1600 – 990 cm^{-1} in three different orientations. Each experiment consisted of ten replicates spectral measurements for each bacterium for each of the substrates studied. As shown in Figures 6.5 and 6.6., reflectance signals spectra were easily obtained for each bacteria type, especially when measured on Anodisc™. In Figure 6.5, tentative bands were assigned and found into all bacteria analyzed, as are shown in Table 6.1.

Table 6.1. Tentative bands assignment of FT-IR ATR spectra for bacteria studied.

All Bacteria	Tentative band assignments
1528-1533	Amide II coupled C-N stretching N-H bending
1523	Amide II β Sheet,
1490	Cytosine
1463-1465	Diaminopimelic acid, C-H def.
1385	N-acetyl muramic
1360-1365	LD-Alanine
1128-1131	N-acetyl glucosamine
1105-1107	D-glutamine
1096	C-C skeletal and COC stretching from glycosidic linkage

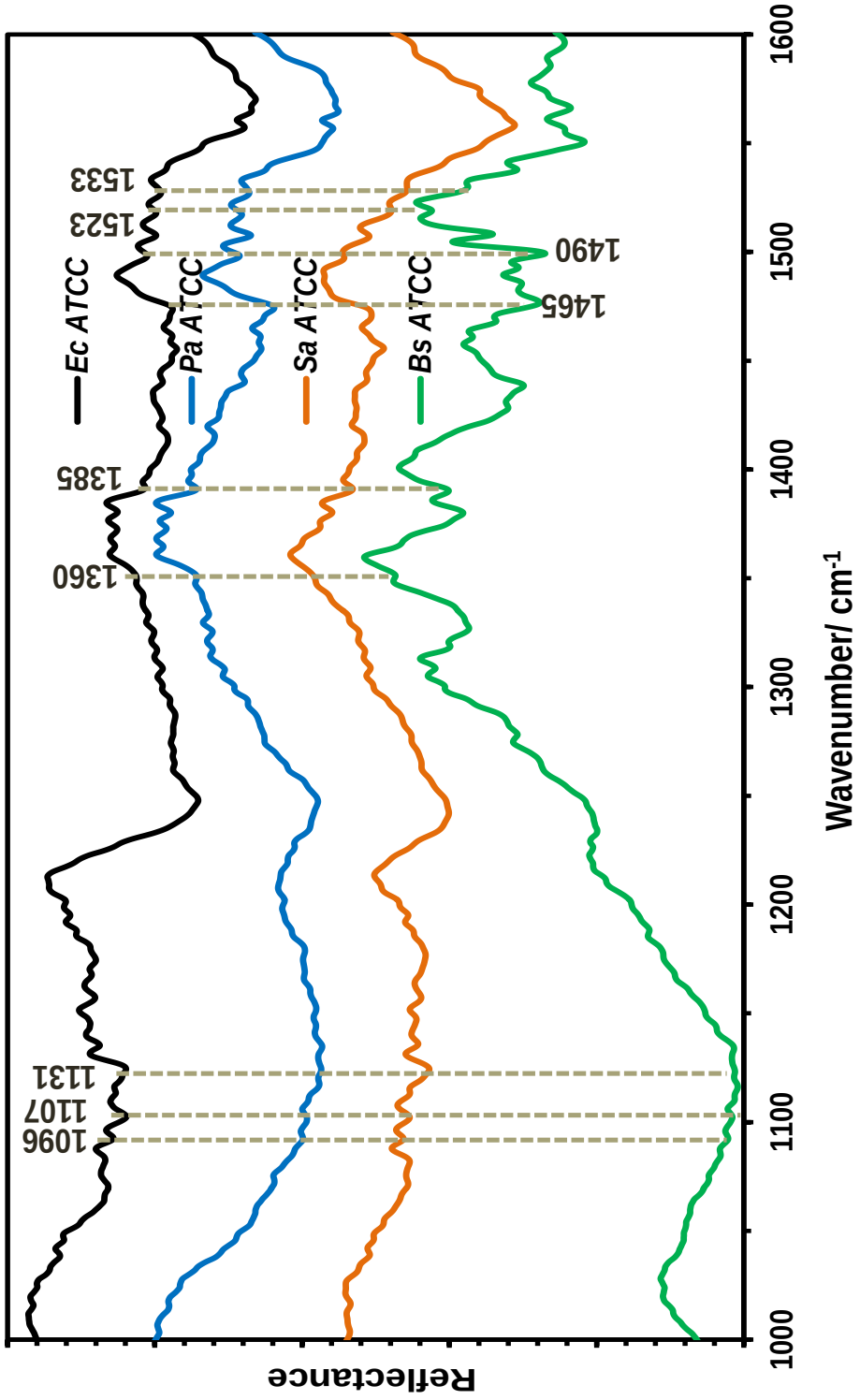

Figure 6.5. MIR spectra of certified bacteria by ATCC (*S. aureus, E. coli, B. subtilis, P. aeruginosa*) deposited on aluminum oxide Anodisc™ by QCLs.

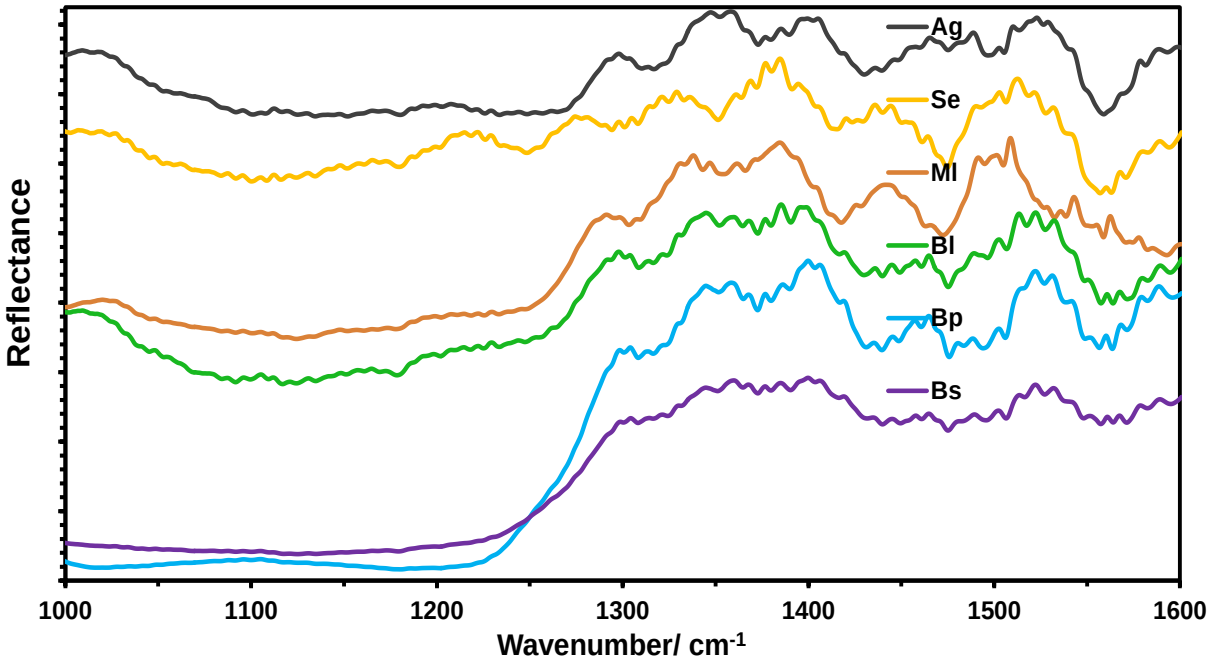

Figure 6.6. FT-IR spectra of isolates bacteria [*Bacillus subtilis (Bs), Bacillus pumilus (Bp), Bacillus licheniformis (Bl), Micrococcus luteus (Ml), Staphylococcus epidermidis (Se)* and *Acinetobacter genomospecies 3 (Ag3)*] deposited on aluminum oxide Anodisc™.

To determine whether the spectra for each bacterium on each of the substrates studied, could be distinguished for these bacteria types, the averages of the spectra of each bacterium were computed and plotted as illustrated in Figure 6.7. As shown, the spectral regions where the characteristic features of bacterium on various substrates appear did not exhibit any significant differences between different surfaces the average spectra. Despite, that the spectra for *M. luteus* were acquired on different substrates can be observed that many spectral features (vibrational modes) of lysine and ribitol are maintained. The main vibrational bands were: 1585, 1542, 1518, 1457, 1417, 1405, 1350, 1321, 1283, 1180, 1061 and 1040 cm^{-1}.

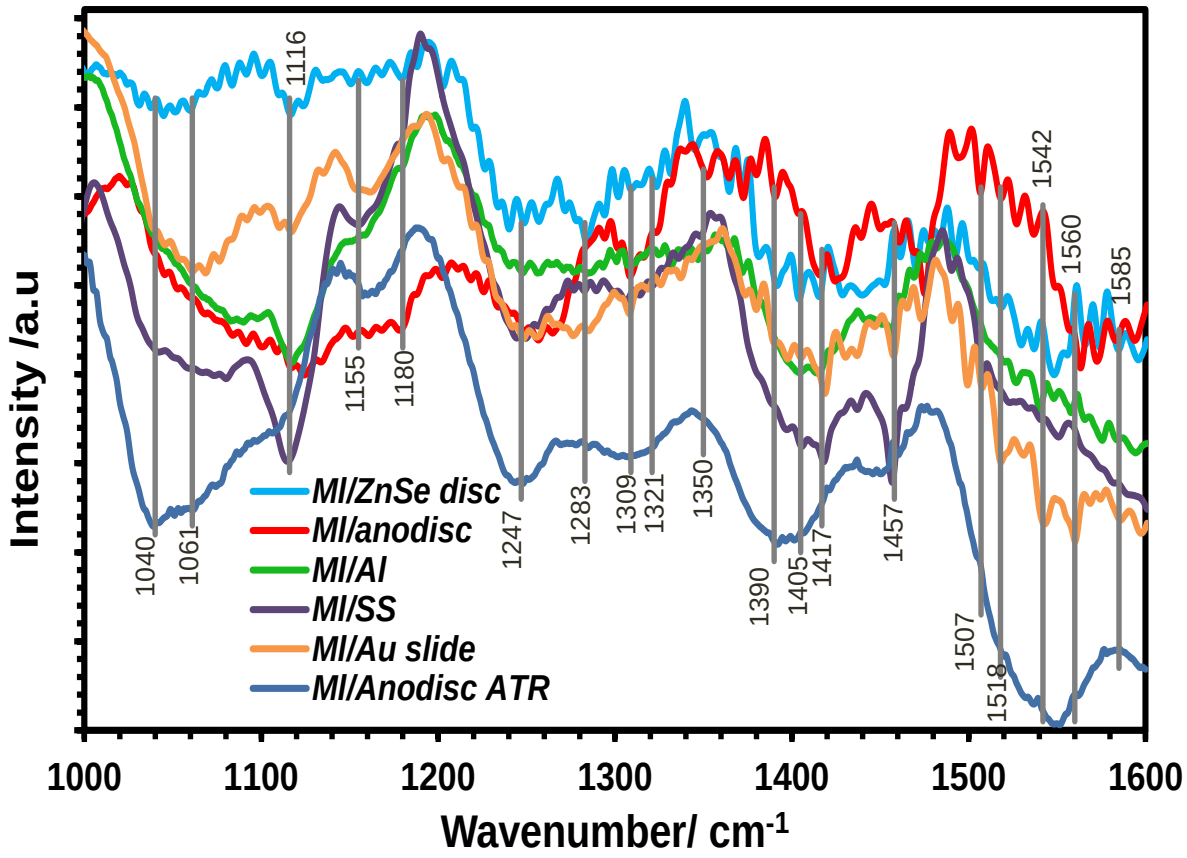

Figure 6.7. Comparison QCLS spectra of *M. luteus* deposited on various substrates.

6.3.3. Statistical analysis

Various manipulations of the spectra were performed to improve the appearance and increase the spectral features to facilitate spectral interpretation and analysis. Spectral preprocessing is generally performed when dealing with bacterial spectra [14]. The preprocessing methods used before spectral comparison using chemometric tools were smoothing, that reduces the high frequency instrumental noise and enhances the information content of a spectrum and normalization, since it eliminates the path length variation and also reduces the differences between each single measurement of the

same sample. As first derivative transformation is generally used for the taxonomic classification of bacteria [15], in this research first derivative was applied too.

Multivariate statistical analysis of FT-IR and QCL spectra used was PCA that is unsupervised methods with the capability of extrapolate the spectral data without a prior knowledge about the bacteria studied. Also, to reduce the multidimensionality of the data set into its most dominant components or scores while maintaining the relevant variation between the data points. Score plots can be used to interpret the similarities and differences between bacteria [16].

The spectral ranges 2800-3700 cm^{-1} and 700-1800 cm^{-1} were chosen as they correspond to the typical biochemical structure of the cell wall and the outer membrane and would therefore maximize the differences in the spectra. There are significant differences in the molecular structures of gram (+) and gram (-) bacteria. Despite these differences, they are not easily recognized in spectra. However, PCA of FT-IR spectra on Anodisc™ does in fact successfully discriminate between five strains of bacteria, two gram (-): *Ec* and *Pa* and three gram (+): *Bs, Bl* and *Sa,* as shown in Figure 6.8. The percent of contribution all samples were: *Bl*-15.9%, *Bs ATCC*-27.3%, *Pa*-15.9%, *Ec ATCC*-18.2%, *Sa ATCC*-20.5% and media control-2.2%.

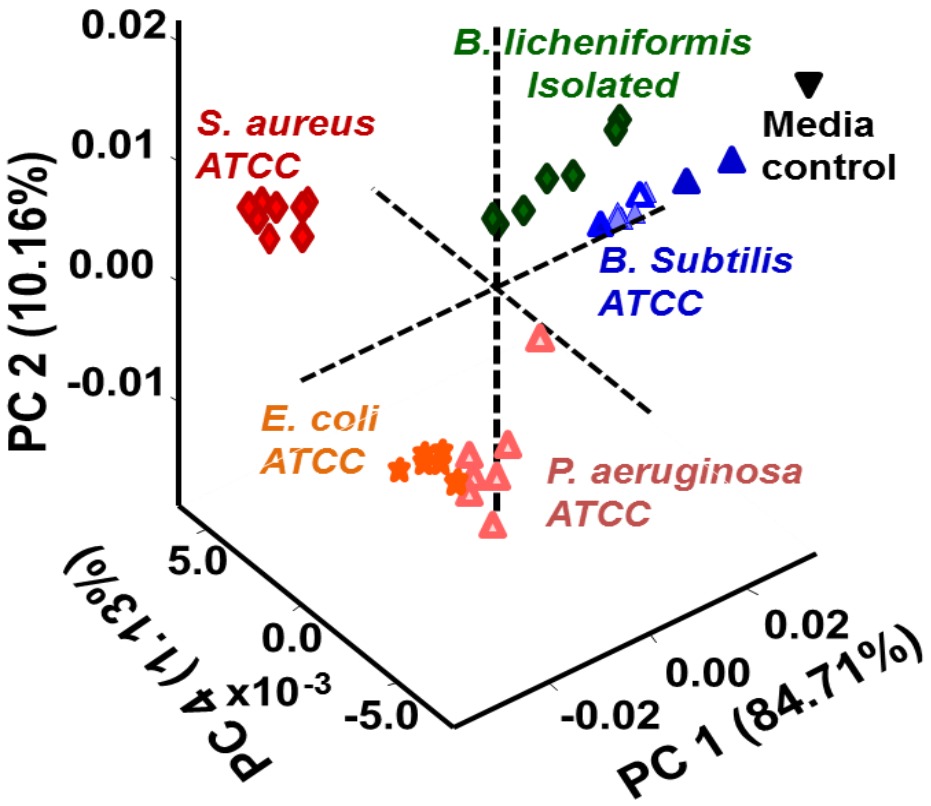

Figure 6.8. Principal component analysis (PCA) for the FTIR-ATR spectra of certified bacteria (*S. aureus, E. coli, B. subtilis, P. aeruginosa*) and isolate *B. licheniformis* deposited on aluminum oxide Anodisc filter.

Scores plots for the bacteria deposited on Anodisc filter required a number of four PCs (PC-1 84.71%, PC-2 10.16%, PC-3 2.79% and PC-4 1.13%) for classification. In addition, only one *Pa* sample was classified as *Bs ATCC* # 6633 with a percentage cases correctly classified of 98.15%. These results in turn indicate that PCA can adequately discriminate between these types of bacteria.

Other PCA models were built by selecting ~ 8 to 10 MIR spectra of samples from each isolate bacterium and certified control bacteria. Scores plot (PC-2 versus PC-1) on

Anodisc™ filter is shown in Fig. 6.9. A poor separation between bacteria species *Bacillus* datasets is shown. PC-1 (68.33% variance) was correlated to the differences between the ten bacteria. Overall, 25% of the *Bp* samples were classified as *Bs ATCC # 6633* and isolate *Bs*, while 16.67%, 50.00%, 81.82% and 90.00% of the *Bp, Bl*, *Pa* and *Ec* were correctly classified, respectively. The other bacteria were classified with 100% indicated good separation between bacteria samples.

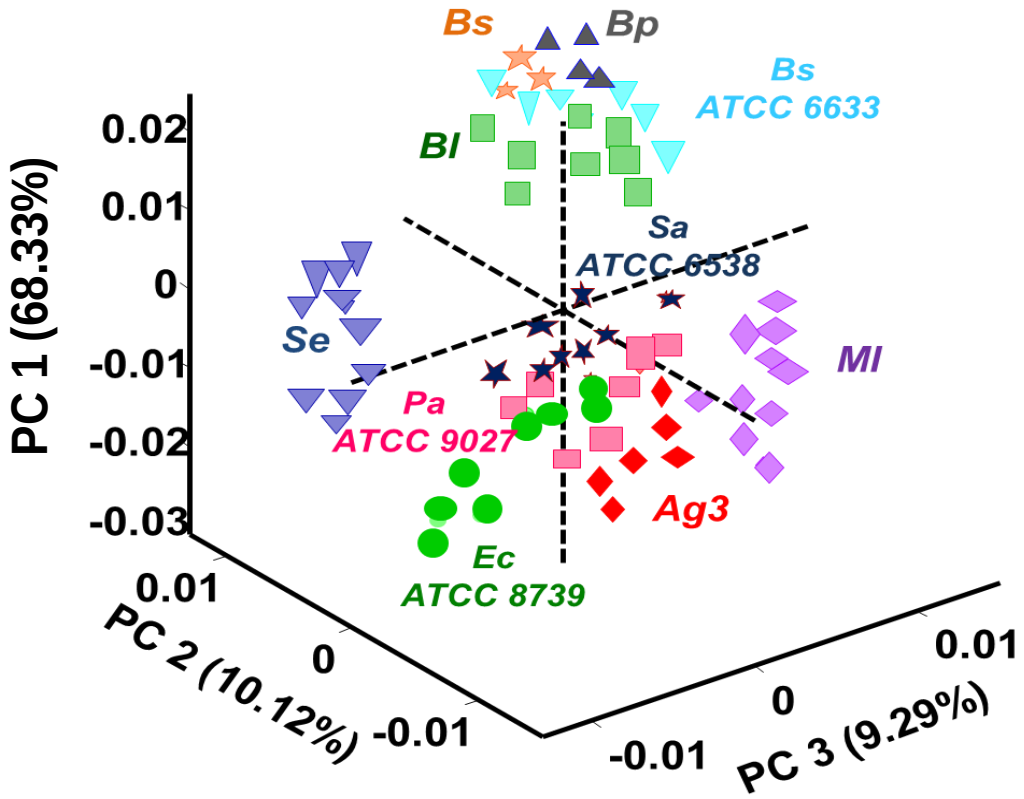

Figure 6.9. PCA for the FTIR-ATR spectra of certified bacteria by ATCC (*Staphylococcus aureus, Escherichia coli, Bacillus subtilis, Pseudomonas aeruginosa*) and isolates bacteria [*Bacillus subtilis (Bs), Bacillus pumilus (Bp), Bacillus licheniformis (Bl), Micrococcus luteus (Ml), Staphylococcus epidermidis (Se)* and *Acinetobacter genomospecies 3 (Ag3)*] deposited on aluminum oxide Anodisc™ filter.

Data from 115 spectra for *Ml, Ml* on Au surface*, Bl, Se, Ag3 and Ag3* on Au surface*,* were used in the PCA models, and the variance that was described by each PC was examined for each isolate bacterium. The percent of contribution all samples were: *Ml*-18.3%, *Ml*/Au-10.4%, *Bl*-13.9%, *Se*-18.3%, *Ag3*-30.4%, and *Ag3*/Au-8.7%. Scores plot (PC-2 versus PC-1) on ZnSe disc compared with two bacteria samples on Au surface is shown in Fig. 6.10. However, these plots only represent portions of the data variance (42.5% and 19.6%, respectively). A good classification was observed between analyzed bacteria. Only nine *Ag3* gram- negative samples were classified as *Ml* on ZnSe disc and one of the *Ag3*/Au samples were classified as *Ml* on Au surface. *Ml, Ml*/Au, *Bl,* and *Se* were correctly classified with 100% indicated good separation between these bacteria samples.

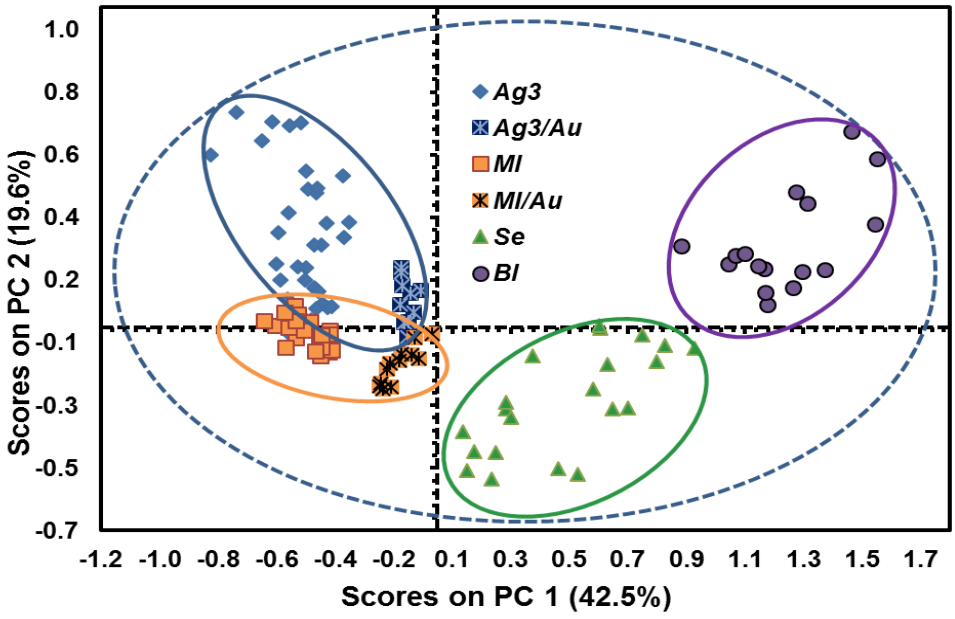

Figure 6.10. PCA for QCLS spectra of isolates *Bacillus licheniformis (Bl), Micrococcus luteus (Ml), Staphylococcus epidermidis (Se)* and *Acinetobacter genomospecies 3 (Ag3)* deposited on ZnSe disc compared to *(Ml)* and *(Ag3) on Au surface.*

6.4. Conclusions

FT-IR spectroscopy methods have attractive features for microbiology applications for their extreme rapidity, simplicity, and uniform applicability to any group of microorganisms. It is a technique highly specific, sensitive and enables identification of bacteria. FT-IR and QCLS MIR spectra of bacteria were successfully used in multivariate classification analyses (PCA). Spectral databases for different bacteria have been created. The results can be used for to produce a full automated handling FT-IR system for detection, quantification, and differentiation of microorganisms using the advancements in MIR technology as is QCLS, helped of computational analysis. The protocol developed could be promising a tool for routine microbial environmental control in the pharmaceutical industries.

6.5. References

[1]. Westwood, N. and Pin-lim, B., Microbial Contamination of Some Pharmaceutical Raw Materials, Pharm. J. (1971) 207: 99-102.

[2]. Bird, R., Microbial spoilage, infection risk and contamination control, in: Stephen P. Denyer, Norman A. Hodges, Sean P. Gorman (Eds.), Pharmaceutical Microbiology, 7th ed., 2004.

[3]. Norris, J. R., and Swain, H. Staining bacteria. Methods in microbiology. Ribbons, D. W. (ed.). 5 (1971): 105-134. Academic Press, Inc., New York, NY.

[4]. Reynolds, J., Moyes, R., Breakwell, D.P. Differential Staining of Bacteria: Endospore Stain. Curr. Protoc. Microbiol. 15:A.3J.1-A.3J.5. (2009) by John Wiley & Sons, Inc.

[5]. Woo, P.C., Lau, S.K., Teng, J.L., Tse, H., Yuen, K.Y. Then and now: use of 16S rDNA gene sequencing for bacterial identification and discovery of novel bacteria in clinical microbiology laboratories. Clin Microbiol Infect. (2008) (10):908-934.

[6]. Clarridge, J.E. 3rd. Impact of 16S rRNA Gene Sequence Analysis for Identification of Bacteria on Clinical Microbiology and Infectious Diseases. Clin Microbiol Rev. (2004); 17(4): 840–862.

[7]. Begot, C., Desnier, I., Daudin, J. D., Labadie J. C. and Lebert, A. Recommendations for calculating growth parameters by optical density measurements, J. Microbiol. Meth. (1996) 25:225–232.

[8]. Rodriguez-Saona, L.E., Khambaty, F.M., Fry, F.S. and Calvey, E.M. Rapid detection and identification of bacterial strains by Fourier transform near-infrared spectroscopy, *J. Agric. Food Chem.* (2001) 49: 574–579.
[9]. Rodriguez-Saona, L.E., Khambaty, F.M., Fry, F.S., Dubois, J. and Calvey, E.M., Detection and identification of bacteria in a juice matrix with Fourier transform-near infrared spectroscopy and multivariate analysis *J. Food Prot.* (2004) 67: 2555–2559.
[10]. Akerlund, T., Nordstrom, K. and Bernander, R. Analysis of cell size and DNA content in exponentially growing and stationaryphase batch cultures of Escherichia coli. J. Bacteriol. (1995),177, 6791– 6797.
[11]. Oberreuter, H., Seiler, H. and Scherer, S., Identification of coryneform bacteria and related taxa by Fourier-transform infrared (FTIR) spectroscopy. *Int. J. Syst.. Evol. Microbiol.* (2002) 52: 91–100.
[12]. Winder, C.L., Carr, E., Goodacre, R. and Seviour, R., The rapid identification of Acinetobacter species using Fourier transforms infrared spectroscopy, *J. Appl. Microbiol.* (2004) 96: 328–339.
[13]. Davis, R. and Mauer, L.J., Fourier transform infrared (FT-IR) spectroscopy: a rapid tool for detection and analysis of foodborne pathogenic bacteria, *Appl. Microbiol.* (2010) 2(1): 1582–1594.
[14]. Smith B. Fundamentals of Fourier Transform Infrared Spectroscopy, CRC Press, Washington, D.C. 1996.
[15]. Rebuffo-Scheer, CA, Dietrich J, Wenning, M, Scherer, S., Identification of five Listeria species based on infrared spectra (FTIR) using macrosamples is superior to a microsample approach, *Anal. Bioanal. Chem.* (2008) 390:1629-1635.
[16]. Al-Qadiri, H.M, Al-Holy, M.A, Lin, M.S, Alami, N.I, Cavinato, A.G, Rasco, B.A., Rapid detection and identification of Pseudomonas aeruginosa and Escherichia coli as pure and mixed cultures in bottled drinking water using Fourier transform infrared spectroscopy and multivariate analysis, *J. Agri. Food Chem.* (2006) 54:5749-5754..

Chapter 7

GENERAL CONCLUSIONS

Vibrational spectroscopic methods: Infrared and Raman are applicable to real-world issues, with usefulness in medical diagnostics, environmental screening, and bioterrorism research. The methods discussed can be readily used in these fields and in others where a limited amount of bacteria need to be identified from amino acids studies. The identification of microorganisms is of high relevance not only for medical applications but also for monitoring of special facilities such as clean rooms or process rooms environments in pharmaceutical and biotechnology industries. For all these applications a fast and reliable identification is necessary. Using these techniques research on two amino acids with different SERS Ag/Au NPs substrates and bacteria on various substrates supports (including cardboard, stainless steel, travel baggage, wood, glass, Au coated slides, ZnSe discs, aluminum oxide Anodisc™ filters) were tested and successful results were obtained by using their characteristic fingerprint spectrum in the MIR. Satisfactory results were found for discrimination of bacteria with good values of sensitivity, specifity and low values of cross validations (RMSCV).

The most important contribution of this research endeavor is the first application of a tunable MIR quantum cascade laser (QCL)-based spectrometer for identification and discrimination of bacteria. While the spectroscopic optical system is relatively simple in

design, it was important to show the feasibility of using QCL for identifying biochemical components of bacterial cell wall of various microorganism species from the vibrational signatures of molecular components in the biosamples. QCLS is a viable spectroscopic technique for potential implementation in the field since it can also be easily adapted to portable equipment to obtain fingerprint information of biomolecules and microorganisms in the field. The results suggest the potential capability of this methodology, with use of powerful multivariate analysis of chemometrics: principal component analysis (PCA) and partial least squares analysis coupled to discriminant analysis (PLS-DA) of QCL spectra to classify and discriminate between gram (+) and gram (-) bacteria at a 95% confidence level. Also, highly interfering contributions from the substrates can be accounted for and separated from spectral information for the rapid identification of microorganisms. The complex cellular composition of bacteria produces MIR vibrational modes, forming the basis for identification. Thus, addition Fourier transform-infrared (FT-IR) spectroscopy was used to rapidly and nondestructively analyze bacteria by the reference spectra presented.

A database of spectroscopic signals including strains of *Bacillus thuringiensis ATCC 35646 (Bt), Staphylococcus epidermidis ATCC 2228 (Se),* isolate *Bacillus subtilis (Bs), Bacillus pumilus (Bp), Bacillus licheniformis (Bl), Micrococcus luteus (Ml),* isolate *Staphylococcus epidermidis (Se), Acinetobacter genomospecies 3 (Ag3), Bacillus subtilis ATCC 6633 (Bs), Staphylococcus aureus ATCC 6538 (Sa), Escherichia coli ATCC 8739 (Ec),* and *Pseudomonas aeruginosa ATCC 9027 (Pa)* was initiated and spectral characteristics of these bacteria were assigned, with special care taken to

optimize sample preparation, because bacterial MIR spectra display signatures of the entire chemical composition of the cell.

Furthermore, this new technology can potentially be used to identify biological contaminants on surfaces and providing fast and accurate analyses for security, safety and quality control purposes when nondestructive analytical methods are preferred. Substrate porosity clearly plays an important role in diminishing the number of microorganisms available to reflect MIR light on the substrate surface. These investigations provide promise and direction for the study of additional parameters and variables for pathogenic and nonpathogenic bacteria. The protocols developed could be promising tools for routine microbial environmental control in pharmaceutical and biotechnology industries.

Appendix A

GROWTH CURVES OF BACTERIA

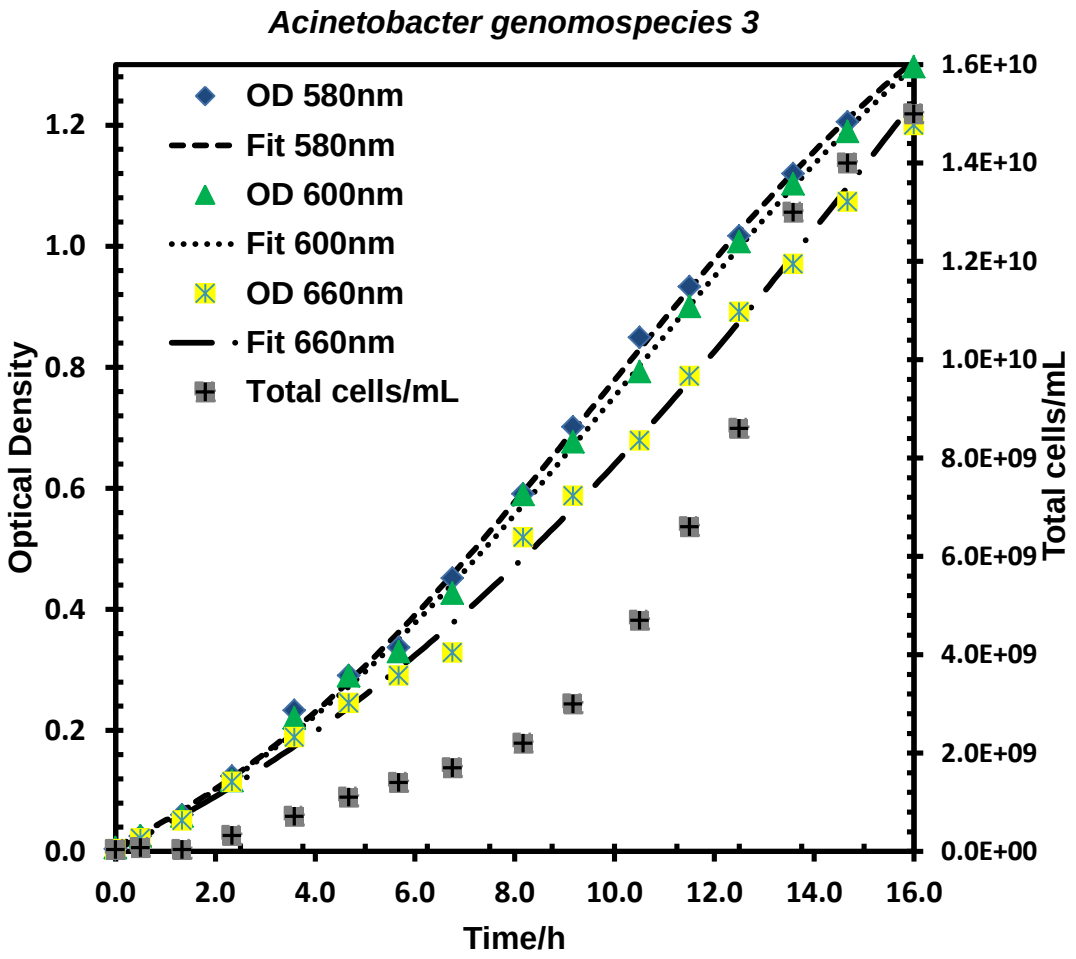

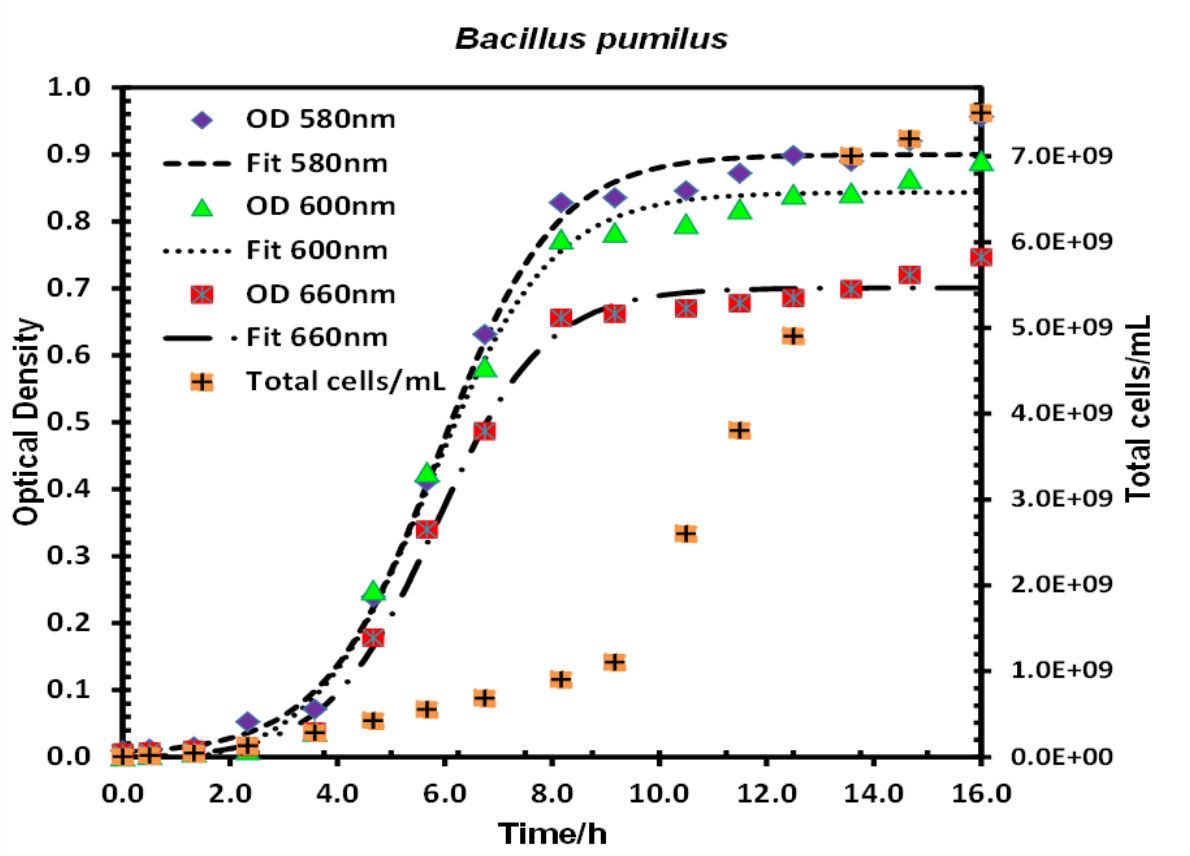
Bacillus pumilus
OD 580nm
Fit 580nm
OD 600nm
Fit 600nm
OD 660nm
Fit 660nm
Total cells/mL
Optical Density
Total cells/mL
Time/h
1.0
0.9
0.8
0.7
0.6
0.5
0.4
0.3
0.2
0.1
0.0
7.0E+09
6.0E+09
5.0E+09
4.0E+09
3.0E+09
2.0E+09
1.0E+09
0.0E+00
0.0
2.0
4.0
6.0
8.0
10.0
12.0
14.0
16.0

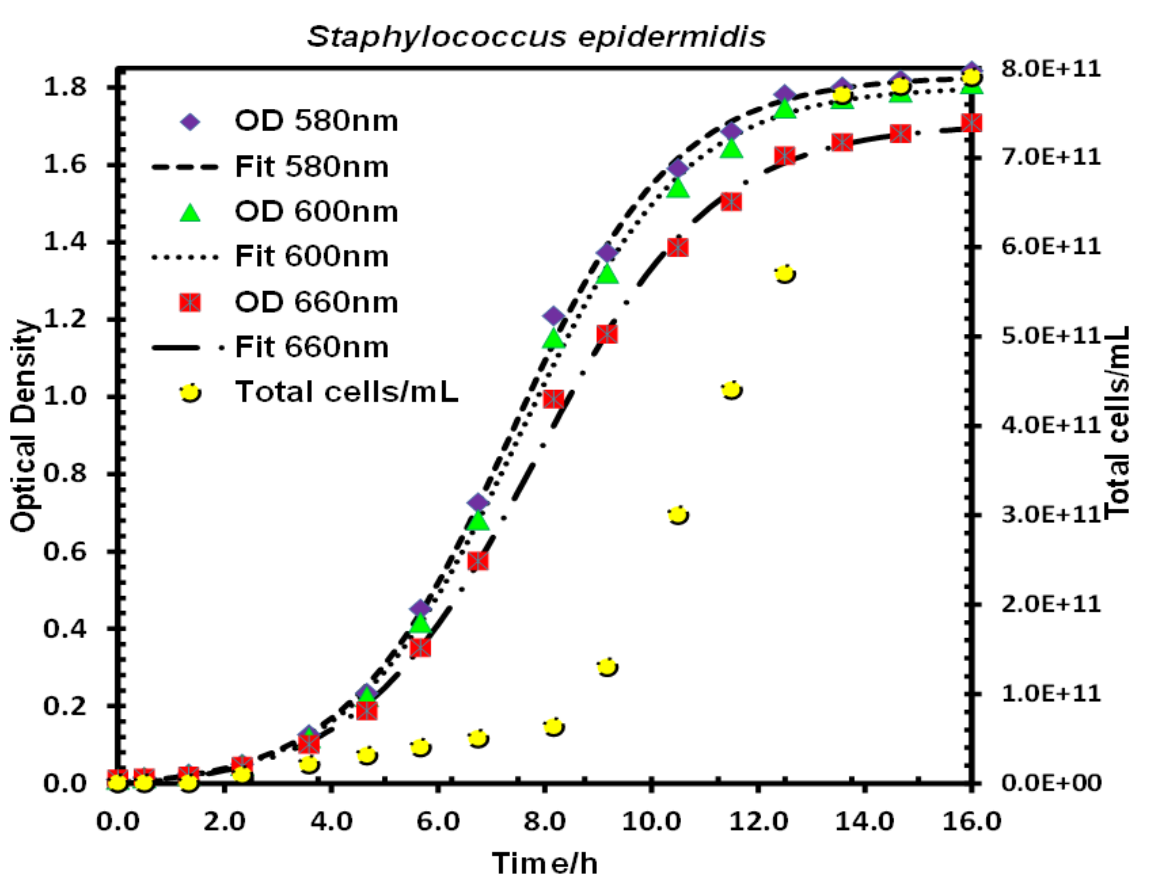
Staphylococcus epidermidis
OD 580nm
Fit 580nm
OD 600nm
Fit 600nm
OD 660nm
Fit 660nm
Total cells/mL
Optical Density
Total cells/mL
Time/h
0.0
0.2
0.4
0.6
0.8
1.0
1.2
1.4
1.6
1.8
0.0E+00
1.0E+11
2.0E+11
3.0E+11
4.0E+11
5.0E+11
6.0E+11
7.0E+11
8.0E+11
0.0
2.0
4.0
6.0
8.0
10.0
12.0
14.0
16.0

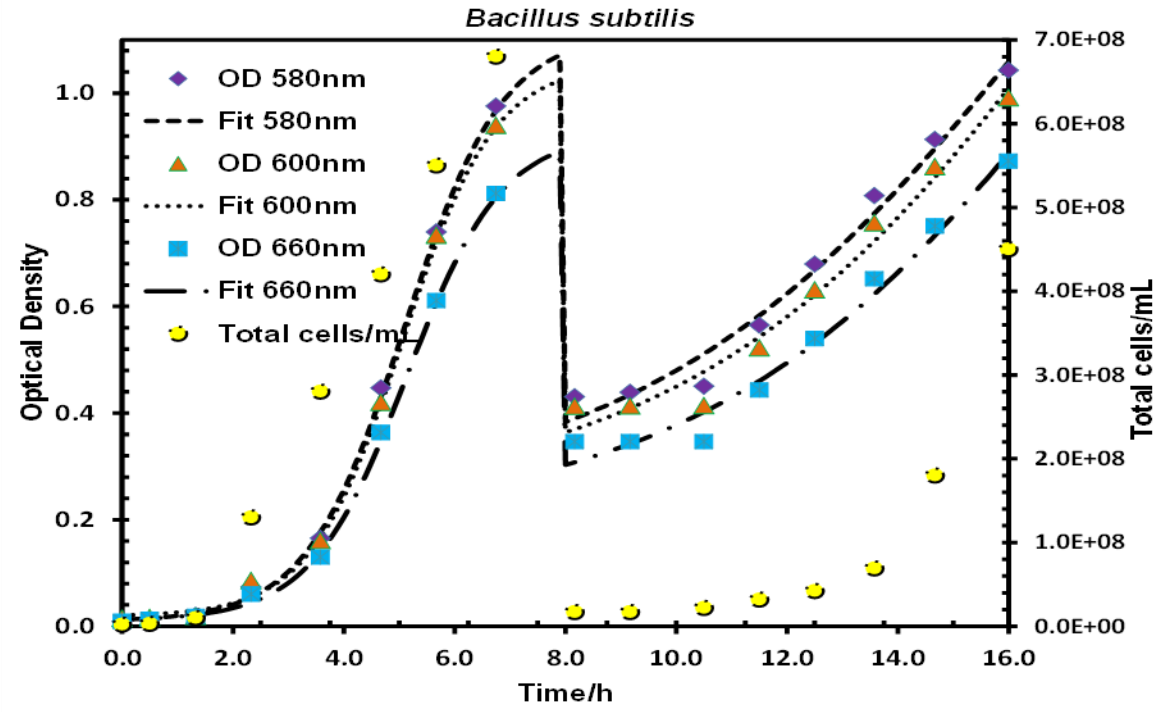
Bacillus subtilis
OD 580nm
Fit 580nm
OD 600nm
Fit 600nm
OD 660nm
Fit 660nm
Total cells/mL
Optical Density
Total cells/mL
Time/h
0.0
0.2
0.4
0.6
0.8
1.0
0.0E+00
1.0E+08
2.0E+08
3.0E+08
4.0E+08
5.0E+08
6.0E+08
7.0E+08
0.0
2.0
4.0
6.0
8.0
10.0
12.0
14.0
16.0

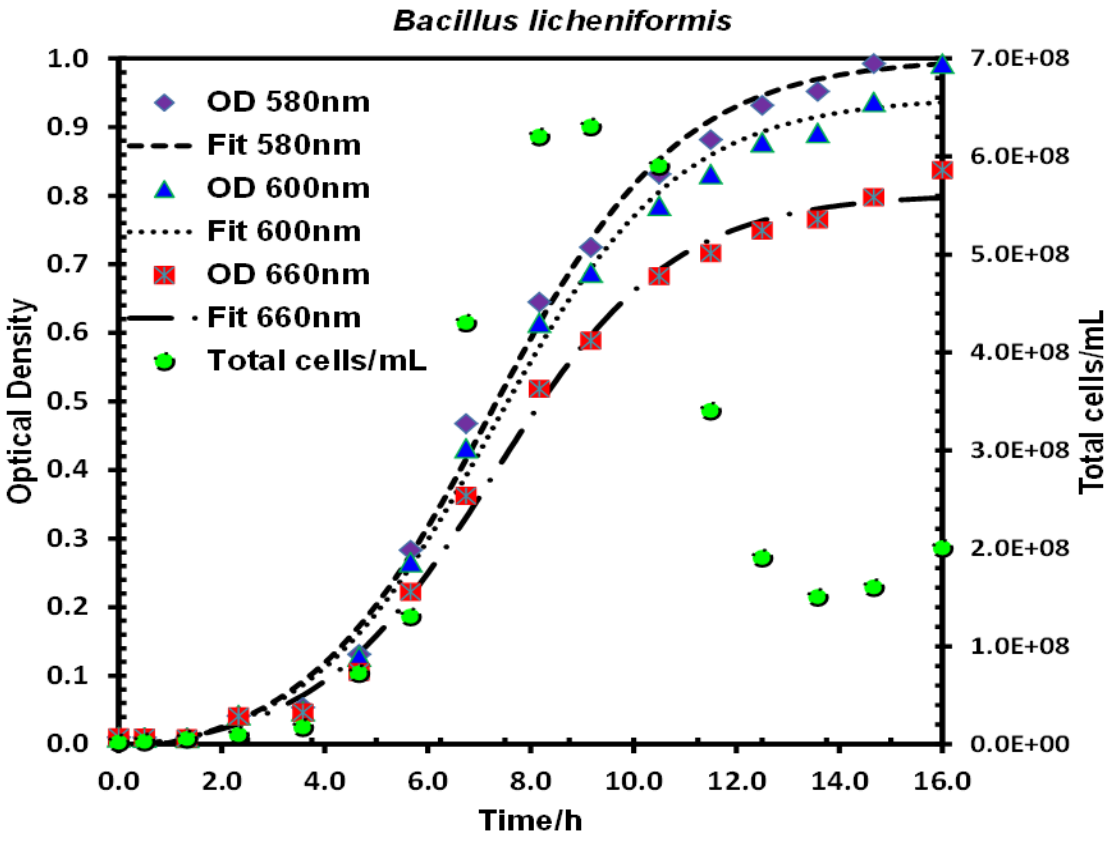
Bacillus licheniformis
OD 580nm
Fit 580nm
OD 600nm
Fit 600nm
OD 660nm
Fit 660nm
Total cells/mL
Optical Density
Total cells/mL
Time/h
1.0
0.9
0.8
0.7
0.6
0.5
0.4
0.3
0.2
0.1
0.0
7.0E+08
6.0E+08
5.0E+08
4.0E+08
3.0E+08
2.0E+08
1.0E+08
0.0E+00
0.0
2.0
4.0
6.0
8.0
10.0
12.0
14.0
16.0

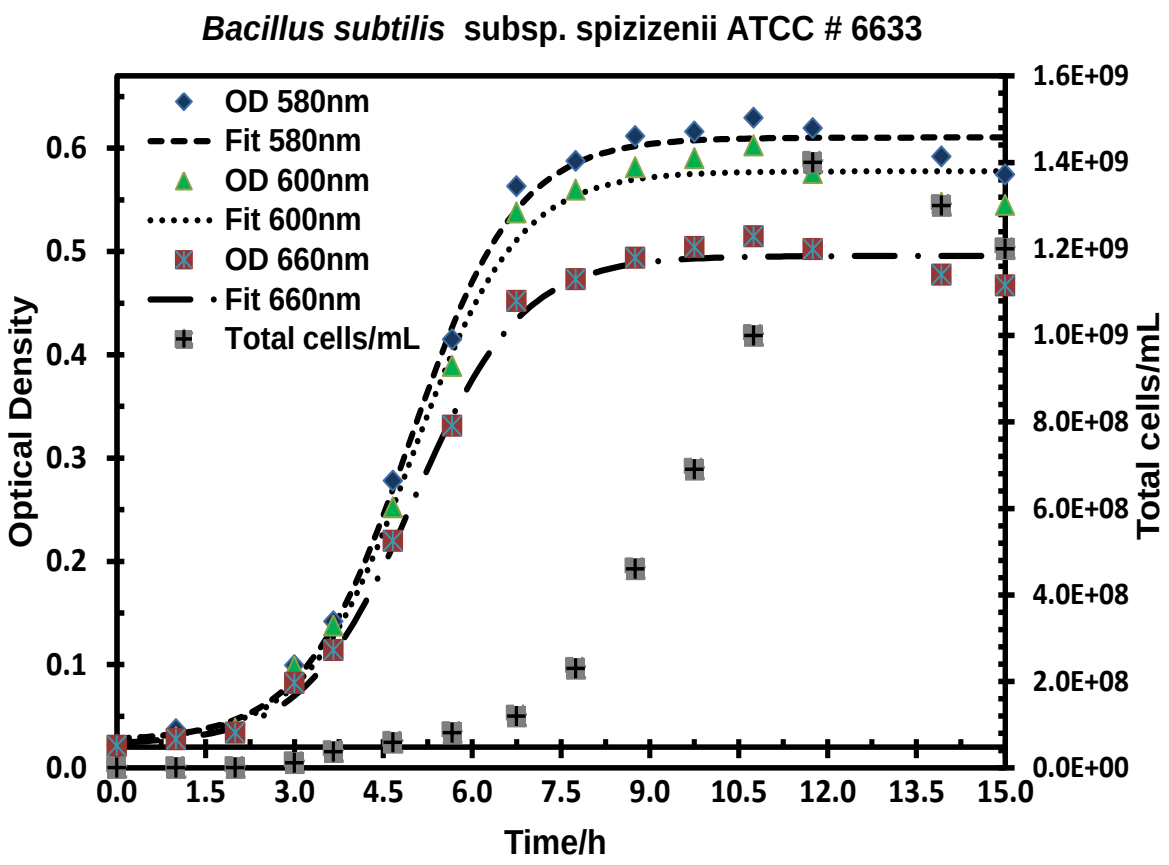
Bacillus subtilis subsp. spizizenii ATCC # 6633
OD 580nm
Fit 580nm
OD 600nm
Fit 600nm
OD 660nm
Fit 660nm
Total cells/mL
Optical Density
Total cells/mL
Time/h
0.0
0.1
0.2
0.3
0.4
0.5
0.6
0.0E+00
2.0E+08
4.0E+08
6.0E+08
8.0E+08
1.0E+09
1.2E+09
1.4E+09
1.6E+09
0.0
1.5
3.0
4.5
6.0
7.5
9.0
10.5
12.0
13.5
15.0

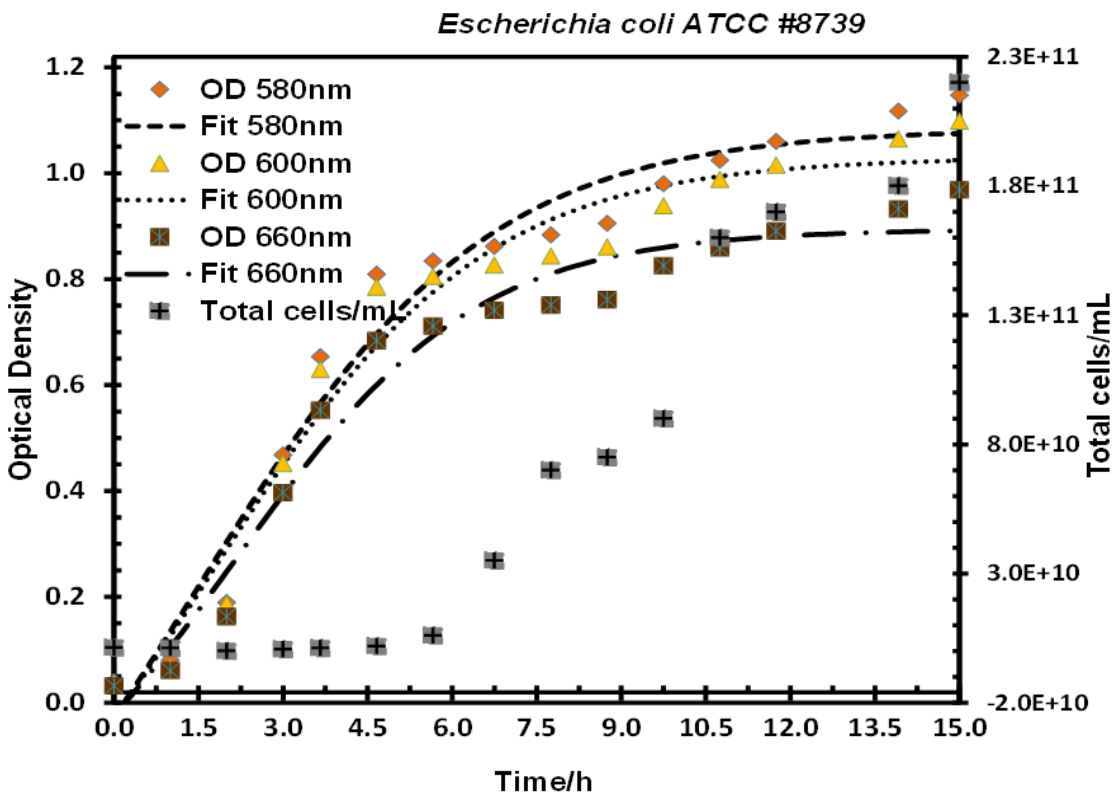
Escherichia coli ATCC #8739
OD 580nm
Fit 580nm
OD 600nm
Fit 600nm
OD 660nm
Fit 660nm
Total cells/mL
Optical Density
Total cells/mL
Time/h
1.2
1.0
0.8
0.6
0.4
0.2
0.0
2.3E+11
1.8E+11
1.3E+11
8.0E+10
3.0E+10
-2.0E+10
0.0
1.5
3.0
4.5
6.0
7.5
9.0
10.5
12.0
13.5
15.0

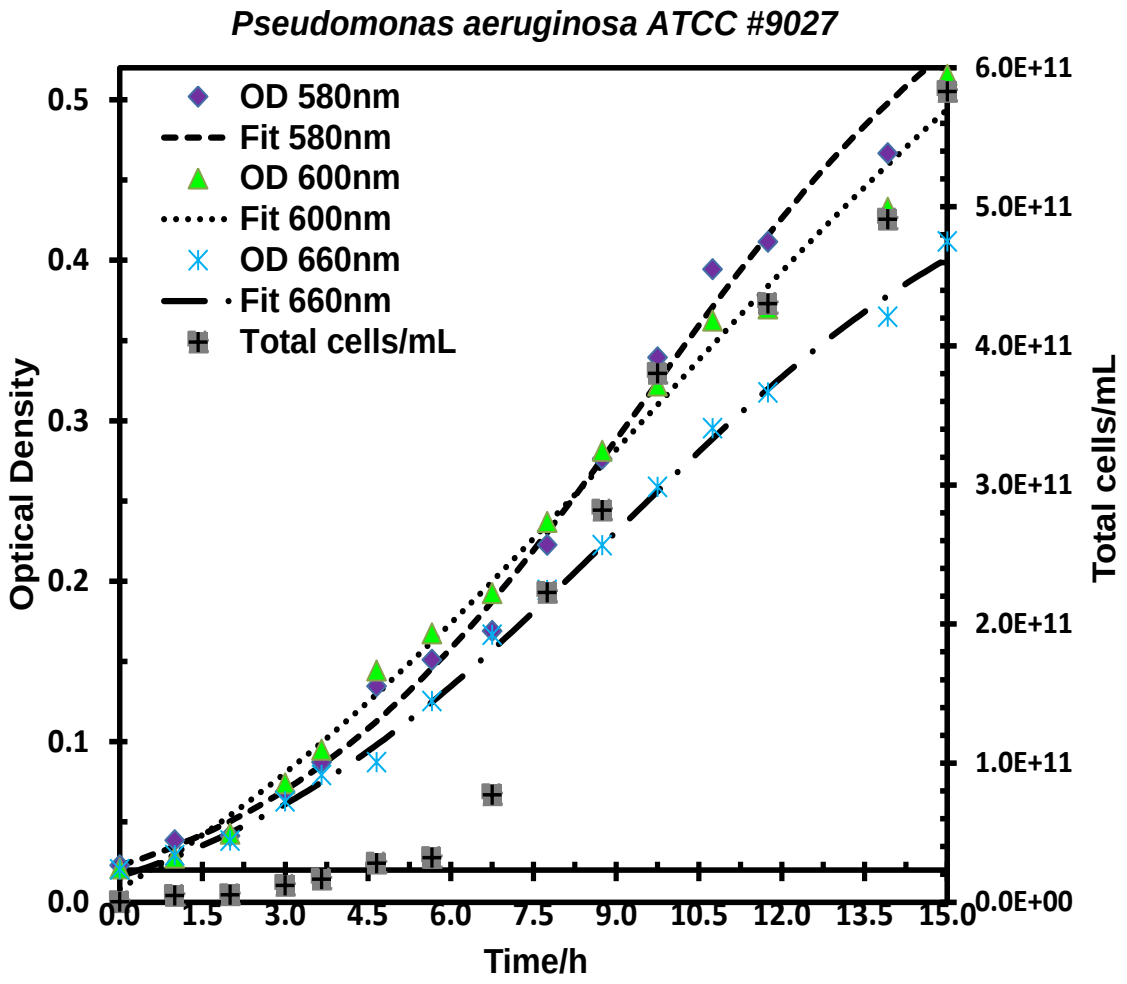
Pseudomonas aeruginosa ATCC #9027
OD 580nm
Fit 580nm
OD 600nm
Fit 600nm
OD 660nm
Fit 660nm
Total cells/mL
Optical Density
Total cells/mL
Time/h
0.0
0.1
0.2
0.3
0.4
0.5
0.0E+00
1.0E+11
2.0E+11
3.0E+11
4.0E+11
5.0E+11
6.0E+11
0.0
1.5
3.0
4.5
6.0
7.5
9.0
10.5
12.0
13.5
15.0